NTNU – Trondheim
Norwegian University of
Science and Technology

CO2 Enhanced Oil Recovery in Strong Water-Drive Reservoirs

Thibaut Forest

Earth Sciences and Petroleum Engineering
Submission date: June 2012
Supervisor: Ole Torsæter, IPT

Norwegian University of Science and Technology
Department of Petroleum Engineering and Applied Geophysics

Summary

This study deals with a subject that has not been deeply under research so far but caused some EOR projects to be reconsidered: CO_2 EOR in the particular case of strong water-drive reservoirs. Despite the lack of field data on actual or previous projects, a simple one-dimensional model and some two-dimensional models were analysed with Eclipse 100 and Eclipse 300. The first part lists the CO_2 properties which will be implemented in the simulation files and describes the benefits of this type of tertiary recovery technique using carbon dioxide. Basic flow equations are applicable in the one-dimensional case and enable to determine the oil, water and CO_2 rate in a strong aquifer configuration. Both the blak-oil and computational simulations lead to concluding results which validated the derived equations. Further simulations permited to make a sensitivity analysis on the pressure drop or the distance between the wells, leading to optimum well location depending on the production needs. A better understanding of the model gave birth to a scaling number for the one-dimensional simulation that was verified by the construction of Walsh Diagrams. This model was further extended from one to two producers to account for gas losses due to the aquifer. It turns out that two scaling numbers are then necessary to describe this flow and eventually scale it up to real dimensions. Multiple-well simulations illustrated the effect of the aquifer on the CO_2 plume in the oil zone; however this loss in sweep efficiency needed to be quantified. A Matlab program was built in order to analyse the simulation pictures. By measuring the pixels of the plume compared to a reference area, the areal and vertical sweep efficiency were computed and gave a better feeling of the effect of the aquifer strength on the EOR process. For the model studied, the volumetric sweep efficiency falls from 15% for a weak aquifer, to 2% for a strong aquifer. The major part of the gas is blown away at a certain water rate which leads to a significant decrease in oil production for the production well next to the CO_2 injector. The industry has faced this problem for many years and some technological solutions turned out to be succesfull, this study can provide useful insights before implanting those solutions, by indicating the ideal well location and the expected fluid rates.

Acknowledgments

It has been a great opportunity to write my master thesis in collaboration with the University of Texas at Austin during this semester, and more specifically with Dr. Larry W. Lake. I was strongly determined to find a topic about CO_2 EOR that would have industrial applications; Dr. Lake managed to figure out exactly what I would like to work on and suggested a brand new research subject. Thanks to his availability I have been through several aspects of this research topic, even though some pratical data would have made it even more meaningful.

I had the chance to attend an EOR class taught by Shell professionals, which provided me with better knowledge about the EOR processes and new methods as the Walsh diagrams. Working with world experts in this field could have been a challenging task in the first place, however I believe this experience has been really rewarding personnaly and professionaly. I have also taken part in seminars concerning my research topic and had the opportunity to attend a conference on CO_2 storage in Denver. I am convinced that my master thesis has been enhanced by this experience and that my future career as an engineer will benefit from all I learnt during this semester.

Finally I would like to thank NTNU, my university in Norway, and my supervisor Ole Torsaeter for their support regarding my application to go study at UT Austin. I also thank Dale Mary Licata from the International Office, Marit Snilsberg and Jon Kleppe, head of the department, for their help during the application process. I hope that many other students from NTNU will have the opportunity to write their thesis in partnership with UT Austin in the future. It was a pleasure to work at the petroleum department during this semester and I am greatly thankful to all employees for their help on a daily basis, particularly Tersian Roger concerning the several IT issues I had. I am thankful to the University for letting me use its facilities and making my stay as a visiting researcher even more pleasant.

Table of Contents

List of figures

List of tables

Introduction

In its latest energy outlook (The U.S. Energy Information Administration, 2012), the international Energy Agency expects the total world carbon emissions to increase by 1% per year until 2035, which is lower than the past years. However this growth is mainly dependent on the fuel mix, too many countries such as China or the United States still use coal-fired plants generating large amounts of CO_2. Since the Kyoto protocol in 1997, many countries have commited themselves to reduce global warming by tackling their CO_2 emissions. Among other technologies, Carbon Capture and Storage (CSS) and Enhanced Oil Recovery (EOR) have been under research in order to cut emissions and reach the targets.

CCS consists in capturing CO_2 produced in large quantities from industrial plants, then transport it and pump it in the ground in order to store it permanently (What is CCS?, 2012). Nowadays the biggest issue with this technology is its cost, due to the expensive processes needed to capture the CO_2. It is a relatively new technology with a few commercial projects up to date, and the regulation frame is yet to be well defined. On the contrary, EOR has been widely used to treat CO_2 even though surprisingly the supply of carbon dioxide can be an issue in some cases. This method can be used as a tertiary recovery method, which consists in injecting CO_2 to produce incremental oil. As the oil price is increasing, this solution has been of interest to oil companies since it increases the life of the field and eventually reduces the carbon footprint by storing significant quantities of CO_2.

Several projects are now under development notably the CCS project in the Sleipner gas field where 12MMT of CO_2 have been injected (Abdelhakim Deghmoum, 2012) as of today, and the biggest CO2-EOR project in the world is currently running in the Denver unit located in west Texas. The United States has conducted many CO_2-EOR projects, notably in the Permian Basin during the last decades and still represents a great potential for EOR[1] (Childers, 2011). Despite the success of these projects, oil companies are facing some challenges in implementing EOR in the existing fields.

[1] 240 billion barrels according to the Department of Energy

For example three operational problems are to be investigated when dealing when CO_2-flooding: corrosion, asphaltene deposition and handling of the CO_2 (Hocott, 1983). More precisely the heterogeneity of the reservoir may create unexpected flow paths, which will affect the sweep efficiency and impact the oil recovery. Finally the presence of an aquifer, especially when it creates a strong water stream accross the reservoir, compromises the CO_2 injection.

The company Hilcorp would like to know if some wells are eligible for CO_2-flooding, however the reservoir contains a strong aquifer that may blow the injected CO_2 away. Following an interview with Hilcorp in Houston, Dr Larry W. Lake suggested me to evaluate the possibility of CO_2 as an EOR process in this type of configuration. This research topic is hardly found in the literature, that's why as a first approach a simple simulation model was studied.

1. Introduction to the problem

The aim of the master thesis is to study the faisability of CO_2 EOR in strong water-drive reservoirs. The company Hilcorp wanted to know if this type of reservoir would be eligible for CO_2-flooding. Some pilot projects exist, injecting CO_2 to recover more oil out of reservoirs with strong aquifers. However in many cases the CO_2 is lost in the formation, thus the carbon dioxide does not displace correctly the oil.
Several explanations can then be assumed to explain the failure of the EOR process in such conditions. A significant part of the CO_2 can be dissolved in the aquifer, generating a first loss. Indeed the carbon dioxide is preferred to dissolve in the oil so the oil mobility ratio is reduced. The quantity of CO_2 able to dissolve in the aquifer is known from lab experiment and cannot be the only explanation of the phenomenon. The most probable explanation is believed to be the sweep of the CO_2 away from the well by the aquifer, so that the surrounding well cannot produce it. This CO_2 swept away by the water has also an impact on the sweep efficiency; the CO_2 will not be in contact with the oil on a large surface. As a consequence the CO_2 is lost and the oil not recovered.

This first part will present a state-of-the-art of strong water-drive reservoirs and CO_2 EOR, to better understand the following simulations.

1.1. Strong water-drive reservoirs

A water-drive reservoir is a reservoir-drive mechanism whereby the oil is driven through the reservoir by an active aquifer. As the reservoir depletes, the water moving in from the aquifer below displaces the oil until the aquifer energy is expended or the well eventually produces too much water to be viable[2] (Schlumberger, 2012). This water influx from the aquifer has obviously an impact on the material balance of the reservoir, it is one way to detect and measure the strength of the aquifer.

[2] Definition from the Schlumberger Oilfield glossary

For example in the Black oil material balance equation (Kleppe, 2011), the term W_e has to be included in case of aquifer influx.

$$F = N\left(E_o + mE_g + E_{f,g}\right) + (W_i + W_e)B_{w2} + G_iB_{g2} \quad (1.1.1\text{-}1)$$

Where F is the production term, E_o the oil and solution gas expansion term, E_g gas cap expansion term and $E_{f,g}$ the rock and water compression/expansion term.
In equation the contribution of the aquifer is contained in the W_e term, which in the case of a strong aquifer would be positive.

There are other ways to measure the strength of the aquifer, for instance the recovery factor, the water production, the cumulative Water-Oil ratio (WOR) and Gas-Oil ratio (GOR) and finally the pressure histories.

In case of the water-oil ratio (WOR), which is the ratio of produced water to produced oil, it is considered that an aquifer is strong if the WOR is greater than 0.25, and weak if less than 0.15. If the WOR is between those two values, another parameter, the GOR is calculated. In this case strong aquifer is indicated by a cumulative GOR less than 1000 m^3/m^3, otherwise the aquifer is weak (Stefan Bachu & Jerry C. Shaw, 2004).

1.2. Literature review

Even though little research has been conducted so far about the topic of this master thesis, several studies are of interest before creating any model or using any formula. Firstable strong water-drive reservoirs issues appear in some case studies, mainly to explain the suitable technology to optimize recovery. Several EOR techniques have been evaluated under such conditions, however CO_2-flooding is hardly considered. The effect of aquifer on CO_2 injection and storage, which is useful in order to extend the study to strong aquifers, is tackled in some publications.

1.2.1. New technologies

Several pilot projects happen to be subject to a strong water influx during production, the first solution is then to accuratly monitor the aquifer to prevent early breakthrough in the producing well (C.A.M. Veeken, 2000). The main physical parameters to monitor in case of a gas injection project can be the rates (oil, water and gas), the pressure drop, the H2S concentration in the produced gas, the gas saturation and gas cap advance. By monitoring those parameters in a gas injection pilot for a massive carbonate reservoir, it is possible to increase the oil production and double the recoverable reserves from the field (Shahsavari, 1991).

To significantly improve the oil production from this type of reservoir once it is carefully monitored, several drilling techniques can be implemented. Multiple laterals but also total and dual penetration methods are promising technology in order to delay the water breakthrough and enhance production (Ehlig-Economides, Chan, & Spath, 2012). An example from a carbonate reservoir in Abu Dhabi with high water cut shows that horizontal wells and electric submersible pumps (ESP) can overcome this challenge, together with a better understanding of the heterogeneities of the reservoir thanks to the monitoring of the field (Abdullatif Ibrahim, 2009).

Developping a strong water-drive reservoir is generally very challenging, that's why new technologies are constantly designed in order to make pilot projects succesful. This is the case for the Bilateral Water Sink (BWS), a cold production method developped for heavy oil reservoirs with severe coning (Wenting Qin, 2011).

1.2.2. Recovery optimization examples

One of the challenges is to improve the gas or oil recovery from such reservoirs, since a major part of the production is water due to water coning. Following the water breakthrough it can turn out that the gas is trapped in water invaded regions; it is then necessary to use a secondary recovery method to produce this gas by depressuring the reservoir (Thomas P. Chesney, 1982).

The previous paragraph introduced some technologies to improve the recovery, however the companies are more and more looking into integrated solutions that can be easily managed. Once the field is monitored, an accurate history match enables to determine the best field development to improve recovery (Ramli, 1995).

1.2.3. EOR techniques

Despite the lack of literature on CO_2 EOR, some strong water-drive reservoirs have been developped with other EOR techniques. First a successful microbial EOR pilot project in Argentina, where nutrients, biocatalizers and microorganisms have been injected to colonize the pore volume. In this case the oil rate increased and the water rate decreased, due to lower residual oil saturation and lower oil mobility (L.A. Strappa & M.A. Maure, 2004). In addition to this EOR technique, several other techniques are faisable and assessed everytime a strong aquifer is located. Among those techniques, the in-situ combustion, high-pressure steam injection and polymer flooding appears to be the best in case of a medium-heavy oil reservoir (A. D. Brooks & and W. Al-Ajmi and M. Mukmin, 2010).

Concerning CO_2 EOR, the screening criterias are determined in the literature by some authors; nevertheless the impact of the aquifer on those parameters is yet to be determined in further studies.

Table 1 Criterias for C02-flooding (Stefan Bachu & Jerry C. Shaw, 2004)

Physical parameter	Criteria for CO_2 EOR
Oil saturation	Greater than 0.25
Reservoir pressure	Greater than 1100 psia or at least 200 psia, greater than the minimum miscibility pressure (MMP)
Oil gravity	Between 27 and 48° API
Permeability	Greater than 5 mD
Reservoir depth and oil viscosity	Dependant on other parameters

The impact of the aquifer strength on CO_2 sequestration and EOR has been investigated in several pools in Canada, resulting in some ineresting plots showing the quantity of CO_2 trapped in the pool depending on the aquifer. Firstable it turns out that at the initial pressure the CO_2 sequestrated with an aquifer effect and/or EOR is always reduced compared to the amount sequestrated without aquifer. However if the reservoir can be pressured beyond its initial pressure, the CO_2 sequestration capacity increases as water is expelled from the reservoir and his capacity is even higher if coupled with EOR.

1.3. CO2 properties

1.3.1. Physical properties

Carbon Dioxide is a non-toxic stable compound found in a gaseous state at standard conditions. In petroleum engineering application it can be in liquid or gas state depending on the PVT conditions. The table below gives the main physical properties of CO_2.

Table 2 CO_2 physical properties

Molar mass	44.01 kg/kgmol
Critical Temperature	88°F
Critical density	1,070 psia
Critical Z factor	0,274

The knowledge of those parameters is important because they will serve as inputs for the simulator, together with the following properties described below. The simulator asks for the density of the fluid, the viscosity, the relative permeability and the Formation volume Factor (FVF) versus pressure. The graphs which served as a basis for the input data are in appendix 1 (Curtis H. Whitson, 2000).

Concerning the formation volume factor, for most CO_2 projects 2 Mscf of CO_2 is required to recover an additional 1 barrel of oil at standard conditions by the CO_2 miscible process. Since carbon storage is related to EOR, a significant part of the injected CO_2 (up to 50%) can remain in the reservoir. Finally since the study concerns aquifers, the formation of carbonic acid by mixing CO_2 and water is to be considered. It may generate corrosion, reduce the injectivity of the well and damage the drilling equipment.

The phase diagram of CO_2 is also a key data since we can inject the gas under different temperature and pressure conditions. The three phases are delimitated in the above diagram, with the triple and critical point. Above the critical point the fluid is supercritical, the liquid and vapor phases cannot be distinguished. When injected as a liquid the CO_2 is often supercritical, and this will be the case in the simulations.

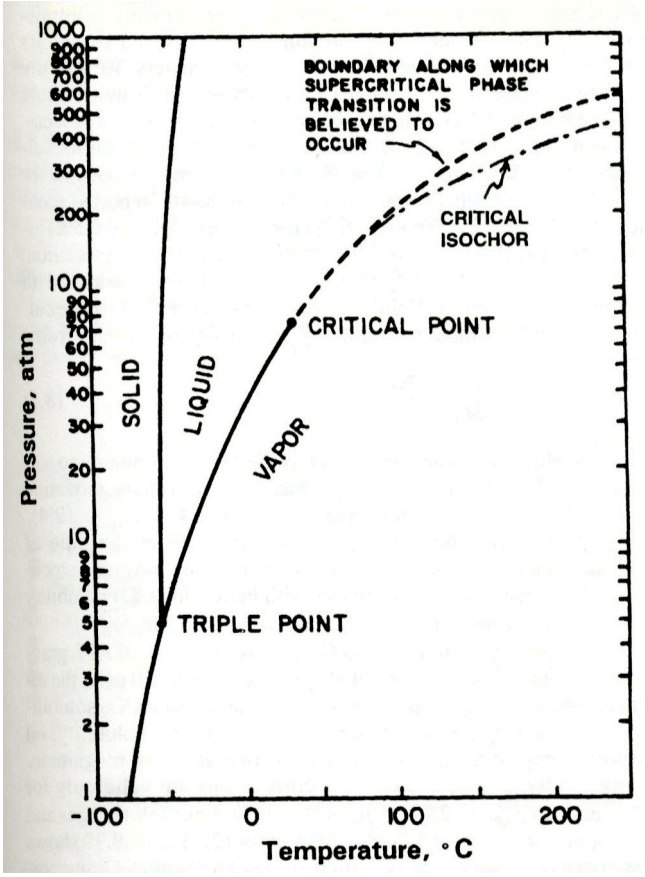

Figure 1 CO_2 Phase Diagram (Curtis H. Whitson, 2000)

1.3.2. Immiscible and miscible displacement

CO_2 injection has been applied to various types of oil reservoirs, in order to reduce the viscosity and increase the oil swelling. The swelling factor can be defined as follows:

$$swelling\ Factor = \frac{CO_2\ saturated\ stock\ tank\ oil\ volume}{original\ stock\ tank\ oil\ volume} \quad (1.3.2\text{-}1)$$

This factor is an indicator of how effective the displacement will be since the more CO_2 dissolves in the oil the less viscous it becomes.

The immiscible displacement is used in viscous heavy oil reservoirs, the following graphs show in which extent the viscosity is reduced with increasing pressure and the swelling factor increases with increasing mol fraction of CO_2. It also shows that high viscosity oil is affected the most, showing a steeper curve for both parameters.

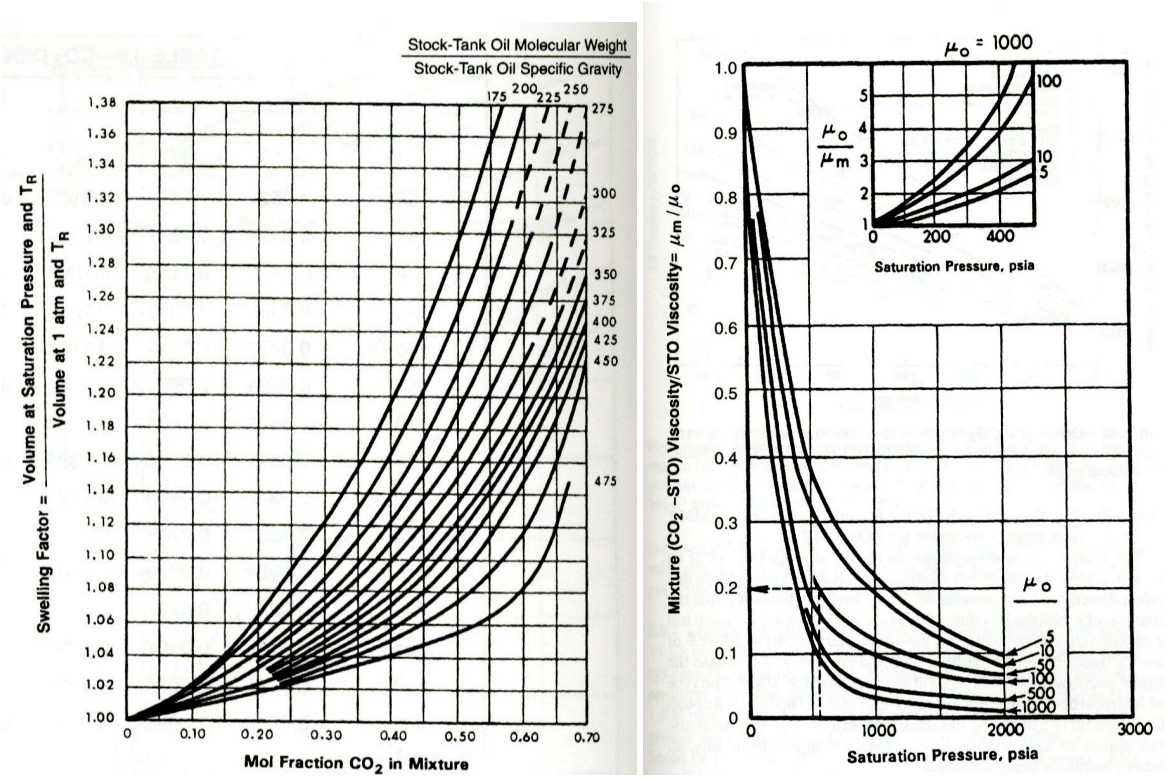

Figure 2 Swelling Factor and effect of CO2 on oil viscosity in case of a miscible displacement

Regarding the miscible displacement of oil, the swelling factor has been reported in many publications (Holm, 1976).An experiment was settled, where a cell was filled with one third of CO_2 and two third of oil, as pressure increases the relative volumes are then measured. The experimental setup is presented in Figure 3, with the results.

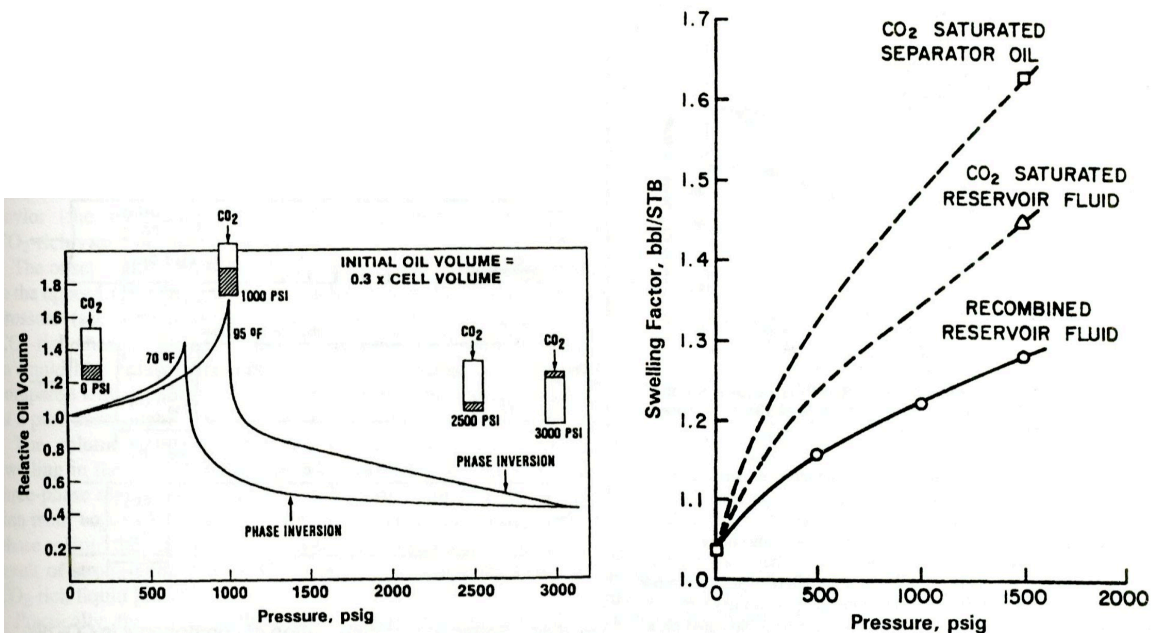

Figure 3 Experimental setup (Curtis H. Whitson, 2000)

Physical properties of CO_2 explain why it has been widely used for EOR, it reduces the viscosity and increases the swelling efficiency of the oil. It results in an incremental oil recovery and CO_2 storage, the produced CO_2 can be recycled. One issue can be the supply of CO_2, even though it seems like a paradox. The CO_2 has to be transported from a source which can be a coal-fired plant for instance; in some cases the CO_2 needed is so large that finding a reliable supply of CO_2 is complicated.

2. Simulation

Considering all the physical parameters listed in the previous part as inputs, several simulations have permited to illustrate the problem and confront the results with the theory. Two different versions of the Schlumberger software Eclipse have been used, both having their pros and cons regarding the accuracy of the results. After a brief description of the method used and the related keywords, the simulation cases will be presented and discussed.

2.1. Simulator characteristics

2.1.1. Eclipse 100

An example of simulation file for this version can be found in appendix 2. A quick review of the RUNSPEC section indicates that 3 phases are present, the keyword DISGAS means that we allow the gas to dissolve in the oil phase, and we work in field units[3]. We then use the black-oil model to simulate the behavior of oil and gas, the gas is taken with CO_2 properties and can dissolve only in the oil phase. It is practical as a first approximation, however this is not a good assumption since we know the solubility of CO_2 in brine or pure water can be significant: around 190 scf/STB in fresh water at 4000 psia (Curtis H. Whitson, 2000).

The GRID section comprises physical parameters for the gridblocks, and also keywords as AQUNUM and AQUCON used to simulate an aquifer in a gridblock. Although the number and the size of the gridblocks have slightly changed depending on the simualtion files, the parameters listed below remained unchanged.

[3] Implies the following units : STB/D for oil and water rates, MSCF/D for gas rate, volumes in cubic feet, pressure in psi.

Table 3 Grid Parameters

Porosity	30 %
Absolute Permeability (isotropic media)	500 mD
Depth at the top	8325 feet
Transmissibility	1

The PROPS section sums up the CO_2 properties described earlier, the water and oil properties are added, notably their relative permeabities. The residual oil saturations have been defined so that 20% oil remains after the waterflood and 5% oil after the CO_2-flood. Initially the bubble point pressure was set to 4014.7 psia, allowing the gas to come out of the oil below this pressure. However it was observed that a large amount of gas would then appear whenever a severe pressure drawdown would occur due to a new producing well. The Rs Value was then set to 0 in order to cancel this effect.

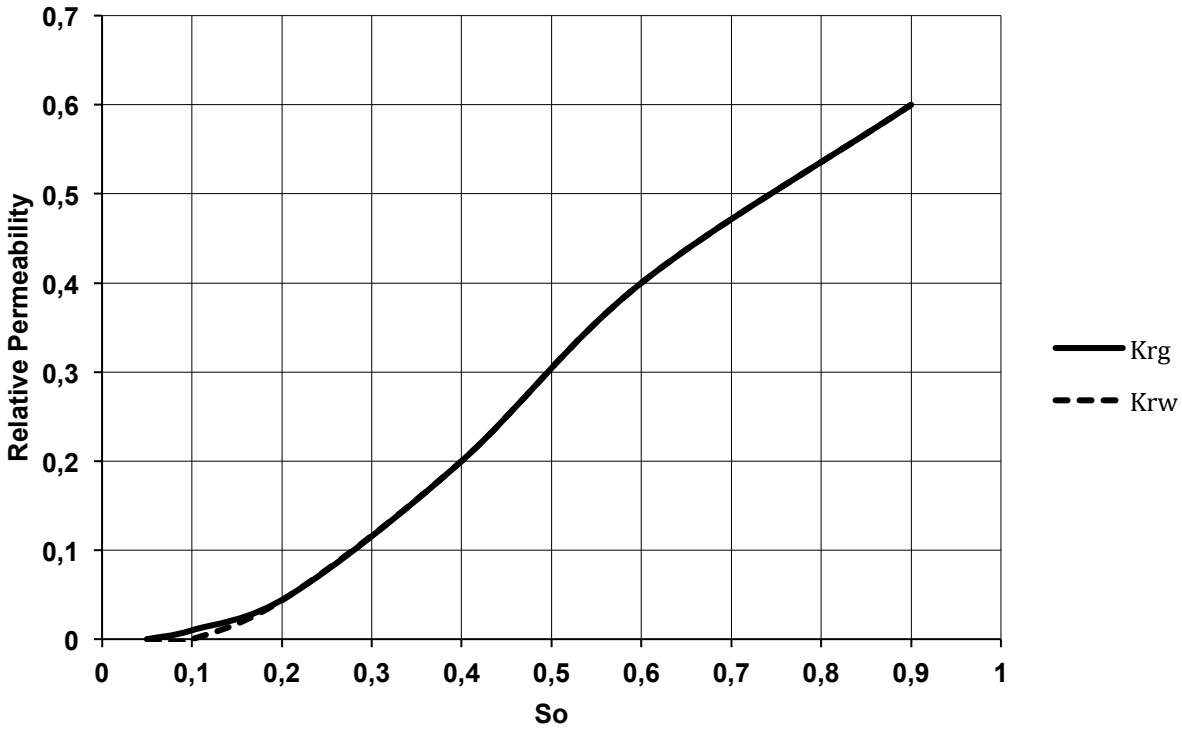

Figure 4 Water and Gas permeabilities versus oil saturation

The SOLUTION section states the initial state of the solution variables, they also remain unchanged in the various simulation file and are listed in the table below. Obviously the simulation had to take place in the oil zone between the gas-oil contact and water-oil contact depths, therefore the block size has to be chosen carefully.

Table 4 SOLUTION section properties

Initial pressure in the model	4800 psia
Gas-Oil contact depth	8440 feet
Water-Oil contact depth	8200 feet
Initial Gas saturation	0
Initial Water Saturation	0

In the SUMMARY Section all the injection and production rates are recorded, together with the saturation in a single block for plotting fractional flow curves. The configuration of the wells, defined in the last section and represented in the scheme, was not significantly modified. It always comprises a water injector simulating an aquifer on the left, a CO_2 injector in the middle and two producing wells on the right. The wells are controlled by Bottom Hole Pressure (BHP), so that the rates are constant. In this section the no-resoluton option DRSDT was set to 0, it has also been necessary to tune the parameters to increase the number of Newtonian interations to run the simulation faster.

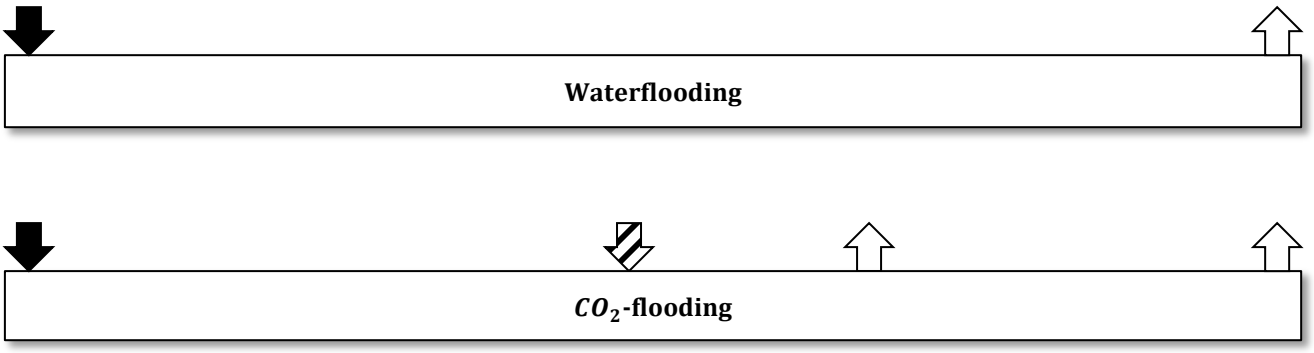

Figure 5 Schematic of the well configuration

2.1.2. Eclipse 300

The E300 simulation file is in appendix 3, in this version the same grid has been chosen with the same fluid properties. However the keywords may not be similar and a compositional model is chosen.It means that we now consider the components of the oil :C1,C2,C3,C4,C5,C6,C7+. The file does not include an oil phase since it can be defined once practical data are given about the field. Consequently this simulation models contains water and CO_2, taking in account the solubility of the gas in the aquifer. In the RUNSPEC section the CO2SOL option illustrate this possibility, also in this file the data is given in METRIC units[4].

Regarding the computation method, it uses the full implicit method, and for the Equation of State the Peng-Robinson method. The COMPS keyword shows that we only have one component which is CO_2. CO_2 properties are indicated in the PROPS section in a different way than the other version since the critical values are implemented in the model.

2.2. One-dimensional simulation

In order to quantify the influence of the aquifer strength on water, oil and CO_2 rate, a one-dimensional model was first built. In this simple case a theoretical relationship can be established between the rates and the pressure.

2.2.1. Theoretical approach

1. We can write the partial differential flow equation in a simple case:

$$\frac{\partial^2 P}{\partial x^2} = \left(\frac{\Phi \mu c}{k}\right) \frac{\partial P}{\partial t} \qquad (2.2.1\text{-}1)$$

[4] Main units : m^3/day for rates, pressure in bars.

The derivation of this equation includes the following assumptions:

- One-dimensional flow
- Linear flow
- Horizontal flow
- One phase flow
- Darcy's equation applicable
- Small fluid compressibility
- Permeability and viscosity are constant

Some of the assumptions are questionnable, for instance there is a gas phase in the simulation that has a high compressibility and this is a three-phase flow. The other assumptions are reasonable; however there may be some discrepancies due to the presence of three phases. In the configuration shown in Figure 5 the pressure profile will fit the one in Figure 6 : the dotted line is the pressure profile during the CO_2-flood and the plain line at the end of the waterflood.

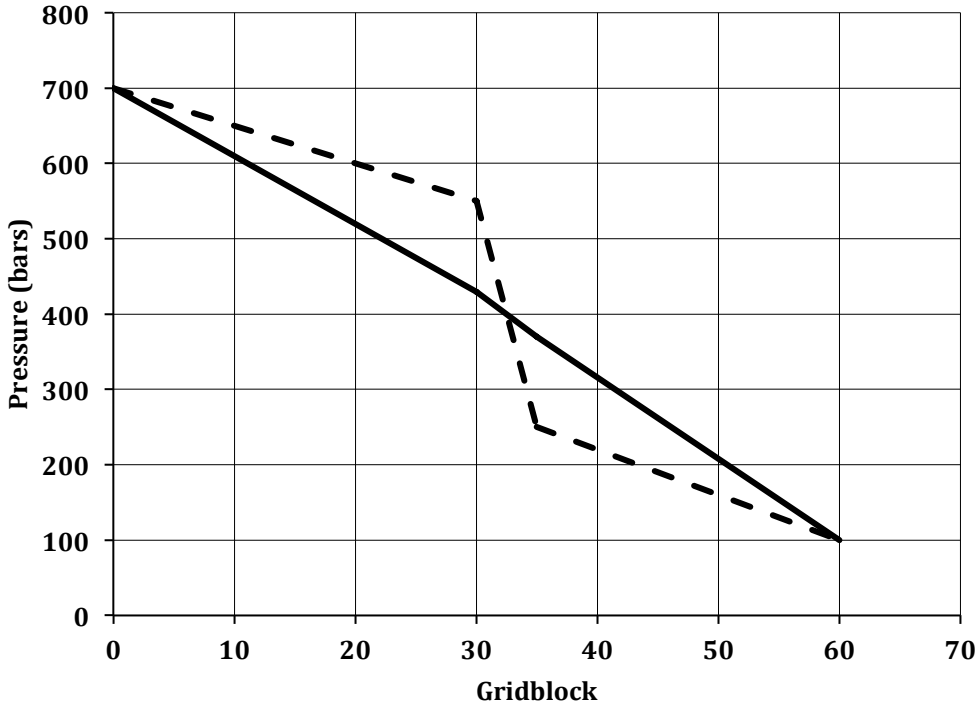

Figure 6 Pressure profile for Pl=700 bars Pr=100 bars Pj=650 bars Pi=250 bars

This graph is predicted by the steady-state condition for equation (2.2.1-1) :

$$\frac{\partial^2 P}{\partial x^2} = 0 \tag{2.2.1-2}$$

Solving equation (2.2.1-2) with dirichlet conditions gives:

$$P = \frac{(P_r - P_l)}{d} x + P_l \tag{2.2.1-3}$$

Then if we use Neumann's conditions using Darcy's law for a zone i between two pressures:

$$q_i = \left(\frac{KA}{\mu}\right)\left(\frac{\partial P}{\partial x}\right)_i \tag{2.2.1-4}$$

It leads to the following rate equations:

$$q_i = \left(\frac{KA}{\mu}\right)\frac{(P_{li} - P_{ri})}{d_i} \tag{2.2.1-5}$$

This expression implies that the rate is higher in the middle zone since the gap between the two pressures is maximum. The flow rate for the injector and producer can be computed using equation (2.2.1-5) for each zone. Then the injection rate is:

$$q_j = q_2 - q_1 = \left(\frac{KA}{\mu}\right)\left(\frac{(P_j - P_i)}{d_2} - \frac{(P_l - P_j)}{d_1}\right) \tag{2.2.1-6}$$

$$q_i = q_3 - q_2 = \left(\frac{KA}{\mu}\right)\left(\frac{(P_j - P_i)}{d_2} - \frac{(P_i - P_r)}{d_3}\right) \tag{2.2.1-7}$$

The different rates can be computed with equation (2.2.1-5), (2.2.1-6) and (2.2.1-7), they only depend on the pressure thus they are constant during the simulation. The plotted rates using Eclipse Office are in appendix 4.

2.2.2. Results on Eclipse 100

The aim of the simulation is to show the impact of the aquifer strength on the CO_2 rate and the oil recovery. In this matter a first simulation file using Eclipse 100 was built with 60 gridblocks on a distance of approximately 6000 feet. The water injector is in block 1, the CO_2 injector in block 30, the producers in blocks 35 and 60. Figure 7 shows the pressure profile following the waterflood, as the theoretical graph the pressure is linearly decreasing along the model from the injector to the producer.

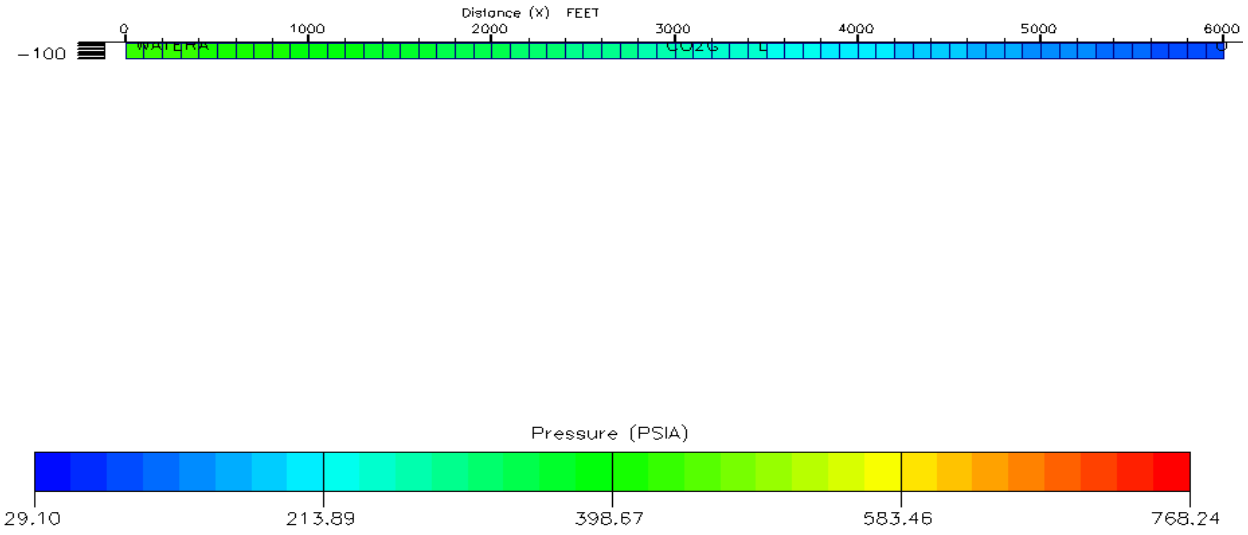

Figure 7 Top view of the gridblocks with the pressure gradient after the waterflood

A first simulation result is shown in Figure 8, it does not fit to the theoretical profile for several reasons. Firstable the injector is rate-controlled so the left pressure is decreasing during the CO_2-flood as the injection rate is constant. Then the point pressure in block 30 and 35 which are supposed to be exactly the value set in the simulation file, are fluctuating. Finally some simulations gave inconsistent results, for example pressures below the waterflood pressure profile.

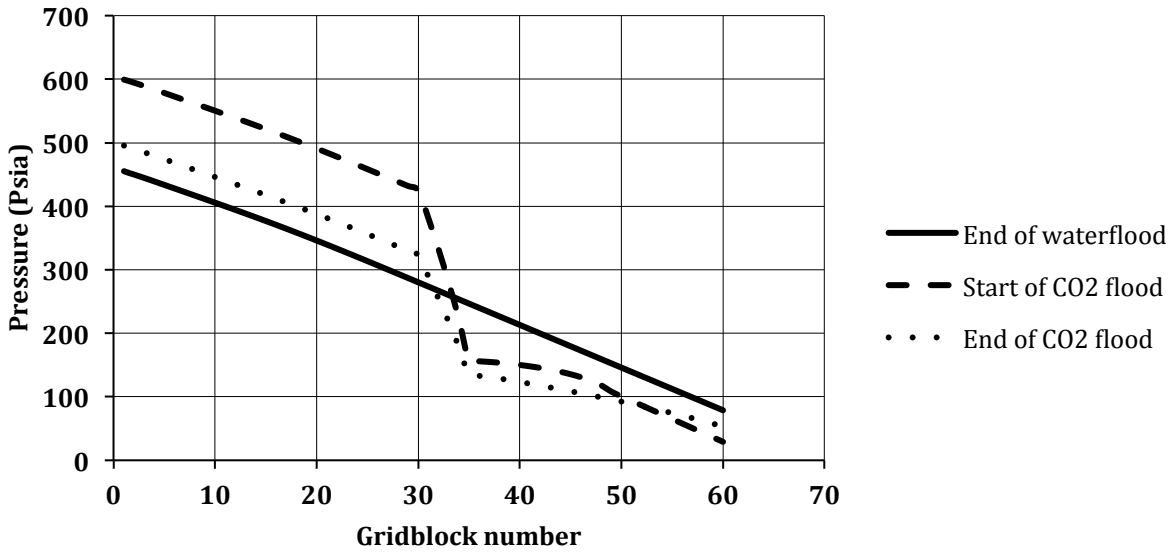

Figure 8 First simulation with a rate constrain on the injector

The solution to this problem is first to set the water injector as rate-controlled, the aquifer strength is then the water injected during the CO_2-flood. Then the gridblock size has been changed since the pressure is taken as an average of the block, this average pressure does not correspond to the Bottom Hole Pressure except if the block is small. The graph below shows the pressure profile at the end of the waterflood and the type of Grid used for the simulation. Figure 9 illustrates this effect with two different block sizes in eclipse E300, with small blocks the pressure reaches the right values (324 and 316 bars).

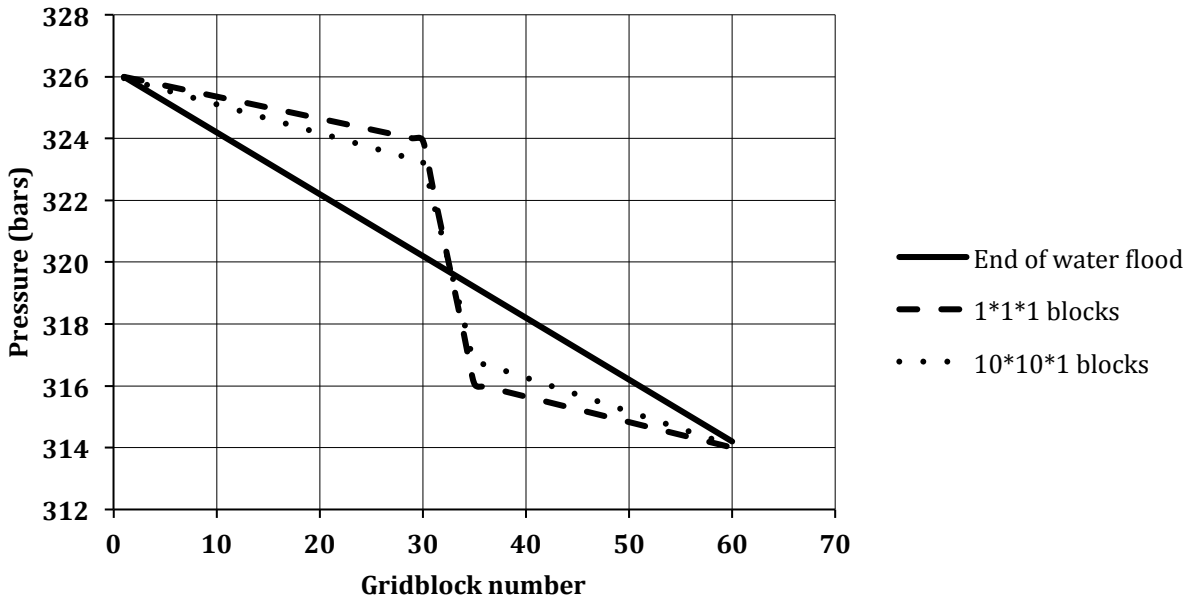

Figure 9 Pressure profile at the end of the waterflood, showing the type of Grid used for the simulation

Once the gridblock size is decreased a first set of simulation files were run using Eclipse 100, with the following pressure profiles. Outside of this range the injecting or producing well was shut due to over or under pressure.

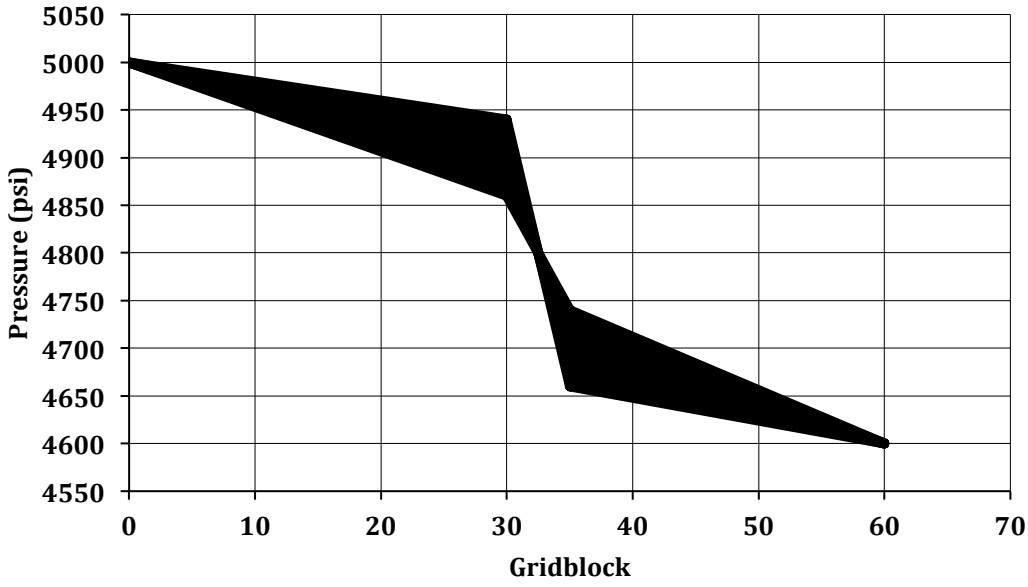

Figure 10 Simulated pressure profiles

It seems logical that the higher the water rate will be, the more CO_2 will be pushed towards the second producer in block 60. Gas rates in both producers were plotted in Figure 11, showing an increasing or decreasing trend as the water rate increases.

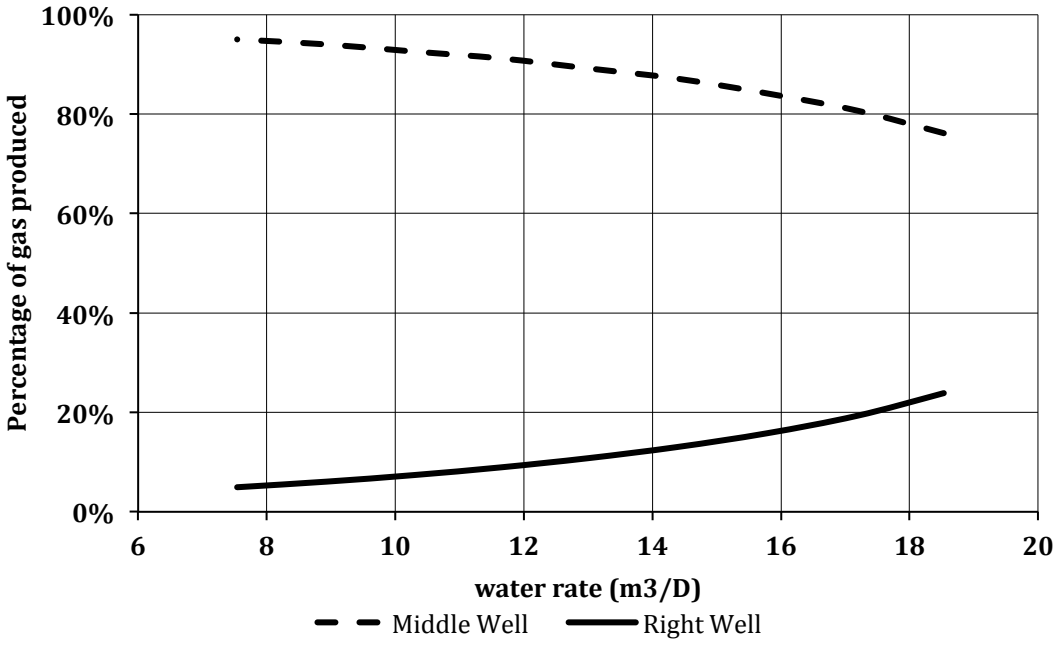

Figure 11 Percentage of gas produced in both wells versus water rate

Both curve follow an exponential trend with a really good fit (R=0,998)

$$\frac{CO2\ production\ in\ right\ well}{Total\ CO2\ production} = 0.0171 * e^{0.141 * water\ rate} \quad (2.2.2\text{-}1)$$

$$\frac{CO2\ production\ in\ middle\ well}{Total\ CO2\ production} = 1 - 0.0171 * e^{0.141 * water\ rate} \quad (2.2.2\text{-}2)$$

The gas rates are also of interest since the gas rate in the middle well is a straight line, in this case :

$$Gas\ rate\ middle\ well = -37{,}247 * Water\ rate\ +\ 761{,}32 \quad (2.2.2\text{-}3)$$

The gas rate in the right well has a parabolic trend with a maximum at a water rate of 14 STB/D. However the main factor affecting the gas ratio is the decrease of the gas rate in the middle. This parabolic trend is also found using Eclipse 300 and will be explained later in this chapter.

Regarding the oil, a significant increase is observed at the beginning of the CO_2 injection because the oil saturation will change from 20% to 5% in the region swept. However the share of incremental production in the middle well decreases with increasing water rate, in fact it decreases from 20% to 16% of the total cumulative oil production during the CO_2-flood as shown in Figure 12 .

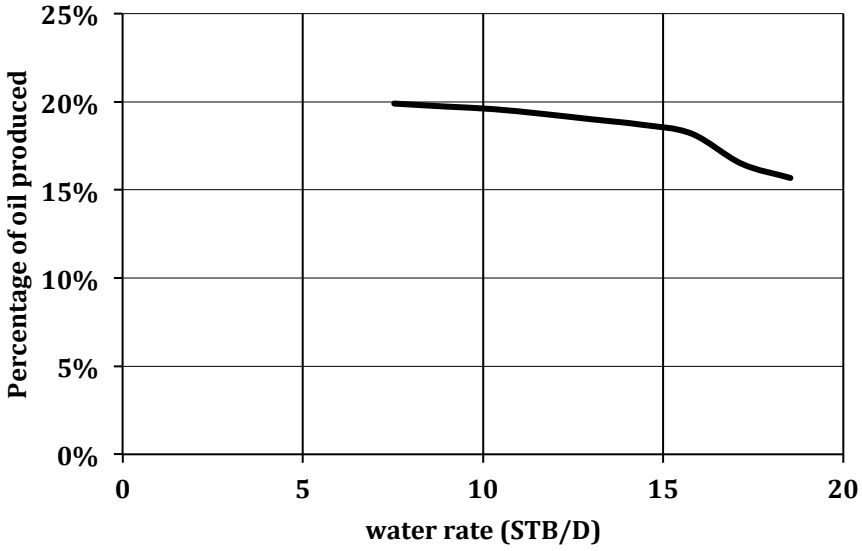

Figure 12 Percentage of oil produced in middle well from Total production

The first reason for the decreasing production is the smaller swept area, then less oil is displaced, this effect will be better described in another part. In fact this is not the main factor here since it is only a 1D simulation, but this effect will occur in the 2D simulation. The second reason is that the stream of water is stronger and will push more oil away from the well in the middle. Table 5 sums up the rate change for oil water and CO_2 during the CO_2-flood and all the rates are plotted in appendix 5.

Table 5 Evolution of the rates with increasing water rate during the CO_2-flood in both wells

	Well in the middle	**Well on the right**
Water rate	Increases	Increases
Gas rate	Decreases	Increases
Oil rate	Decreases	Reaches a maximum

Another parameter was defined in order to establish relationships between the rates, the dimensionless pressure. All simulations were run using different injecting and producing pressure P_i and P_j, whereas the overall pressure gradient used for the waterflood P_l -P_r remained constant. It is then natural to define a parameter as the ratio of those two values, going from 0 to 1.

$$P_{dim} = \frac{P_j - P_i}{P_l - P_r} \quad (2.2.2\text{-}4)$$

The rates are linearly dependent on the pressure drop, as defined in equations (2.2.1-6) and (2.2.1-7), it is verified in the following graphs showing water and CO_2 injecting rates versus dimensionless pressure.

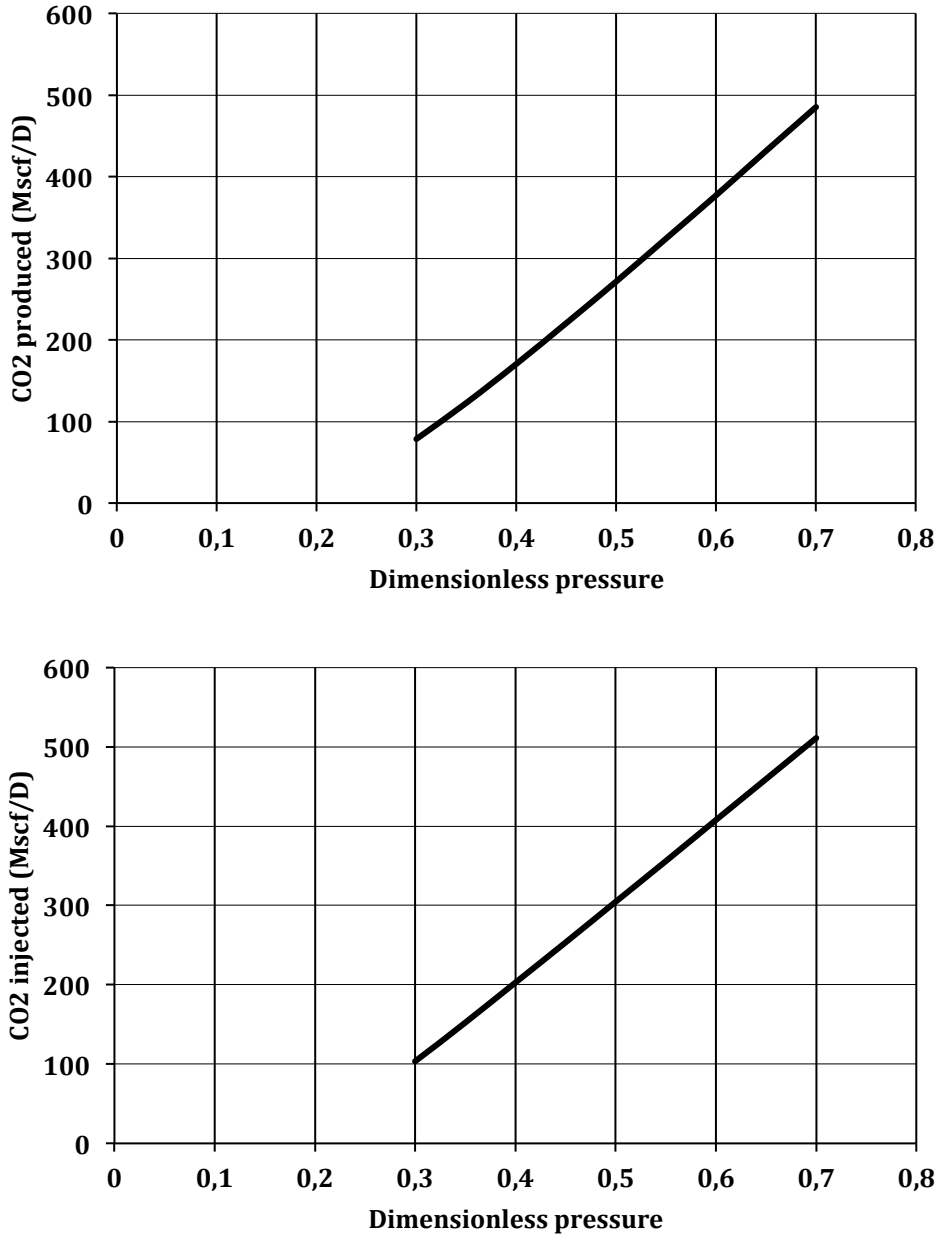

Figure 13 CO_2 production and injection versus dimensionless pressure

Noticing that the simulations have been made with symmetric pressure drops, we have:

$$P_l - P_j = P_i - P_r \tag{2.2.2-5}$$

We can simplify equations (2.2.1-6) and (2.2.1-7) :

$$q_j = \left(\frac{KA}{2\mu}\right)\left(P_{dim}\,(P_l - P_r)\left(\frac{2}{d_2} + \frac{1}{d_1}\right) - \frac{(P_l - P_r)}{d_1}\right)(10) \tag{2.2.2-6}$$

$$q_i = \left(\frac{KA}{2\mu}\right)\left(P_{dim}\,(P_l - P_r)\left(\frac{1}{d_3} + \frac{2}{d_2}\right) - \frac{(P_l - P_r)}{d_3}\right)\,(11) \tag{2.2.2-7}$$

It is then possible to compute the slope and Y-intercept from equation (2.2.2-6) and check with the trend suggested by Excel that for the CO_2 injection:

$$(P_l - P_r)\left(\frac{KA}{2\mu}\right)\left(\frac{2}{d_2} + \frac{1}{d_1}\right) = 1021{,}7\ Mscf/D$$

And

$$(P_l - P_r)\left(\frac{KA}{2\mu}\right)\left(\frac{1}{d_1}\right) = 205{,}3\ Mscf/D$$

The slope and Y-intercept for the CO_2 production in the middle well is found thanks to equation (11), we check that:

$$(P_l - P_r)\left(\frac{KA}{2\mu}\right)\left(\frac{2}{d_2} + \frac{1}{d_3}\right) = 1023{,}9\ m3/D$$

And

$$(P_l - P_r)\left(\frac{KA}{2\mu}\right)\left(\frac{1}{d_3}\right) = 236{,}02\ m3/D$$

According to this first part, we can conclude that the equations derived in 2.2.1 are verified so far with the Eclipse 100 simulation files. Some delay is observed to reach a stable flow rate, in the order of 1 or 2 days as show in the appendix 4. However the discrepancies concerning the pressure or thre rates disappear with larger time-steps and/or bigger grid.

2.2.3. Results of the compositional Simulation with Eclipse 300

Even though the oil is not present in this simulation, the behavior of CO_2 and water can be analyzed in the compositional runs. A broader range of simulation could be run, which allows checking the trend observed with Eclipse 100. The pressure profiles implemented are plotted below, a large number of additional simulations have a really low dimensionless pressure because this area was of interest for the study.

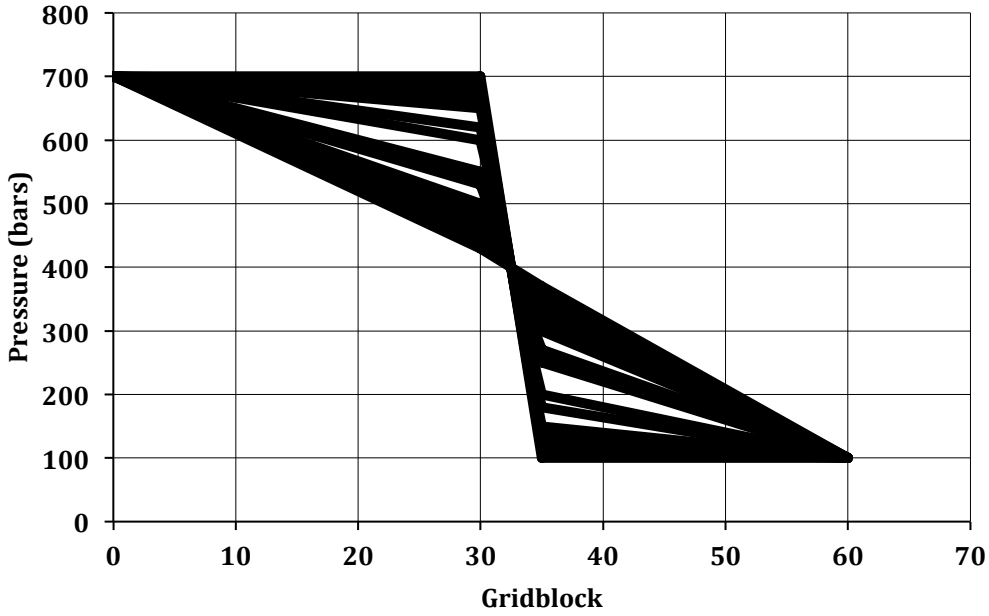

Figure 14 Pressure profiles simulated

The exact same trend was observed for the percentage of gas produced in both wells as shown in Figure 15. Despite the similarity, an interesting fact was observed for the gas produced at a low dimensionless pressure in Figure 16 Gas produced in right well and water produced in middle well versus dimensionless pressure, Eclipse 300., which was thought to be a parabole in the whole range.

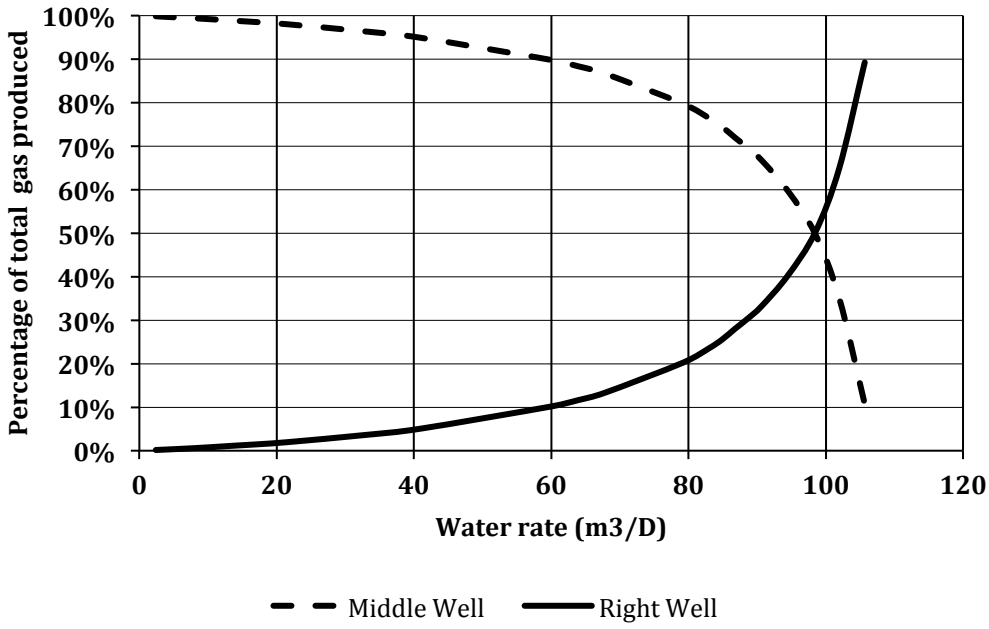

Figure 15 Percentage of gas produced in both wells, Eclipse 300

Once again the gas production in the right well reaches a peak for P_{dim} =0.45 corresponding to a water rate of 60 m^3/D which is the same value as the black-oil simulation. One assumption about this trend is the water effect on the CO_2 flow, indeed we observe in Figure 16 the same parabolic trend for the water flow for the well in the middle.

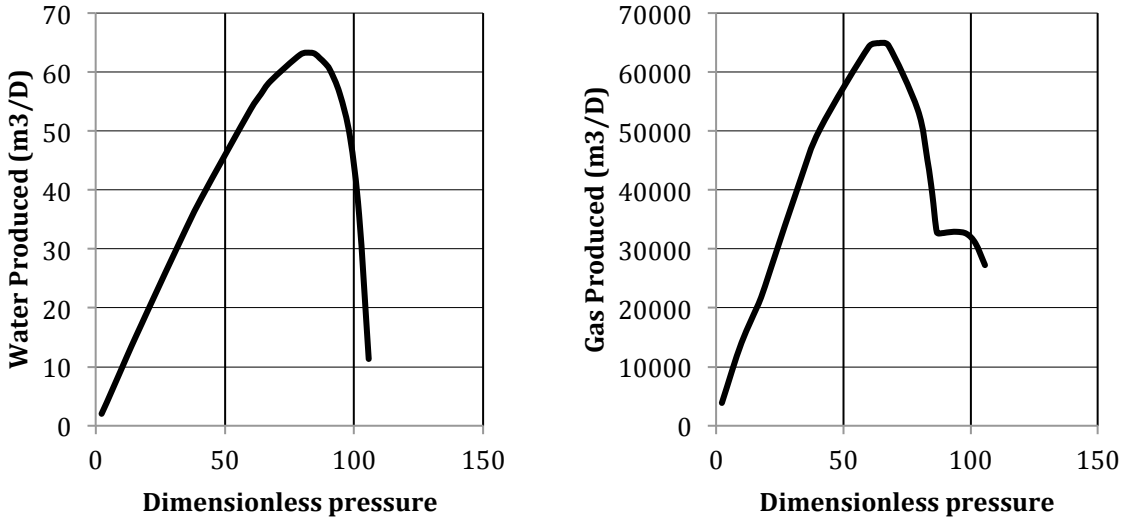

Figure 16 Gas produced in right well and water produced in middle well versus dimensionless pressure, Eclipse 300.

It seems that at a low water rate the gas and the water are immediatly produced by the first well (Figure 15 and Figure 17), then in a second time the increasing water rate pushes the water and the gas away. The gas production reaches a peak and the water stream becomes so strong that the middle well water production is decreasing. At high water rates the CO_2 plume narrows down around the middle well, due to the strong water flow on both sides. As a consequence the gas production in the well at the upper right declines.

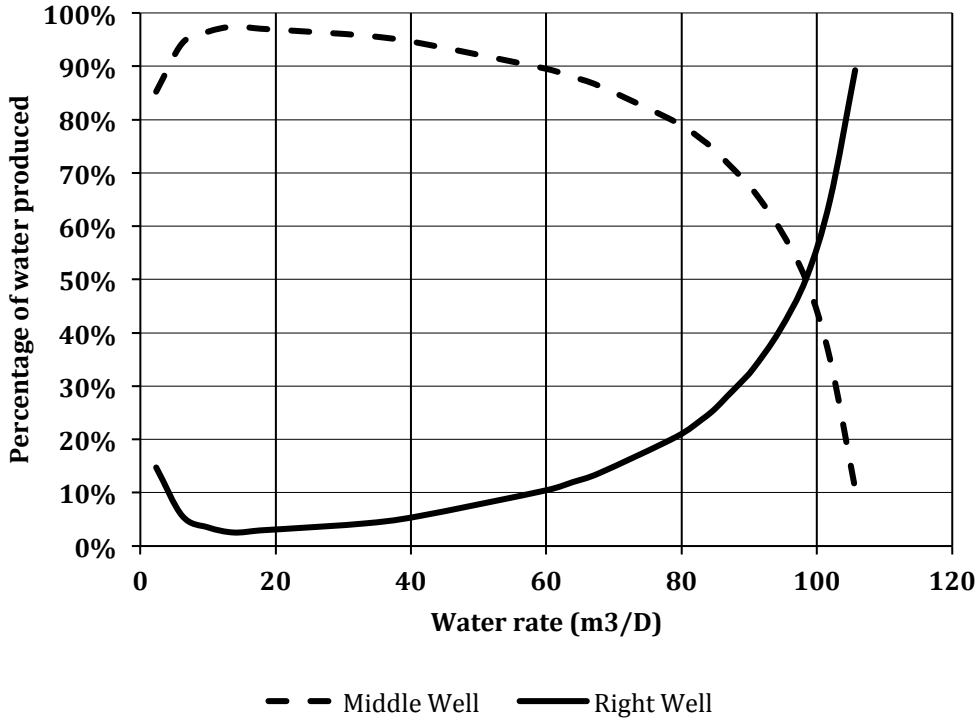

Figure 17 Percentage of water produced in both Wells, Elcipse 300

All the Gas and Water rates are in Appendix 6, the main trends are described in the following table.

Table 6 Evolution of the rates with increasing dimensionless pressure during CO_2-flood

	Well in the middle	**Well on the right**
Water Rate	Reaches a maximum	Decreases
Gas Rate	Increases	Reaches a maximum

2.3. Distance sensitivity

2.3.1. Model, parameters and results

Another parameter was introduced in order to measure the influence of the distance between the wells, the dimensionless distance, as shown in the schematic below. As the previous simulations, the gas and water rates were plotted against this dimensionless quantity in order to determine some trends. In this case the pressure gradient chosen is: P_l=P_j=700 bars and P_i=P_r=100 bars.

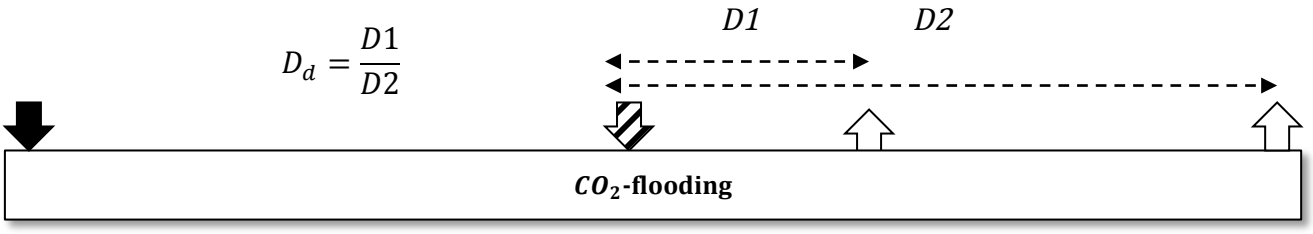

Figure 18 Schematic showing the dimensionless distance

The water rate in the well on the right is found to be constant versus the dimensionless distance, whereas the other rates are plotted in Figure 19 through Figure 21.

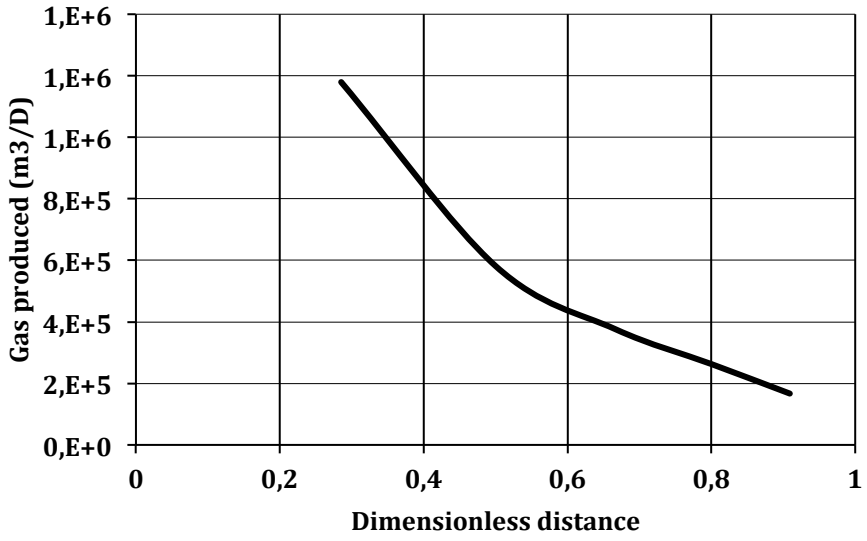

Figure 19 Gas produced in middle Well versus dimensionless distance

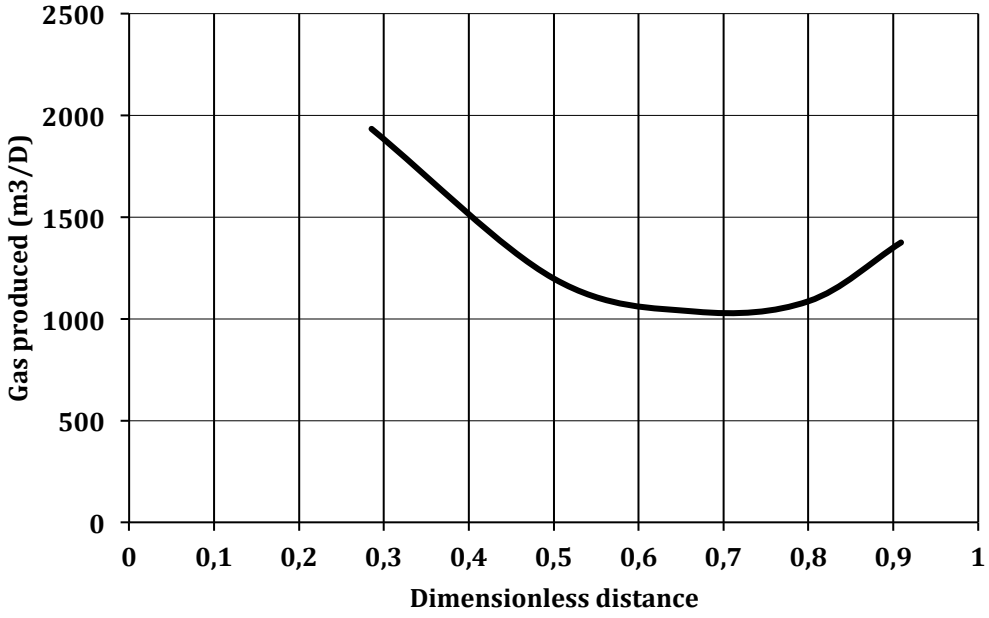

Figure 20 Gas produced in right well versus dimensionless distance

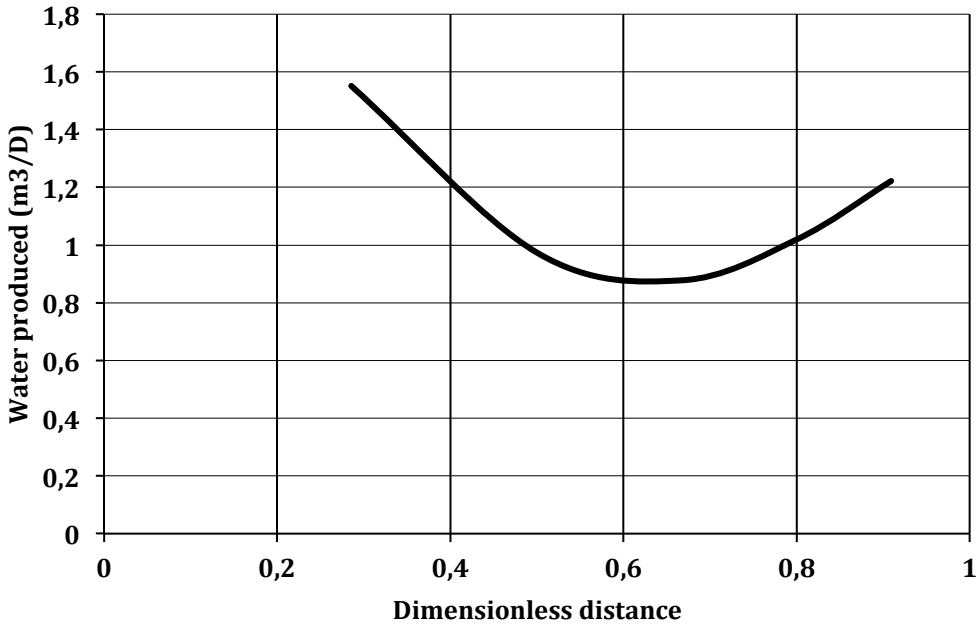

Figure 21 Water produced in the middle well

2.3.2. Observations and conclusion

As for the dimensionless pressure plot, the gas produced in right well and the water in middle well reach a extremum which is a minimum in this case. For D_d=0,65 we have low water produced in the first well and low gas produced in the right well, this is an interesting situation because this configuration prevent the gas from coning towards the second well, maximizing the production in the middle even though it keeps on decreasing. For this pressure drop the quantity of gas produced is negligible in the second well, however as mentioned in the previous part the gas share in this well will increase with the pressure, reaching a maximum for a given pressure.

As a conclusion of this part, to maximize the gas produced in the well on the right, the dimensionless pressure has to be as high as possible which corresponds to a strong aquifer. Then for this pressure gradient a very low or very high dimensionless pressure can be chosen, depending on the reservoir characteristics.

Secondly to maximize the CO_2 production in the well in the middle, the dimensionless pressure has to be low, that is to say the injecting pressure will be close to the pressure of the reservoir. This configuration will prevent the gas from being blown away since it will set a low water rate. Preferably the dimensionless distance will be chosen low, even though the gas production in the other well reaches a minimum. The reason for that is the small share of the gas produced in the second well compared to the first one.

2.4. Several producers and injectors patterns

The one-dimensional simulation stays close to the theory, that's why several simulations were run to verify the equations derived with several small blocks (1meter) aligned. In reality there are several wells injecting and producing gas, water and oil. In this matter this part will show some results obtained by creating a pattern of wells to illustrate a 2D case closer to reality. Figure 22 shows the pressure gradient after the waterflood for this 2D case. A first row of water injectors is simulating an aquifer, then three rows of CO_2 injectors are ready for the CO_2-flooding and finally two rows of producers in between the CO_2 injector and one row of producers at the upper right.

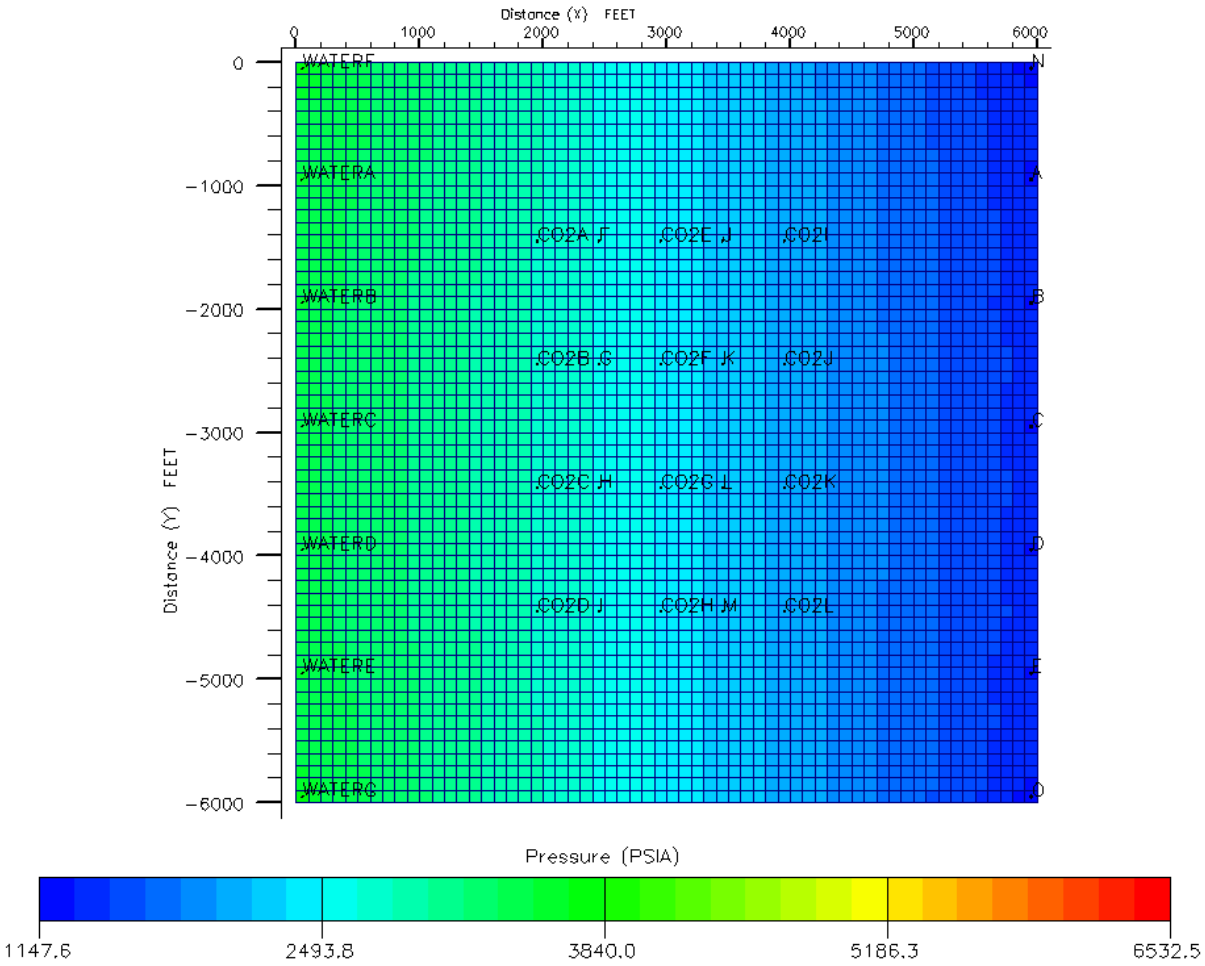

Figure 22 Pressure gradient across the model after waterflood

The pressure gradient across the model is decreasing, around 1psi/foot as a rule of thumb. In this model the water injector and the CO_2 injector are rate-controlled, and the producers BHP-controlled. Figure 23 was obtained using Eclipse 100 with the parameters indicated in Table 7.

Table 7 Rate and pressure inputs

Water injecting Rate	22 STB/D
CO_2 injecting rate	200 Mscf/D
Pressure in all producing wells	1000 psia

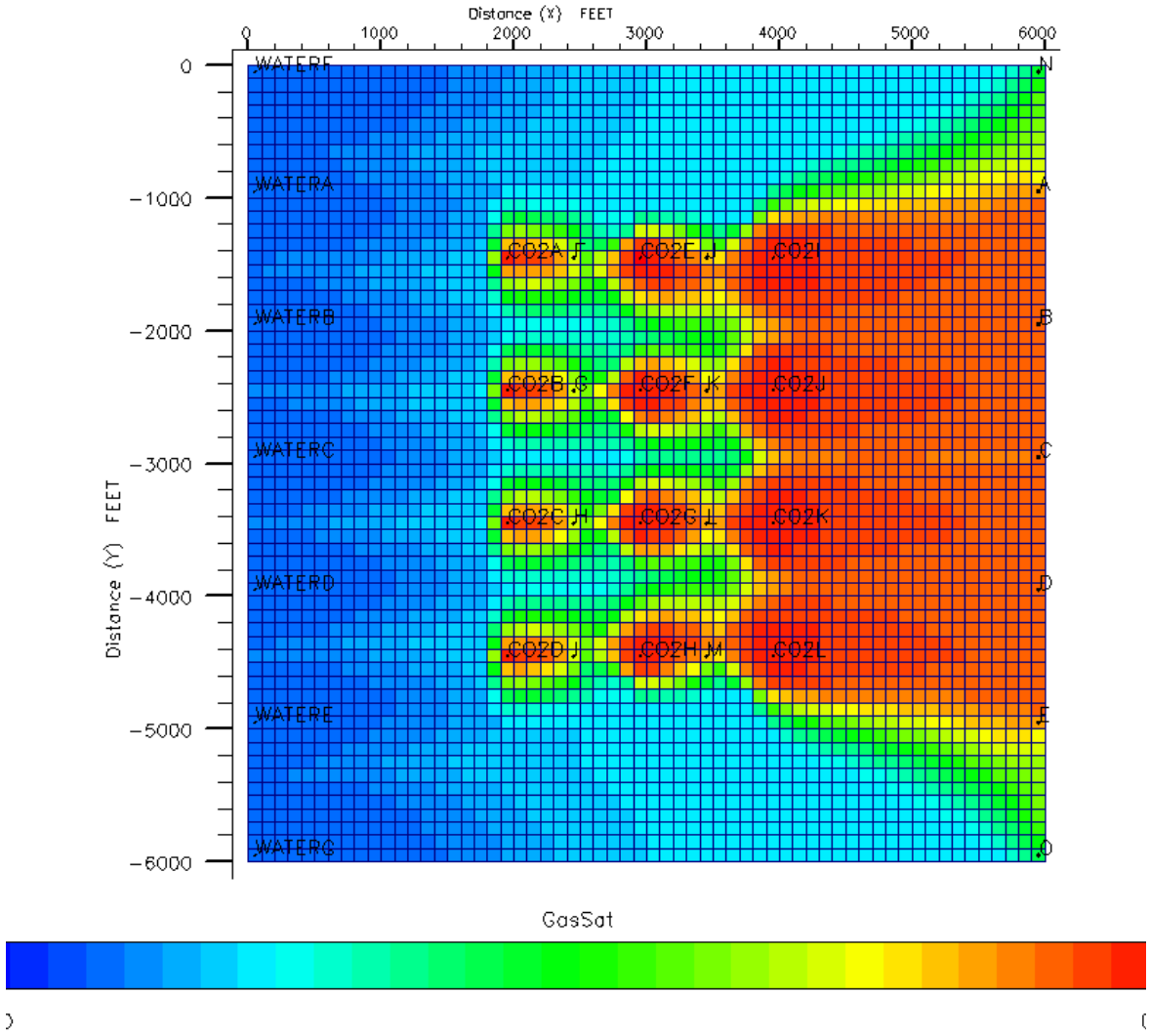

Figure 23 Example of CO_2 saturation pattern with multiple wells using Eclipse 100

This second example shows the CO_2 saturation profile for one CO_2 injector and one gas producer. The pressures can be tuned in order to have greater production in one of the wells; in the example they have been switched from 14 and 1000 psi on the left to 1000 and 14 psi on the right. In the example Figure 24, on the right much more gas is coning towards the right since the pressure in the middle is not low enough to produce all of the CO_2. The two pictures have been taken at the same time, with the same pore volume of gas and water injected.

Table 8 Rates and pressure inputs

	Left	**Right**
Water injection rate	200 STB/D	
CO_2 injection rate	1000 Mscf/D	
Pressure in the center	14 psia	1000 psia
Pressure on the right	1000 psia	14 psia

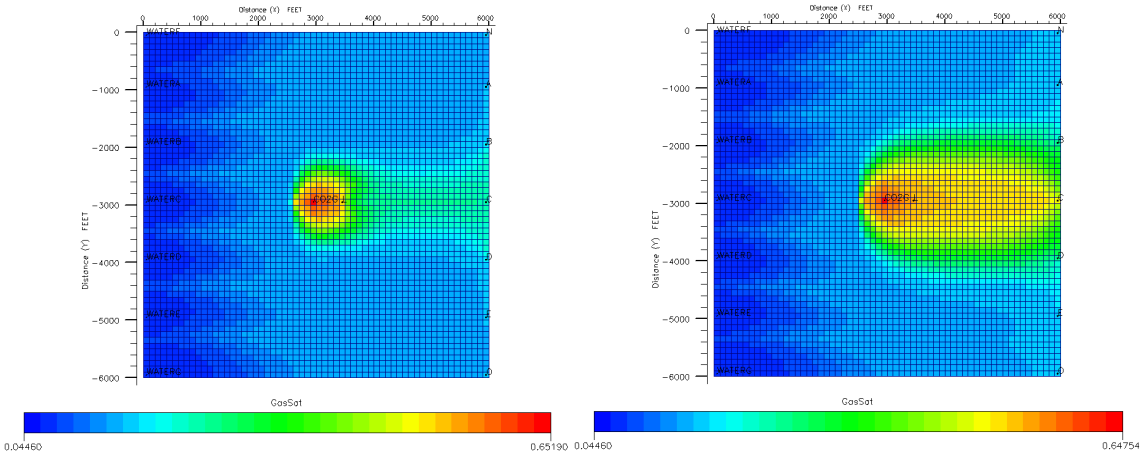

Figure 24 CO_2 saturation patterns for one injector and one producer

The same example has been taken with Eclipse 300 with different rates and pressures. In this example the well on the right is clearly not producing CO_2 in one configuration whereas the CO_2 is pushed away in the second case. The contrast in saturations is much higher with eclipse 300 due to the absence of oil, that's why it will be chosen later to compute the area of the CO_2 plume. In this example the pressure on the right is unchanged, unlike the pressure in the middle which is 50 and 70 bars on the left and right figure respectively.

Table 9 Rates and pressure inputs

	Left	**Right**
Water injection rate	23 m^3/D	
CO_2 injection rate	20000 m^3/D	
Pressure in the center	50 bars	70 bars
Pressure on the right	50 bars	50 bars

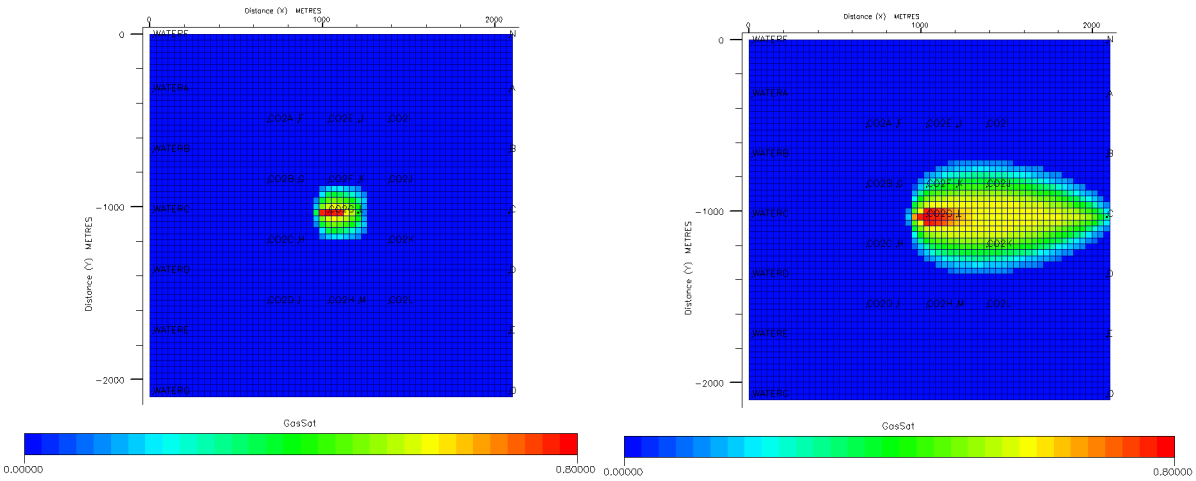

Figure 25 CO_2 saturation patterns, one injector and producer, Eclipse 300

3. Walsh diagrams

3.1. Theoretical approach and adaptation to the problem

3.1.1. Fractionnal flow equations

The Buckley-Leverett theory gives a mass conservation equation for a one-dimensional permeable medium for an isothermal flow (Lake, 1989):

$$\Phi \frac{\partial S_i}{\partial t} + u_i \frac{\partial f_i}{\partial x} = 0 \qquad (3.1.1\text{-}1)$$

The fractionnal flow of each fluid is defined as $f_i = \frac{u_i}{u}$, which can be obtained in Eclipse by recording the water, oil and gas rates for the producing well since the area is constant.
This equation can also be written in terms of dimensionless time and distance :

$$\frac{\partial S_1}{\partial t_D} + \frac{\partial f_1}{\partial S_1}\frac{\partial S_1}{\partial x_D} = 0 \qquad (3.1.1\text{-}2)$$

where $x_D = \frac{x}{L}$ and $t_D = \int_0^t \frac{u dt}{\Phi L} = \frac{Total\ amount\ of\ fluid\ injected}{Pore\ Volume}$

The solution to the new equation can be written as a total differential

$$dS_1 = \frac{\partial S_1}{\partial x_D} dx_D + \frac{\partial S_1}{\partial t_D} dt_D \qquad (3.1.1\text{-}3)$$

which can also be solved for $\frac{\partial x_D}{\partial t_D}$, the specific velocity of the saturation S_1

$$\left(\frac{\partial x_D}{\partial t_D}\right)_{S_1} = -\frac{(\partial S_1/\partial t_D)}{\partial S_1/\partial x_D} \qquad (3.1.1\text{-}4)$$

Replacing one of the derivatives by its expression in the equation gives

$$\left(\frac{\partial x_D}{\partial t_D}\right)_{S_1} = \frac{df_1}{dS_1} \tag{3.1.1-5}$$

Which gives a relationship between the dimensionless variables x_D and t_D.

Those equations allow to construct the Walsh diagrams which contains :

- $f_1 = f(S_1)$ based on the rates and saturation measured in the simulation.
- $f_1 = f(t_D)$ where $t_D$is computed as the ratio of the volume injected and the pore volume.
- $x_D = f(S_1)$ where x_D is computed as the product of the product of the derivative of the fractionnal flow and t_D, for a fixed t_D.
- $x_D = f(t_D)$ containing straight lines of constant saturation.

3.1.2. Scaling number

In this part a scaling number will be derived from the expression of the fluid velocities and the fractionnal flow, the following model is considered :

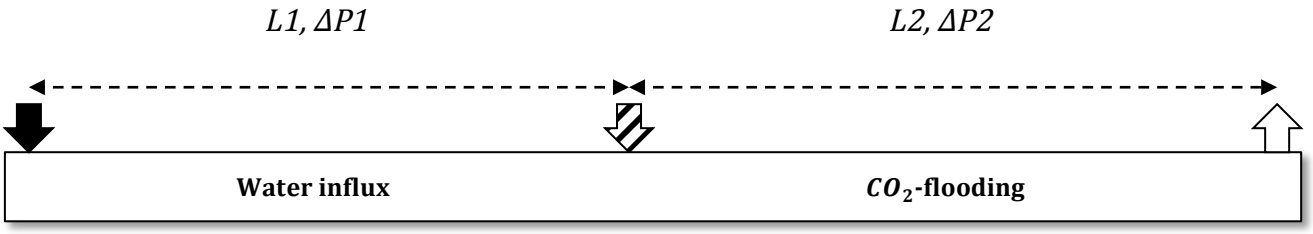

Figure 26 Schematic of the reservoir model for the fractionnal flow diagram

This CO_2-flooding occurs after a waterflooding, the residual oil saturation is 20% after the waterflood and is expected to decrease to 5% . On the upper right a water injector simulates the aquifer, a CO_2 injector and a producer are ensuring the displacement of oil by CO_2. Recall that we have the pressure profile respecting the partial differential equation as shown in Figure 27.

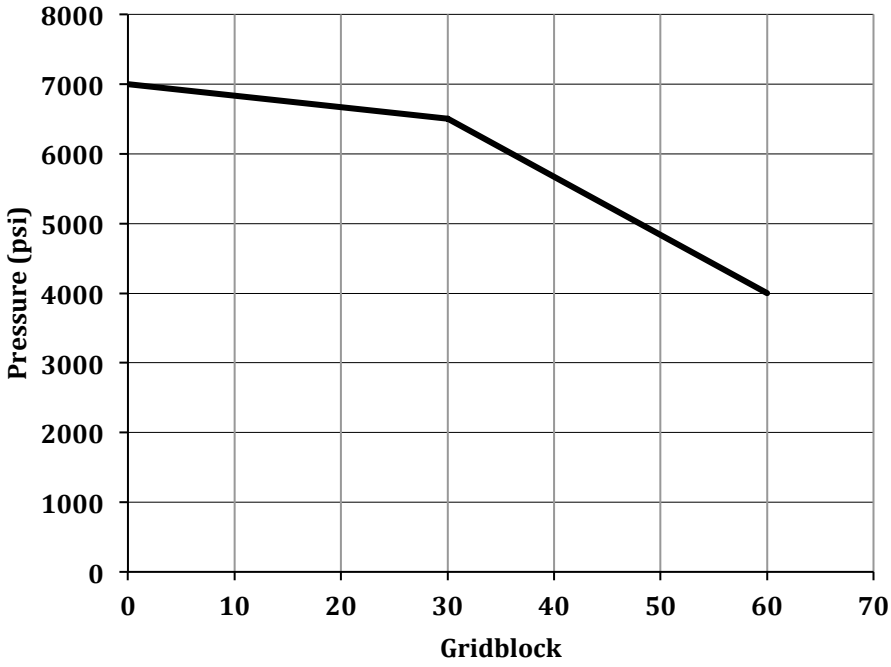

Figure 27 Pressure profile for Pl=7000,Pj=6500 and Pr=4000

The first slope is proportional to the water rate and will always be smaller than the second slope. The reason is that the CO_2 injection pressure cannot be smaller than the reservoir pressure after the waterflood.

The total velocity in the CO_2 injection part can be expressed as the sum of all the fluid velocities

$$u = u_1 + u_2 + u_3 \tag{3.1.2-1}$$

The water velocity can be expressed as the aquifer velocity plus the velocity in this region

$$u_1 = u_{aq} + \lambda_1 \frac{\partial P}{\partial x} \tag{3.1.2-2}$$

With

$$\lambda_i = \frac{K}{\mu_i} \tag{3.1.2-3}$$

if we inject the water velocity in the total velocity we obtain :

$$u = u_{aq} + \lambda_1 \frac{\partial P}{\partial x} + \lambda_2 \frac{\partial P}{\partial x} + \lambda_3 \frac{\partial P}{\partial x} \tag{3.1.2-4}$$

which gives an expression for the pressure gradient in the CO_2-flooding zone :

$$\frac{\partial P}{\partial x} = \frac{u - u_{aq}}{\lambda_1 + \lambda_2 + \lambda_3} \tag{3.1.2-5}$$

If we go back to the expression of the fractionnal flow for one component and we replace the velocity of the fluid we have :

$$f_j = \frac{\lambda_j \frac{\partial P}{\partial x}}{u} = \lambda_j \left(\frac{1 - \frac{u_{aq}}{u}}{\lambda_1 + \lambda_2 + \lambda_3} \right) = \frac{\lambda_j}{\sum_1^3 \lambda_j} \left(1 - \frac{u_{aq}}{u}\right) \tag{3.1.2-6}$$

The factor $\frac{u_{aq}}{u} = N_c$ can be used as a scaling number since the other parameter only depends on the fluids characteristics. N_c is proportionnal to the ratio of the the two slopes of the pressure profile. There are two extreme cases setting the boundaries of this number, a strong or a weak aquifer.

In case of a strong aquifer the slope in the water-only region would be high, however it cannot be higher than the other slope since the injector has to be able to flow. We thus have $N_c \to 1$ in case of a strong aquifer and as a consequence $f_j \to 0$. It makes sense since with a high water rate the fractionnal flow of water tends to 1 whereas the others tends to zero.
In case of a weak aquifer the slope of the water region would flatten and tend to zero. Since the velocity at the denominator is fixed, the factor $N_c \to 0$ and then $f_j \to \frac{\lambda_j}{\sum_1^3 \lambda_j}$.

Since $N_c \propto \frac{\Delta P_1 / L_1}{\Delta P_2 / L_2}$, several simuations can be designed by changing the pressure drop and the lengths to have a strong or a weak aquifer situation. To check this scaling number several runs were made for the same value of N_c using different pressure drops and lengths, from very low to very high water rate.

3.2. Walsh diagram construction

The following pages show the Walsh diagrams for the water, oil and gas for a low water rate. The dimensionless time selected for the gas was 0.2 which is after the gas breakthrough.

3.2.1. Gas diagrams

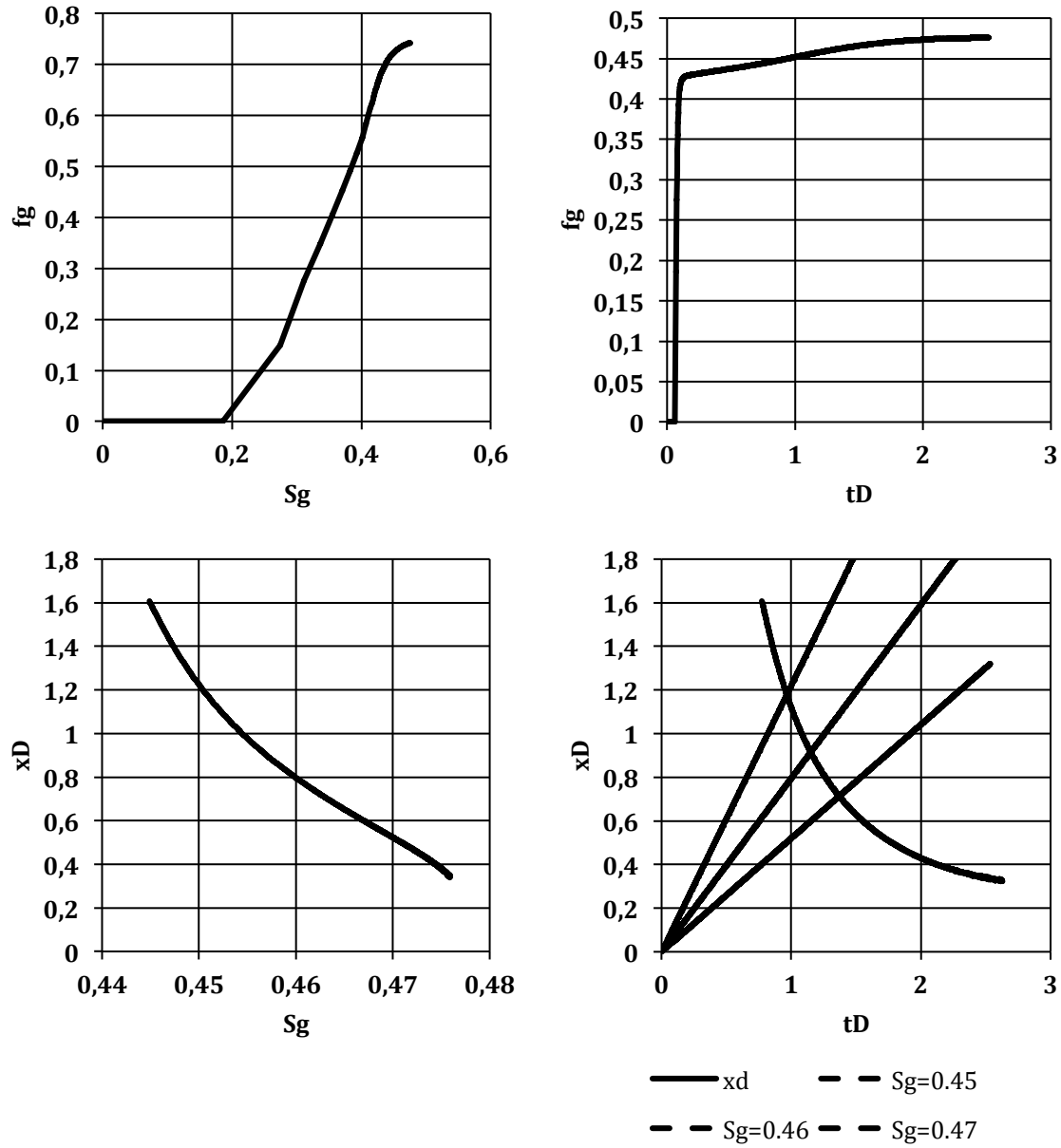

Figure 28 Walsh diagrams for the gas phase, low rate simulation with Eclipse 100

3.2.2. Oil diagrams

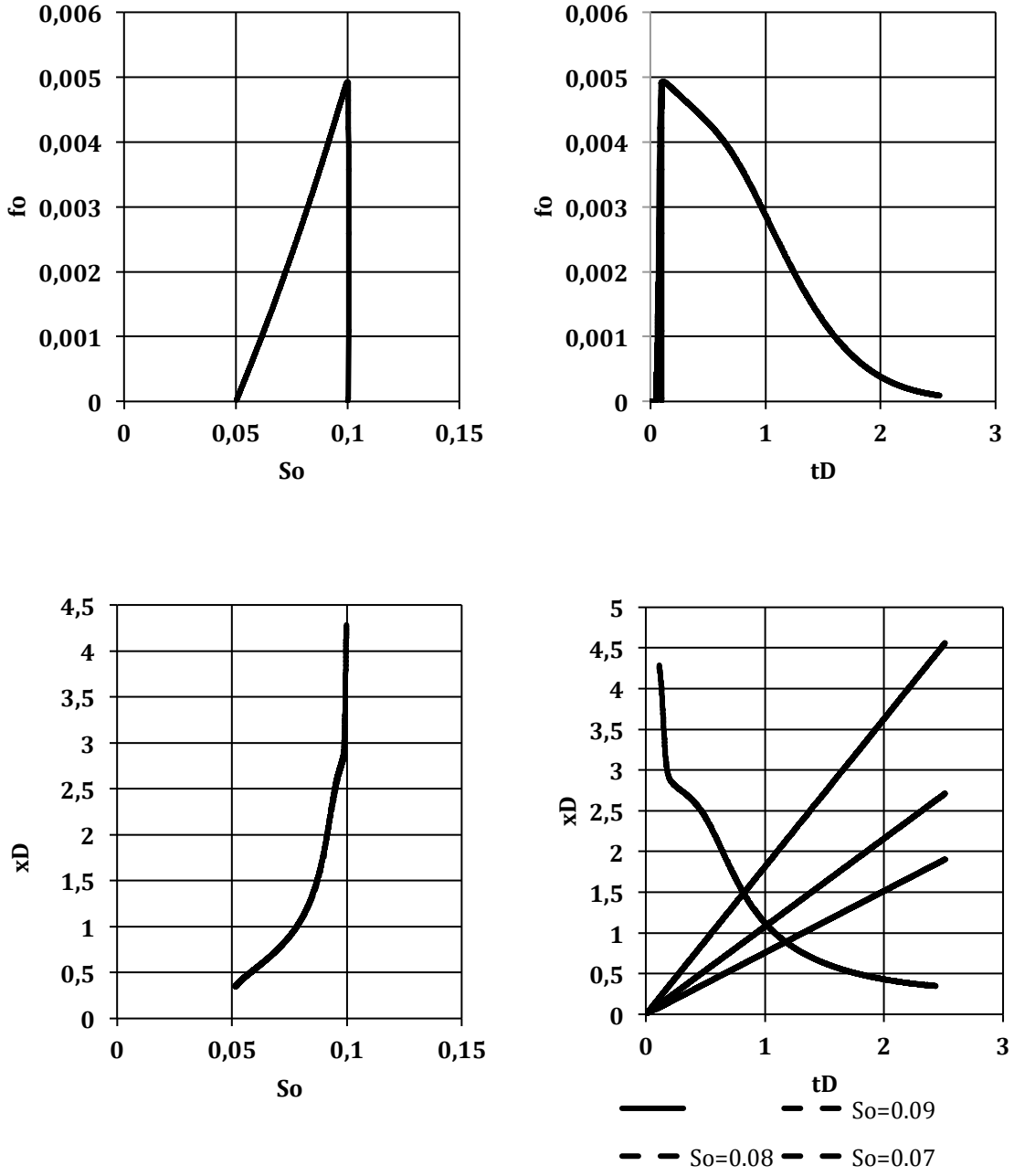

Figure 29 Walsh diagrams for the oil phase, low rate simulation with Eclipse 100

3.2.3. Water diagrams

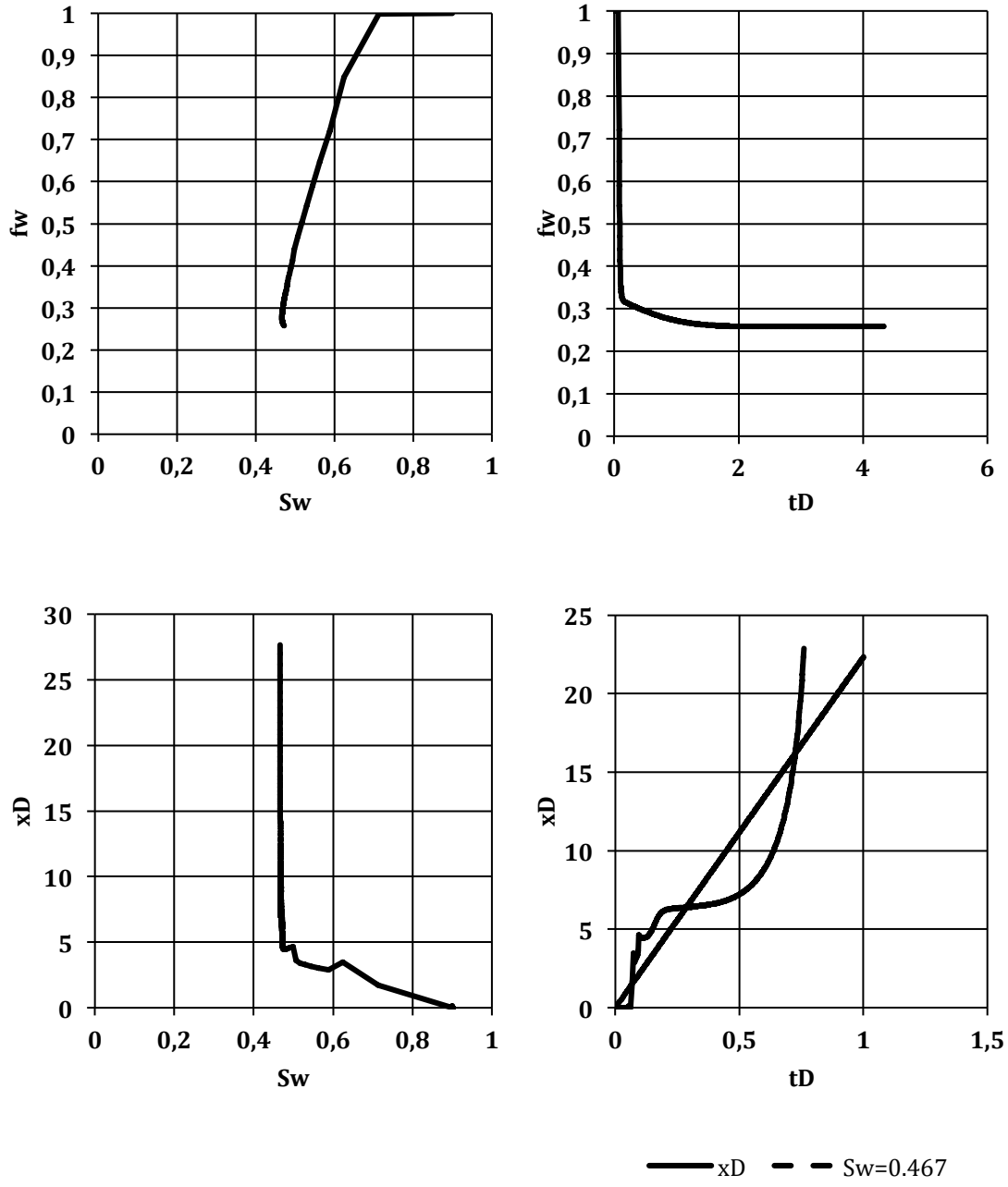

Figure 30 Walsh diagrams for the water phase, low rate simulation with Eclipse 100

3.2.4. Observations and conclusion

The gas diagrams present a very early breakthrough, the fractionnal flow curve reaches a rather high saturation of 50% since the water flow is low. The saturation in the front has a typical Buckley-Leverett shape, with a quick calculation in excel we find the saturation at the front to be 0.445[5]. Several constant gas-saturation lines were plotted in order to observe the different saturation regions.

The oil diagram is interesting since the oil saturation and rate are first increasing and then both decreasing, giving a curve going slightly onwards and then backwards. The increase in oil saturation is not visible here, however we clearly notice that the oil saturation is going from the waterflood residual saturation (10% in this simulation) to the CO_2-flood residual saturation (5%). Unlike the previous front for the gas, the oil front has an increasing saturation with increasing distance since it is pushed by the gas and water. The oil fractionnal flow is really low meaning that the quantity of water and gas are very large, it has to be discussed from an economic point of view when applied to real cases.

The water fractionnal flow curves shows a water saturation strongly declining from 1 to 0.3, and slightly increasing afterwards. The water is first swept by the gas in the region, the saturation increase happens after the CO_2-flood occured, the saturation increase is due to the water influx which slowly displaces CO_2 at the end. As for the gas, the fractionnal flow quickly changes and we see that the water front is pretty sharp. Since the water saturation goes way and back, some saturations are attained several times, it is the case of the saturation indicated by a straight line in the bottom left graph.

[5] We plot a straight line on the fractional flow curve going from zero and containing the inflexion point, the intersection with the maximum horizontal line gives the gas saturation at the front.

3.3. Validity of the scaling number

The goal of the following simulations is to verify the scaling number N_c , derived in the first part. Three cases have been tested, from a small N_c corresponding to a low water rate, to a high N_c for a high water rate. Even though the expression of the fractionnal flow suggest that the scaling number is only valid for gas, the plots have been made for all the fluids.

3.3.1. Low water rate

Table 10 Simulation cases for a low water rate

$\mathbf{P_l}(psi)$	$\mathbf{P_j}(psi)$	$\mathbf{P_r}(psi)$	$\mathbf{\Delta P_1}(psi)$	$\boldsymbol{L_1}(\mathbf{ft})$	$\mathbf{\Delta P_2}(\mathbf{psi})$	$\boldsymbol{L_2}(\mathbf{ft})$	$\mathbf{N_c}$
7000	6000	4000	1000	50	2000	10	0.1
6000	5500	3000	500	60	2500	30	0.1
7000	6500	4000	500	20	2500	10	0.1

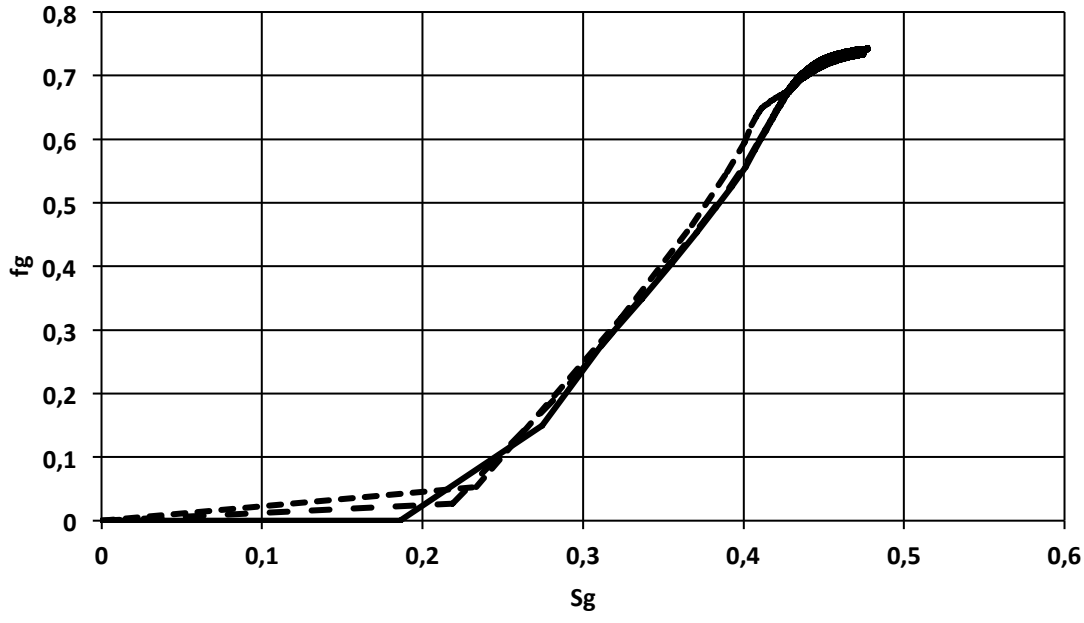

Figure 31 Gas fractionnal flow for a low water rate

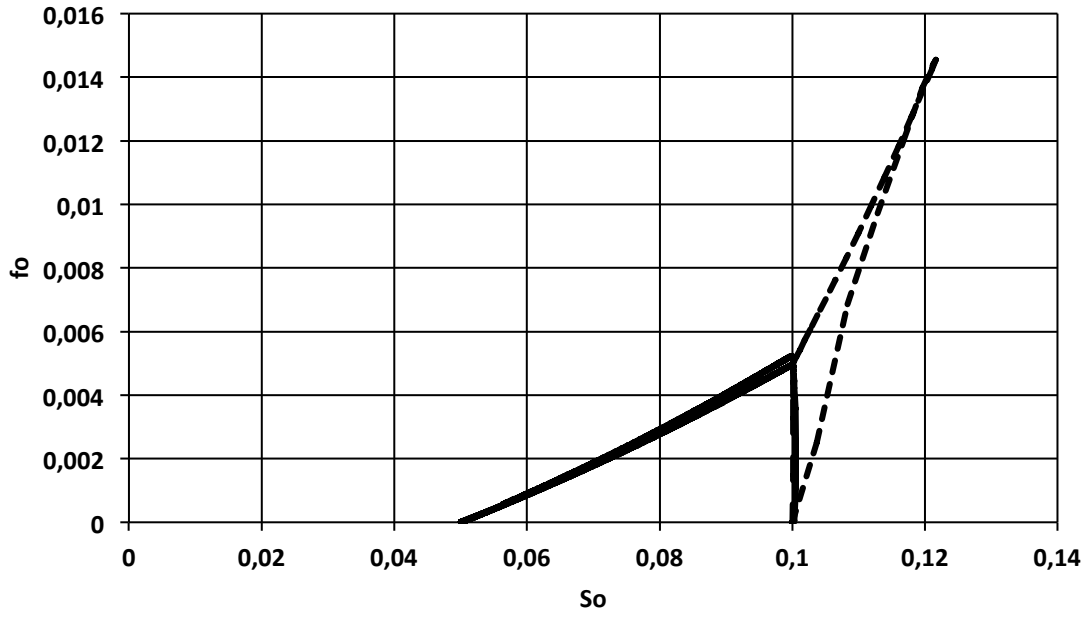

Figure 32 Oil fractionnal flow for a low water rate

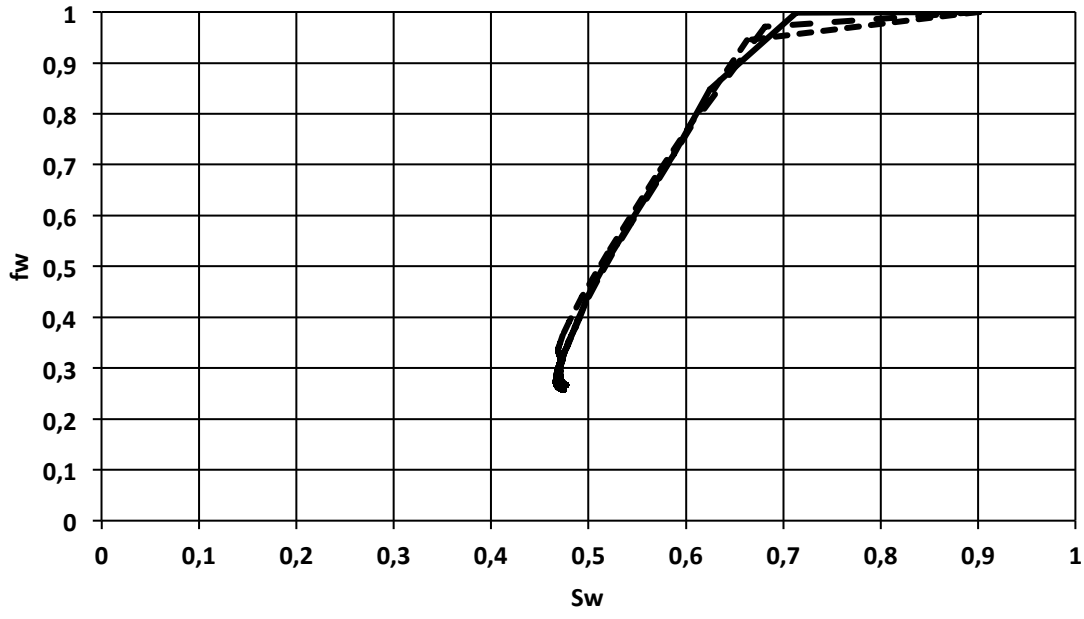

Figure 33 Water fractionnal flow for a low water rate

3.3.2. Moderate water rate

Table 11 Simulation cases for moderate water rate

$P_l(psi)$	$P_j(psi)$	$P_r(psi)$	$\Delta P_1(psi)$	$L_1(ft)$	$\Delta P_2(psi)$	$L_2(ft)$	N_c
7000	5000	4000	2000	40	1000	10	0.5
6000	5250	3000	750	30	2250	45	0.5
6000	5000	3000	1000	20	2000	20	0.5

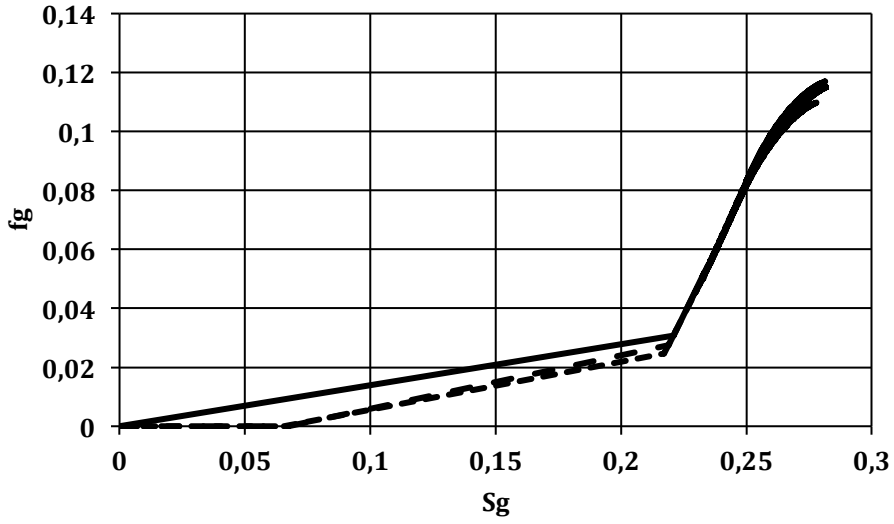

Figure 34 Gas fractionnal flow for a moderate water rate

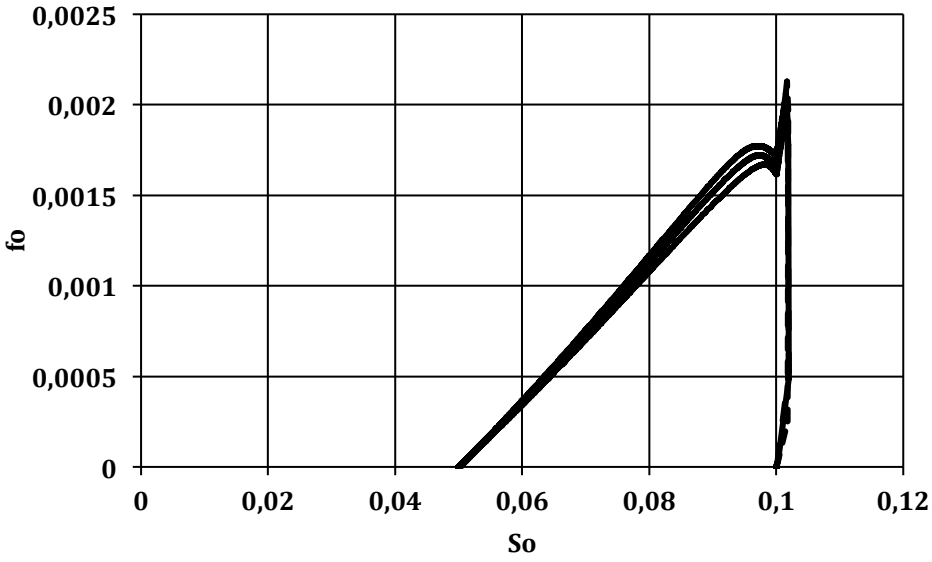

Figure 35 Oil fractionnal flow for a moderate water rate

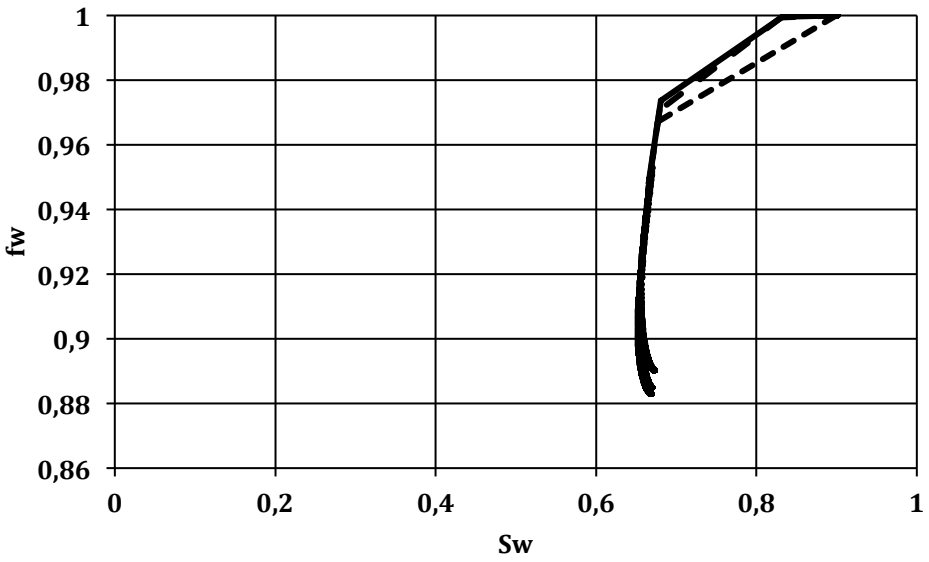

Figure 36 Water fractionnal flow for a moderate water rate

3.3.3. Strong water rate

Table 12 Cases for high water rate

$P_i(psi)$	$P_j(psi)$	$P_r(psi)$	$\Delta P_1(psi)$	$L_1(ft)$	$\Delta P_2(psi)$	$L_2(ft)$	N_c
7000	6000	4000	1000	50	2000	75	0.75
7000	5666	3000	1334	40	2666	60	0.75
7000	6333	3000	667	20	3333	75	0.75

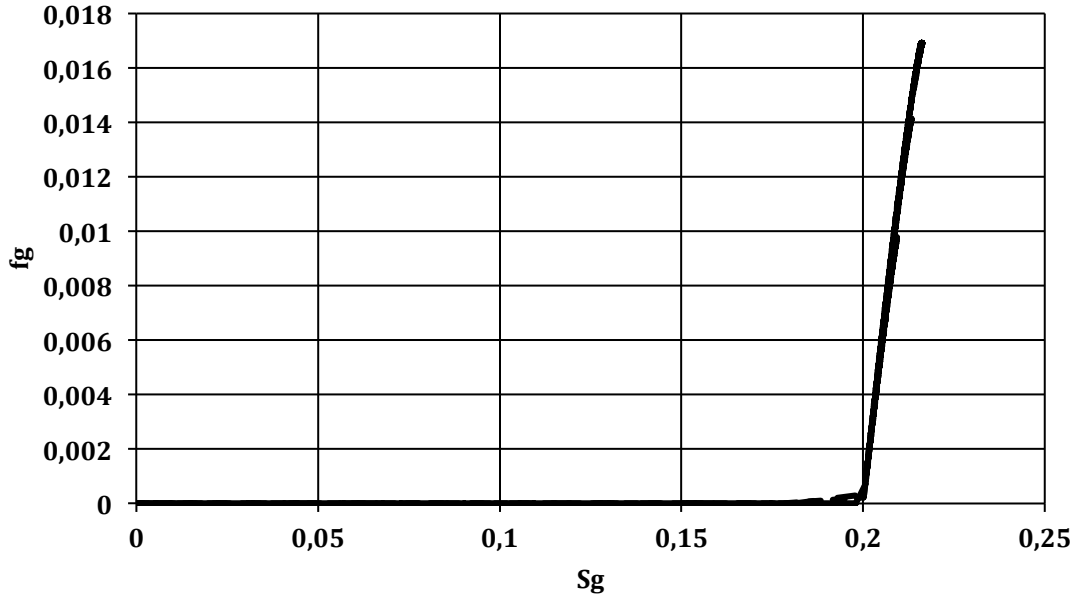

Figure 37 Gas fractionnal flow for a high water rate

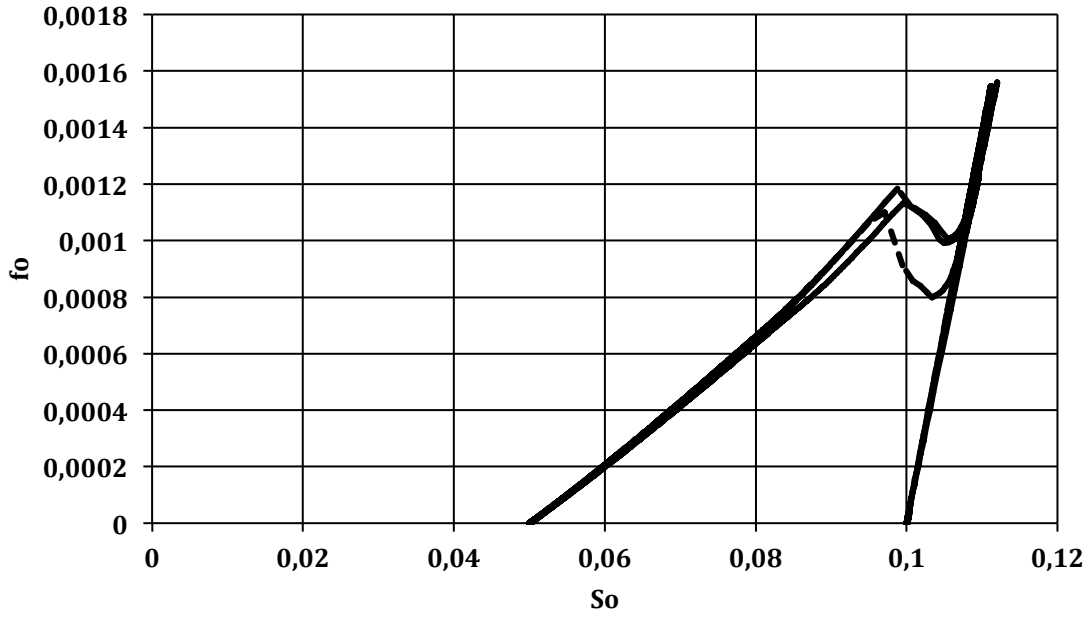

Figure 38 Oil fractionnal flow for a high water rate

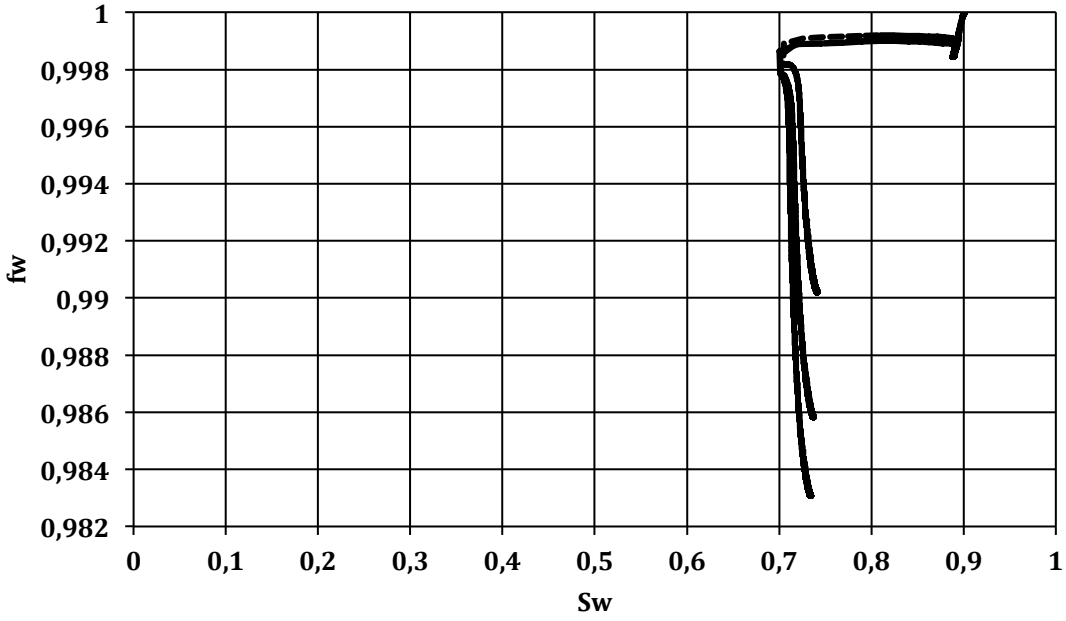

Figure 39 Water fractionnal flow for a high water rate

3.3.4. Observations and conclusion

Surprisingly there is a good match for oil, water and gas in all the graphs. Despite some differences it can be infered that the scaling number leads to a good match of the data, the gap between the curves does not exceed 1% in most simulations. This is in the one dimensional case, it is then possible to observe if this scaling number is still applicable in a 2D case, even though the derivation must be much more complicated.

3.3.5. Comaparison with the two dimensional simulation

A two dimensional model as the one explained in the simulation chapter wa used to measure the rates and the saturation in the producing well, and infer a possible match with the one-dimensional scaling number. Two situations were chosen : a low water rate and a medium water rate, the high water rate did not work because the injecting pressure was to low. The injecting pressure was normally computed assuming a straight line pressure gradient as for the one-dimensional case, thus this problem encouraged me to plot the pressure profile of the two dimensional case. Figure 40 shows the pressure profile for the two-dimensional case compared to the one-dimansional simulation.

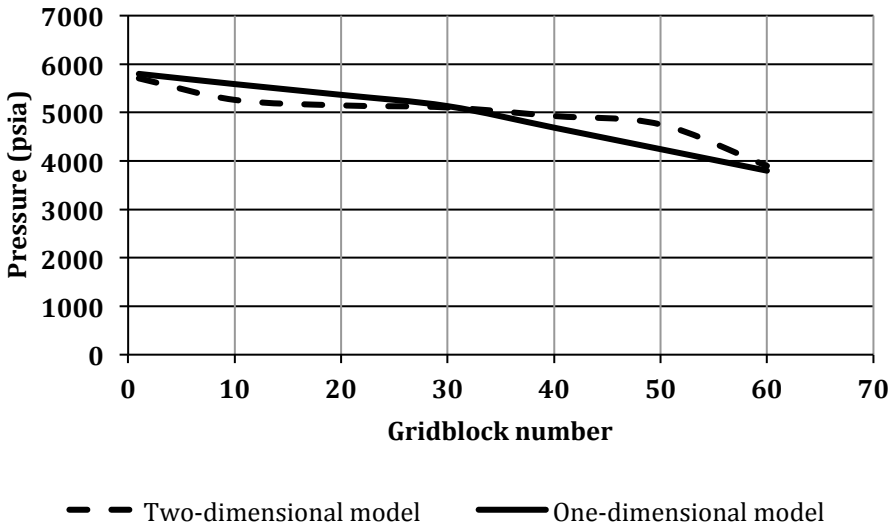

Figure 40 Pressure profile for the one and two-dimensional cases, Eclipse 100

The pressure profiles do not match, which explains the injection or production issues with the wells, the reservoir pressure is indeed below or over the theoretical profile. Nevertheless the scaling number can still be applicable, maybe not between the two models given the pressure profile difference but between the same two-dimensional simulations. Then two simulations with the same scaling number were tested, to be compared between them and with the one-dimensional case.

Table 13Simulation cases for the two-dimensional scaling number

$\mathbf{P_l}(psi)$	$\mathbf{P_j}(psi)$	$\mathbf{P_r}(psi)$	$\mathbf{\Delta P_1}(psi)$	$L_1(\mathbf{ft})$	$\mathbf{\Delta P_2}(\mathbf{psi})$	$L_2(\mathbf{ft})$	$\mathbf{N_c}$
5800	5133	3800	667	50	1333	10	0.100075
5800	5514	3800	286	15	1714	45	0.500583
5800	5513	3800	287	50	1713	30	0.100525
5800	5338	3800	462	30	1538	50	0.50065

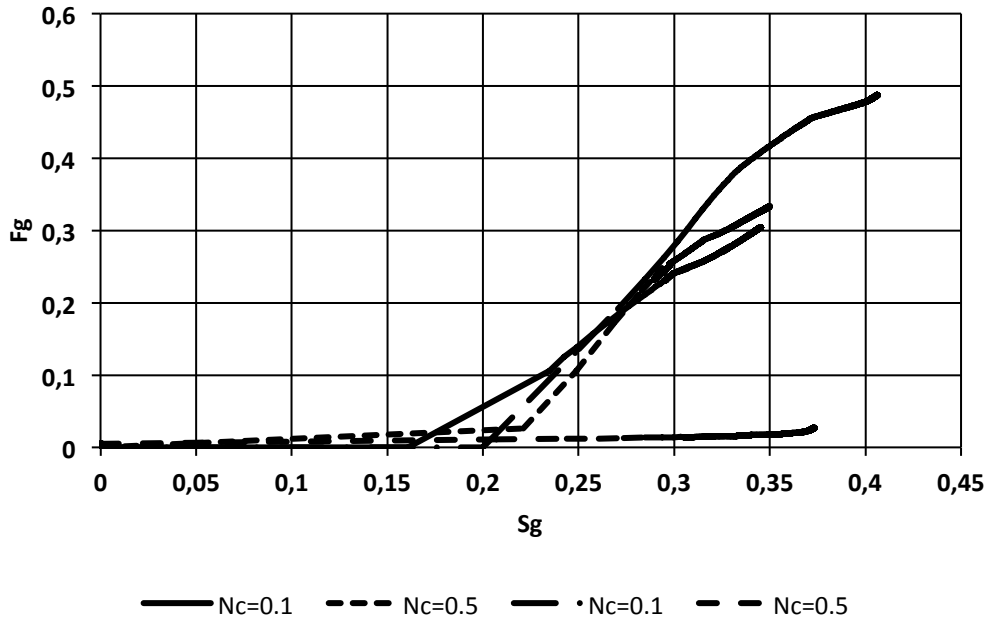

Figure 41 Gas fractionnal flow for the two-dimensional simulation

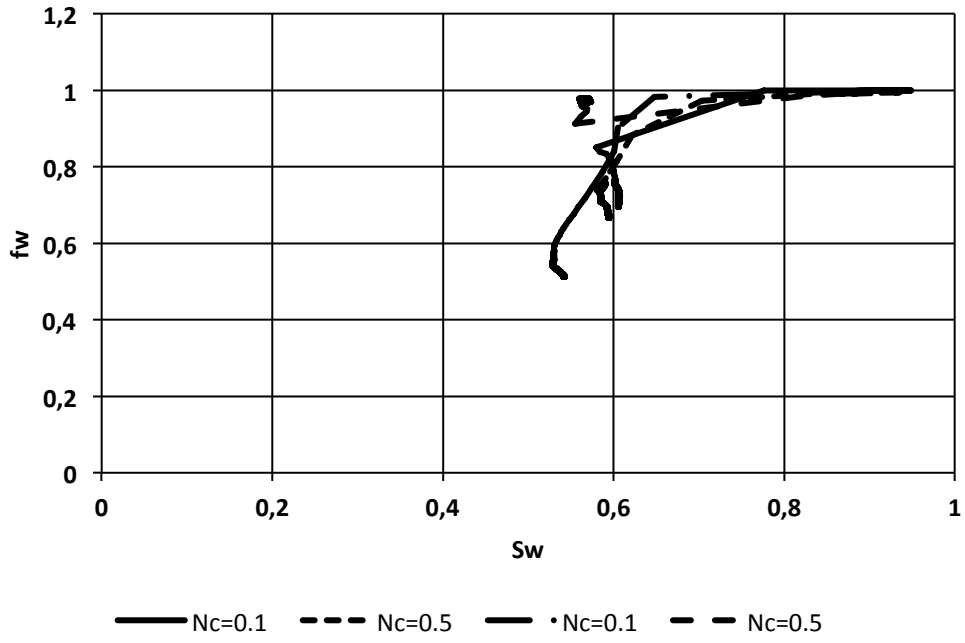

Figure 42 Water fractionnal flow for the two-dimensional simulation

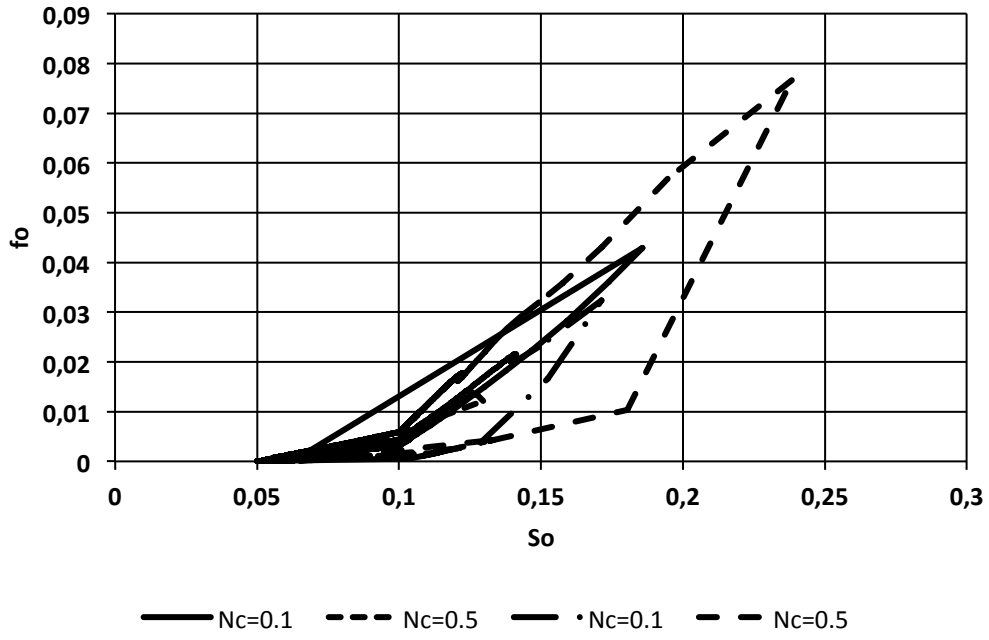

Figure 43 Oil fractionnal flow for the two-dimensional simulation

Figure 41through Figure 43 show that the scaling number derived for one dimension is not applicable. First two similar scaling number lead two different results, and secondly those values does not corresponds to the one-dimensional case since it reaches a different endpoint fractionnal flow. We can explain this mismatch by the pressure profile which is different, there must be an additionnal scaling number taking in account the y-axis distance.

3.4. Scaling number for two producers

3.4.1. Introduction to the model and related scaling numbers

By adding a producer at the end of the model, acting as a "sink" to observe how the gas is shared between the two producers. The parameters are given on the following schematic; with the corresponding pressure profile wich will serve as a basis to derive the scaling numbers.

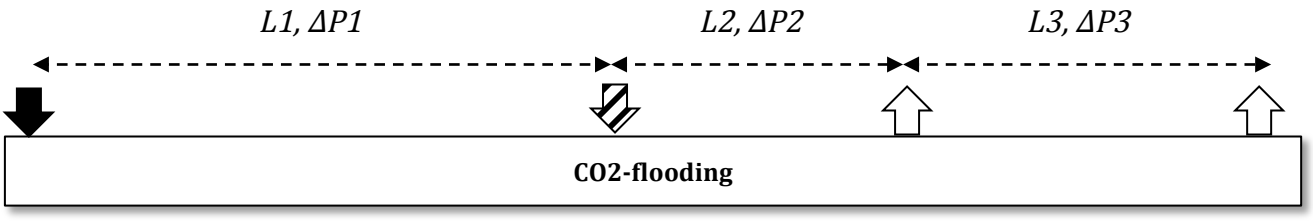

Figure 44 Schematic of the wells for a two producers and two injectors configuration

Figure 45 Pressure profile for two injectors and two producers for a random grid

Since an injector is located at L1 and a producer in L1+L2, the first and last slopes slope will always be smaller than the pressure gradient in the middle, to allow the wells to inject and produce after the waterflood.

We can then define two scaling numbers N_{c2} and N_{c2} defined as

$$N_{c1} = \frac{\Delta P2/L2}{\Delta P3/L3} \tag{3.4.1-1}$$

And

$$N_{c2} = \frac{\Delta P1/L1}{\Delta P3/L3} \tag{3.4.1-2}$$

A set of simulation files were run for fixed values of those scaling number, the results are presented below

3.4.2. Simulation cases for 2 producers

Table 14 Simulation cases for 2 producers

$P_I(psi)$	$P_j(psi)$	$P_i(psi)$	$P_r(psi)$	$\Delta P_1(psi)$	L_1(ft)	ΔP_2(psi)	L_2(ft)	ΔP_3(psi)	N_{c1}	N_{c2}
7333	6000	4000	3000	1333	40	2000	30	1000	0.9	2
7200	6000	3600	3000	1200	20	2400	20	600	1	2
7900	7000	5200	4000	900	30	1800	30	1200	1	2
8000	7000	5000	4000	1000	20	2000	20	1000	1	2

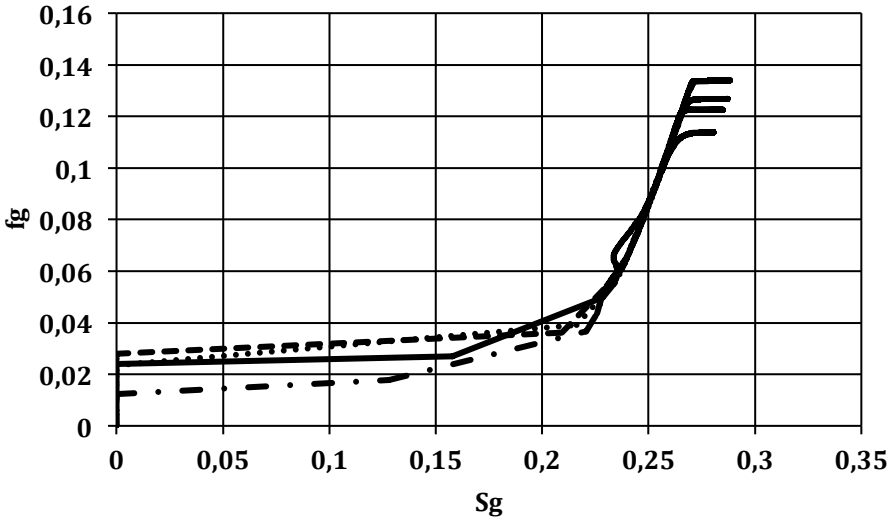

Figure 46 Gas fractionnal flow curves for Nc1=1 and Nc2=2

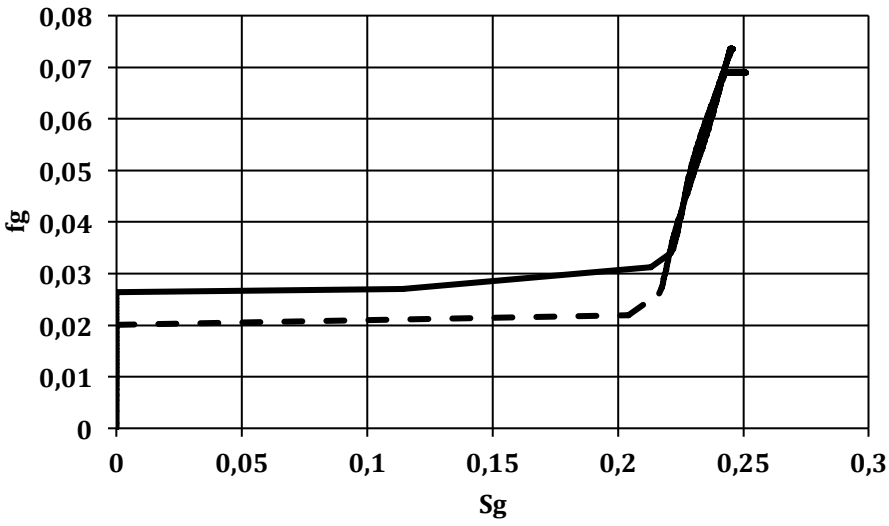

Figure 47 Gas fractionnal flow curves for Nc1=3 and Nc2=5

3.4.3. Observations and conclusions

The match is quite good except at the beginning and at the end of the curve, where the difference is significant[6] in the first case. This discrepancy seems to be related to the sum of the pressure drop in the third zone and the pressure drop in the first zone, however no analytical equation was derived to prove it. As for one injector a two dimensional model can be created to ckeck if this scaling number still works. Given the mismatch for one injector one and two dimensions cases, it seems logical that those new scaling numbers will not work if the model is extended to two dimensions.

[6] More than 1% difference is considered as significant.

4. Volumetric sweep efficiency

4.1. Definition of the efficiencies

The volumetric sweep efficiency can be computed as the product of an areal and vertical sweep efficiency (Lake, 1989) :

$$E_v = E_A E_l \tag{4.1.1-1}$$

With

$$E_A = \frac{Area\ contacted\ by\ CO2}{Total\ area} \tag{4.1.1-2}$$

$$E_l = \frac{Cross - sectional\ area\ contacted\ by\ CO2}{Total\ cross - sectional\ area} \tag{4.1.1-}$$

4.2. One injector and one producer efficiency

4.2.1. Areal sweep efficiency

Firstable for this efficiency to be measured, a set of simulation files had to be prepared. Eclipse 300 was used with a 2D simulation including one water injector, one CO_2 injector and one producer. The pressure gradients are the same as the one-dimensional part : P_l=700 bars and P_r=100 bars, then P_i and P_j are modified to increase the water influx. Figure 48 shows the two extreme cases, one with a high water rate on the right and on the left with a low water rate. All the CO_2 saturation profiles for areal and vertical sweep can also be found in appendix 8. The pore volume chosen for the areal sweep does not matter since it quickly stabilizes, thus despite a similar area the saturation profiles in appendix 8 are not the same.

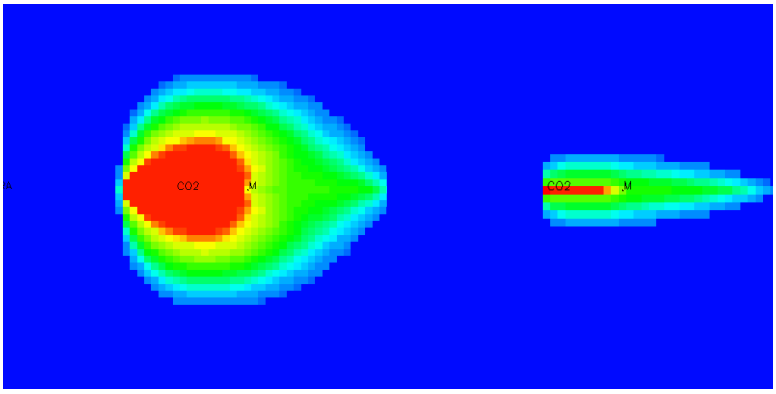

Figure 48 CO_2 saturation profiles in the 2D simulations for a weak and a strong water rate

Secondly to capture the size of the plume in each pictures, one needs to filter the blue color surrounding the plume. The RBG system gives a number from 0 to 250 for each pixels, representing its color. A matlab program added in appendix 7 was created to import the picture and build a matrix with the blue color index of every pixels of the picture, in a chosen window including the plume. A quick look at this matrix shows the number allocated to the blue color representing the water. Once this matrix is created an «if » loop will copy and paste the number 0 if the number corresponds to the blue color and the actual number if this is the plume. Everytime a non-zero value is copied in this matrix the variable « area » is incremented. Figure 49 shows the matrix obtained after filtering the blue color, the red shape represent all the positive CO_2 saturations.

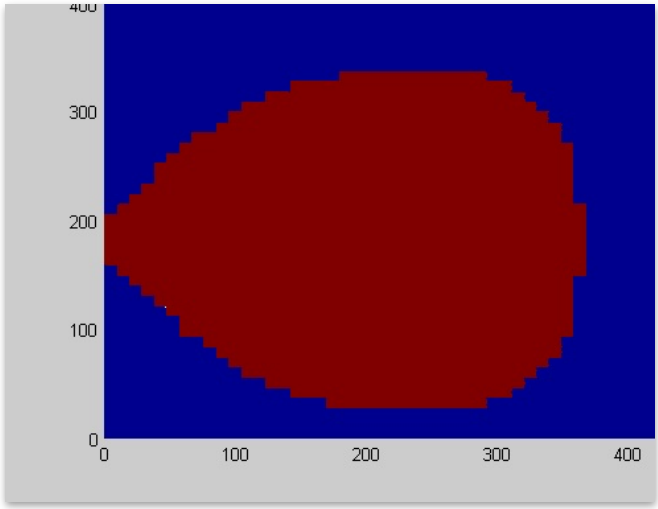

Figure 49 0 and 1 matrix to count the pixels of the plume

This operation is repeated for every pictures, giving the number of pixels of the plume for all the cases. The results appear in the following table, with the sweep efficiency percentage. The reference area has been taken as the reservoir area, which is composed of 318096 pixels, then the sweep efficiency represent the percentage of this total area.

Table 15 Results of the areal sweep efficiency

CO_2 injection pressure (bars)	**Middle well production pressure (bars)**	**Number of pixels of the plume**	**Percentage of the total area**
700	100	87786	28%
650	150	78472	25%
600	200	68543	22%
550	250	56609	18%
500	300	44185	14%
430	370	18895	6%

4.2.2. Vertical sweep efficiency measurement

To be consistent, all the vertical sweep pictures have to be taken for the same pore volume of CO_2 injected. The pore volume of CO_2 needed to begin production in the upper right well will be greater for a low water rate. Indeed a high water rate will push the CO_2 towards this well and the breakthrough will happen earlier.

The simulation with the lowest water rate shows that the top layer reaches the producer on the right for $1.54\ 10^8\ sm^3$ of pore volume injected. This is the reference pore volume for the other simulations. This number is large, however the total pore volume of the reservoir is $3{,}6\ 10^6 m^3$ which would correspond to a volume of $2{,}14\ 10^9\ sm^3$ of CO_2 with a FVF of 0,4 RB/Mscf.

The picture is taken in the cross-section of j=30 which is the middle of the model. The vertical sweep is obviously higher in the middle of the CO_2 front, however we assume here that the same area is swept under all the surface area swept. Figure 50 represents the swept area in the cross section for a strong and a weak aquifer respectively on the right and the left.

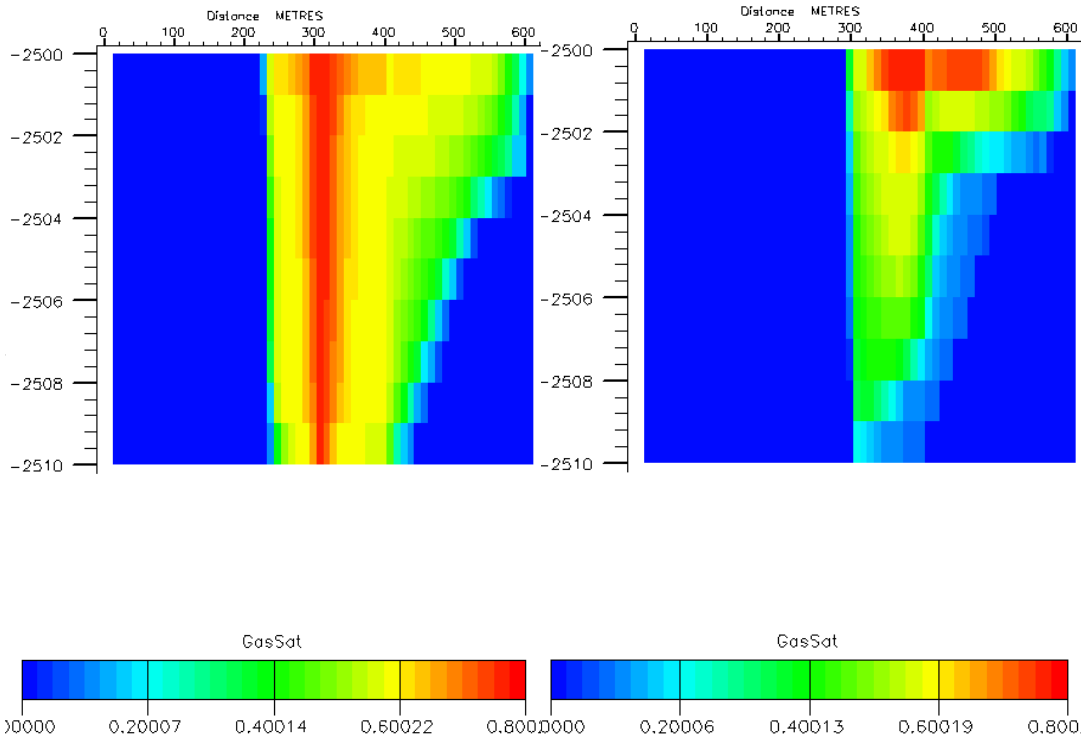

Figure 50 Vertical Sweep for the cross section at j=30, high and low water rate, 2D model using Eclipse 300

Unlike the areal sweep saturation profiles, the high CO_2 saturation location in Figure 50 is strongly changing. The CO_2 still mainly remains between the injector and producer, however in the high water rate case all the CO_2 has moved up to the surface. This effect is not taken in account in the methodology of calculation in Matlab. Nevertheless it partly explains why the vertical efficiency is decreasing with increasing water rate. The same Matlab program gives the matrix of the swept area in Figure 51, with the results in the following table . The reference area wich is the total cross section of the reservoir, represents 123185 pixels.

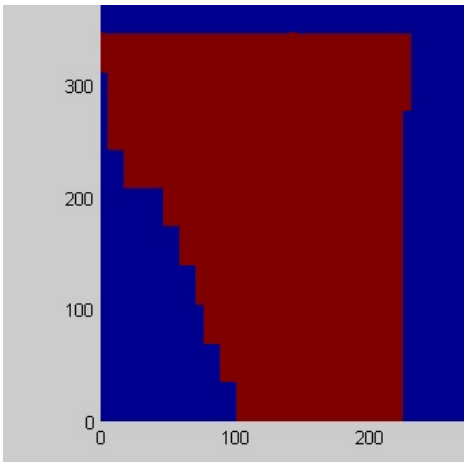

Figure 51 Matrix used for the calculation, showing the vertical sweep

Table 16 Results of the Vertical sweep Calculations

Number of pixels of the CO_2 plume	Percentage of the total Area
62006	50%
62725	50%
62667	50%
59150	48%
54601	44%
41908	34%

4.2.3. Observations and conclusion

Finally Figure 52 sums up all the sweep efficiencies, which all decrease with increasing water rate. The volumetric sweep efficiency goes from 14% to 2% which is very low. This graph first shows that the aquifer has a great impact on the sweep efficiency, and then that in such a reservoir one injector and producer are not enough to recover a significant amount of oil in an EOR process. We could also take another reference area such as the biggest area, to observe how much the area decreases compared to the maximum area.

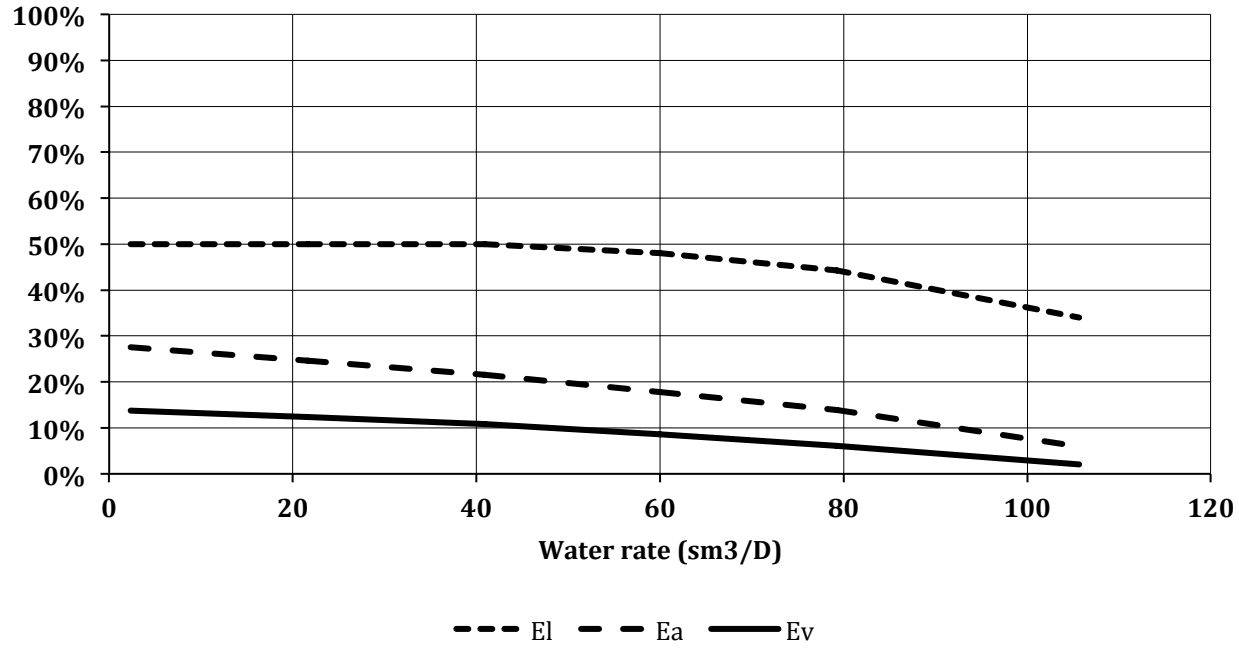

Figure 52 Areal, vertical and volumetric sweep efficiency for the reservoir

4.3. Injection patterns sensitivity

4.3.1. Selected patterns

Several injection patterns are available (Schlumberger, 2012):

- Direct line drive / staggered line drive
- Four-spot / Inverted four-spot
- Five spot / Inverted four spot
- Seven-spot / Inverted seven-spots
- Nine spot / inverted nine-spots

The three configurations experimented in the study are the direct line drive, the four-spot and the five-spot, they are illustrated on Figure 53. On the left side 4 water injectors are injecting water at a rate going from 5 to 1500 m^3/D, and on the right side four wells are producing at a fixed BHP of 100 bars. The injecting pressure was also fixed to 400 bars and all the producers in the pattern to 100 bars, they are located 5 blocks apart from each other which represents 50m.

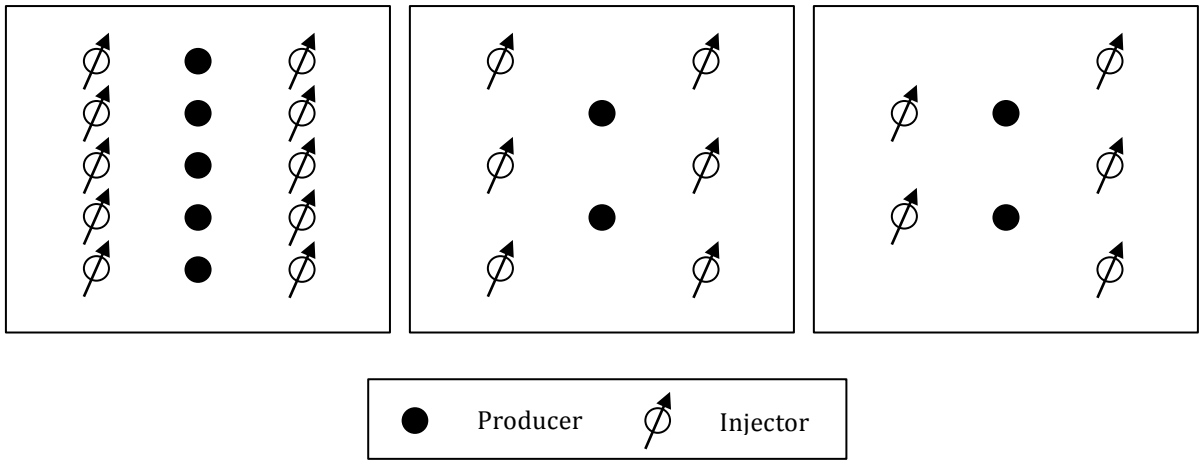

Figure 53 Schematic of the injection patterns tested: Direct line drive, five spot and four spot

4.3.2. Areal efficiency results

As for the single well, the pictures of the well patterns were taken for increasing water rates, using Eclipse 300. Figure 54 shows the results for a low water rate. As the water rate increases the area of the left part of the pattern is decreasing, whereas de right part is only slightly decreasing as shown in Figure 55. The main reason for this effect is that the CO_2 from the first well is pushed away towards the right and is constantly feeding this area with CO_2.

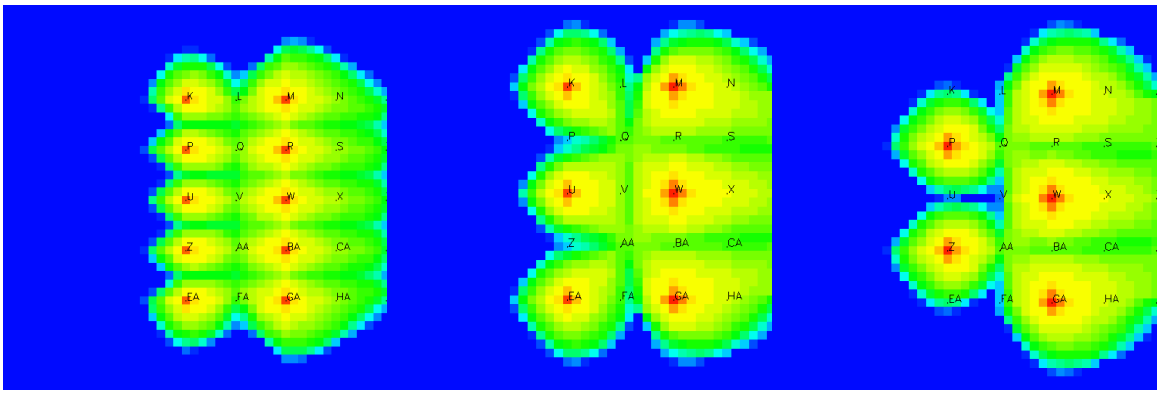

Figure 54 CO_2 plume for the three patterns with a low water rate

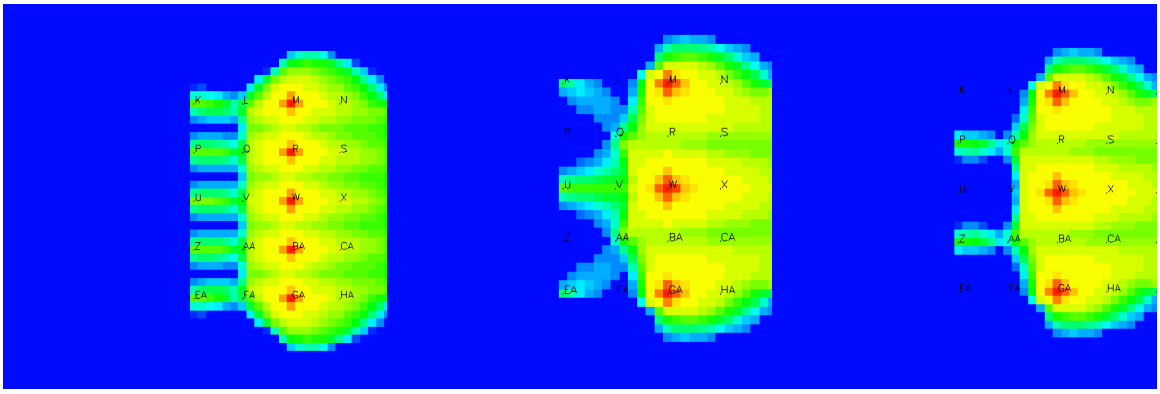

Figure 55 CO_2 plume for the three patterns with a high water rate

Unlike the one-producer case, several patterns are compared to each other with different well number; it is not relevant to compare their efficiency with a total reference area such as the reservoir area. However it is done afterwards in order to choose the most suitable pattern. The reference area chosen is then the biggest area achieved, which is always for the lowest water rate. The results of the relative areal efficiciency between the patterns are in Figure 56.

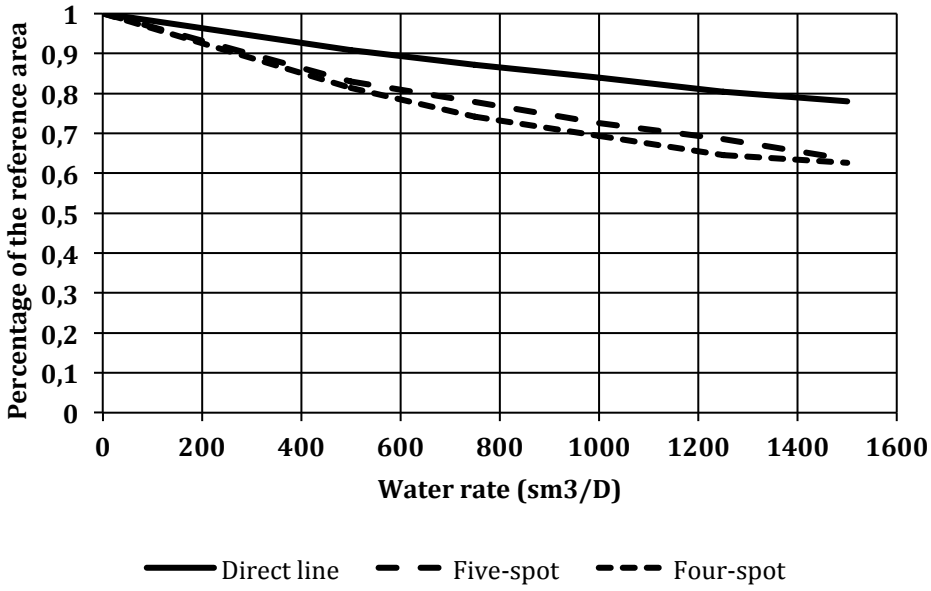

Figure 56 Areal efficiency with the biggest area as a reference

According to this graph, the direct line drive is the one giving the best efficiency based on the efficiency loss when the water rate increases. It does not already mean that this is the best pattern because the efficiency at the beginning compared to the whole field can be very low. The five spot is the second pattern which does not lose much area compared to the initial size, however it is similar to a four-spot pattern in case of a strong aquifer.

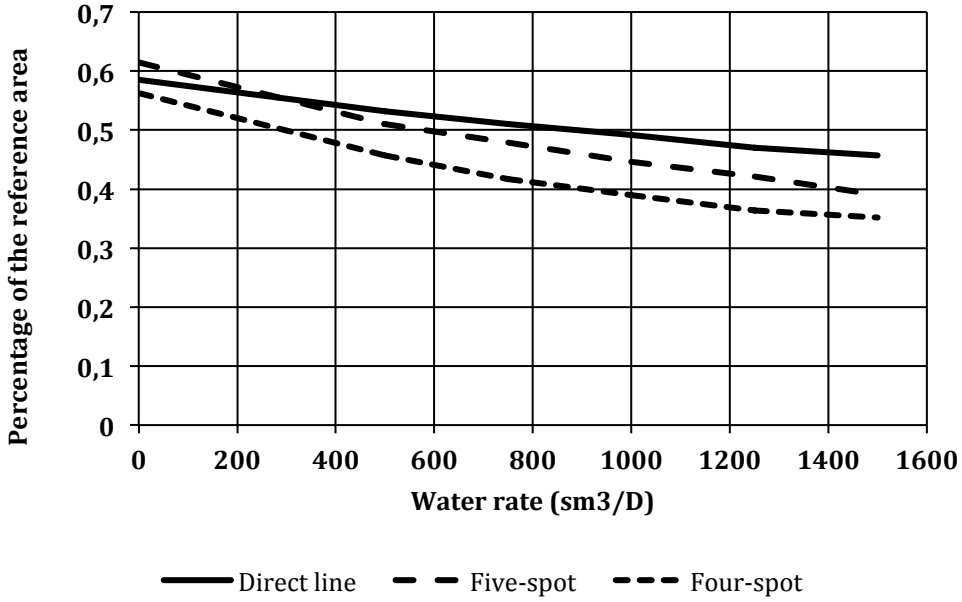

Figure 57 Areal efficiency for each pattern based on the whole area

4.3.3. Observations and conclusion

A five-spot is preferred to a direct line drive with a low water influx, however this tendancy switches as the water rate increases since the five-spot pattern loses swept area. According to Figure 57 a direct line drive would be preferred and would normally give a better oil production. However for this conclusion to be maintained the vertical sweep efficiency has to be measured. This efficiency is difficult to measure given the numerous wells; the cross section is not clearly defined. Nevertheless as a first assumption the vertical sweep efficiency found in the previous part could be a good start. For the range of this sweep efficiency, about 100 sm^3/D, the volumetric sweep efficiency would then be around 30% which is much better than the value of 2% for a single well. This efficiency can be questioned regarding the cost of the new wells to drill in order to increase the recovery.In the same way the direct line drive may be the best option but needs 10 wells, whereas 6 and 5 wells were required in the other patterns. The price of a new well being around 60 million euros, the price of 5 more wells may overbalance a 10% sweep efficiency if the residual oil saturation or the size of the field is not large enough.

5. Conclusion

This study shows that EOR methods involving injection of CO_2 can still be further improved, especially when the reservoir is subject to a strong aquifer. Carbon dioxide has excellent properties as a tertiary recovery method, by dissolving in the oil it decreases its viscosity and increases the swelling efficiency. However these advantageous properties are altered when a water influx is present in the reservoir. Numerous simulation pictures and rate computation show how negative this effect can be regarding the sweep efficiency and thus the oil recovery; it has been finally observed and quantified in the last part of the study.

The problem was first simplified to a one-dimensional study where a theoretical pressure profile was assumed and validated in the simulations. Once the simulation matched with the equations several sensivity analysis regarding the pressure drop between the wells or the distances lead to key observations and conclusions regarding CO_2 injection in such conditions. Unlike the basic model, reservoirs are in three dimensions and heterogeneous, that's why those conclusions have to be checked at a larger scale. Therefore scaling numbers were derived in two simple cases, in order to scale up the reservoir data and obtain the rates. At the same time the Walsh diagrams were built using the simulation data, they represent useful tools to better understand the displacement mechanisms.

The goal of this study was to have a first insight of what is happening during CO_2 EOR with a strong aquifer: evaluate, quantify and eventually solve the problem. The methodology was to build a simple one-dimensional and establish relationship that could explain the behavior of CO_2. This step has been successful since the effect of aquifer on CO_2 was observed and the equations were verified with the fractional flow curves. The study dealt a little with several well cases or two-dimensional simulations; however these simulations remain to be matched with the theory.

The accuracy of the simulator can also be discussed, even though the compositional simulation is as of today the best way to simulate the behavior of carbon dioxide with the aquifer. I have encountered several limitations of the simulator during the study, mainly due to the number of gridblocks, problems of well injection or production or wrong input parameters for the fluids. I would have liked to be closer to the reality of the problem by having companies 'feedback on this issue and be able to build a more realistic model. What strongly motivated be along this study is that it is an actual problem faced in the industry which was not clearly understood. I believe further simulations with field data combined with this basic theoretical approach could already lead to technological solutions. An optimum well configuration can be defined with the corresponding pressure drops, and then other technological solutions can be considered if the water production prevails such as lift methods mentioned in the literature.

Nomenclature

Normal

f_i	Fractionnal flow of component i [=] fraction
λ_j	Mobility of phase i [=] F - t
Φ	Porosity [=] fraction
μ_j	Viscosity of component I [=] F – t/ L^2
c	Compressibility [=] L^2/F
K	Absolute permeability [=] L^2
u_i	Velocity of the component i [=] L / t
U_i	Velocity in the medium number i [=] L / t
K_r	Relative permeability [=] L^2
S_i	Saturation of component i
q_i	Volumetric rate of component i [=] L^3 / t
P_i	Pressure in medium i [=] F/ L^2
P_l	Bottom hole pressure of the water injector at the upper left side of the model
P_j	Bottom hole pressure of the CO_2 injector
P_i	Bottom hole pressure of the first producer
P_r	Bottom hole pressure of the second producer at the upper right side of the model
x	Distance in the x-direction [=] L
x_D	Dimensionless distance in the Walsh diagrams
t_D	Dimensionless time
d_D	Dimensionless distance in the 1D simulation
P_D	Dimensionless pressure
E_a	Areal efficiency [=] fraction
E_l	Vertical efficiency
E_v	Volumetric efficiency
FVF	Formation volume factor
GOR	Gas-oil ratio [=] L^3 / L^3
WOR	Water-oil ratio [=] L^3 / L^3
GOC	Gas-oil contact [=] L

WOC	Water-oil contact [=] L
$N_{c1,c2}$	Scaling number for the two producers case
N_c	Scaling number for the one producer case
ΔP_i	Pressure drop in zone i [=] F/ L^2
B_g	Formation volume factor for gas [=] L^3 / L^3
B_w	Formation volume facto for water [=] L^3 / L^3
G_i	Cumulative gas injected at standard conditions [=] L^3

Subscripts

i	1 for water, i=2 for oil, 3 for gas
j	1,2,3 for zone 1,2 and 3.

References

What is CCS? (2012). Retrieved from Global CCS Institute Website: http://www.globalccsinstitute.com/ccs/what-is-ccs

A. D. Brooks, A. d.-A., & and W. Al-Ajmi and M. Mukmin, P. D. (2010). Evaluation Of EOR Techniques For Medium-Heavy Oil Reservoirs With a Strong Bottom Aquifer In The South Of Oman. *SPE EOR Conference at Oil & Gas West Asia.* Muscat, Oman: Society of Petroleum Engineers.

Abdelhakim Deghmoum, S. D. (2012). A Riveting Review of Worldwide Industrial Geological Carbon Capture and Storage Projects with the Junction of CO2 Emissions in Algeria. *North Africa Technical Conference and Exhibition* (pp. 1-2). Cairo, Egypt: OnePetro.

Abdullatif Ibrahim, S. A. (2009). Challenges in Operating and Developing Strong Bottom Water Drive Reservoir.A Case Hosiery. *SPE/EAGE Reservoir Characterization and Simulation Conference.* Abu Dhabi, UAE: Society of Petroleum Engineers.

C.A.M. Veeken, H.-V. C. (2000). Monitoring and Control of Water Influx in Strong Aquifer Drive Gas Fields Offshore Sarawak. *SPE Asia Pacific Oil and Gas Conference and Exhibition.* Brisbane, Australia: Society of Petroleum Engineers.

Childers, A. M. (2011). *Reducing Onshore Natural Gas and Oil Exploration and Production Impacts Using a Broad-Based Stakeholder Approach.* Oklahoma City: Interstate Oil and Gas Compact Commission.

Curtis H. Whitson, M. R. (2000). *Phase Behavior SPE Monograph volume 20.* Society of Petroleum Engineers.

Ehlig-Economides, C. S., Chan, K. S., & Spath, J. S. (2012). Production Enhancement Strategies for Strong Bottom Water Drive Reservoirs. *North Africa Technical Conference and Exhibition.* Cairo, Egypt: Society of Petroleum Engineers .

Hocott, C. R. (1983). *Improved oil recovery.* Oklahoma City: Interstate Oil Compact Commision.

Holm, L. U. (1976). Status of CO2 and Hydrocarbon Miscible Oil Recovery Methods. *Journal of Petroleum Technology*.

Kleppe, J. (2011). *Reservoir Recovery Techniques 2011, Material Balance Equations.* Trondheim.

L.A. Strappa, J. D.-Y., & M.A. Maure, M. L. (2004). A Novel and Successful MEOR Pilot Project in a Strong Water-Drive Reservoir Vizcacheras Field, Argentina. *SPE/DOE Symposium on Improved Oil Recovery* (p.). Tulsa, Oklahoma: Society of Petroleum Engineers.

Lake, L. W. (1989). *Enhanced Oil Recovery.* Prentice Hall.

Ramli, A. P. (1995). Reservoir Simulation of a High Viscous Crude and Strong Water Drive Reservoir in Sarawak, Malaysia. *SPE Asia Pacific Oil and Gas Conference.* Kuala Lumpur, Malaysia: Society of Petroleum Engineers.

Schlumberger. (2012). *Schlumberger Oilfield Glossary*. Retrieved from http://www.glossary.oilfield.slb.com/

Shahsavari, D. D. (1991). Monitoring and Evaluation of an Immiscible Gas Injection Pilot in a Massive Carbonate Reservoir With a Strong Water Drive. *Middle East Oil Show.* Bahrain.

Stefan Bachu, A. E., & Jerry C. Shaw, R. M. (2004). Estimation of Oil Recovery and CO2 Storage Capacity in CO2 EOR Incorporating the Effect of Underlying Aquifers. *SPE/DOE Symposium on Improved Oil Recovery.* Tulsa, Oklahoma: Society of Petroleum Engineers.

The U.S. Energy Information Administration. (2012). *Annual Energy Outlook 2012 Early Release.* Washington.

Thomas P. Chesney, R. C. (1982). Secondary Gas Recovery From a Moderately Strong Water Drive Reservoir: A Case History. *Journal of Petroleum Technology*, Volume 34, Number 9.

Wenting Qin, A. K. (2011). New Cold Production Technique for Heavy Oil with Strong Bottom Water Drive. *SPE Annual Technical Conference and Exhibition .* Denver, Colorado, USA.

Appendix 1: CO_2 physical properties input in Eclipse

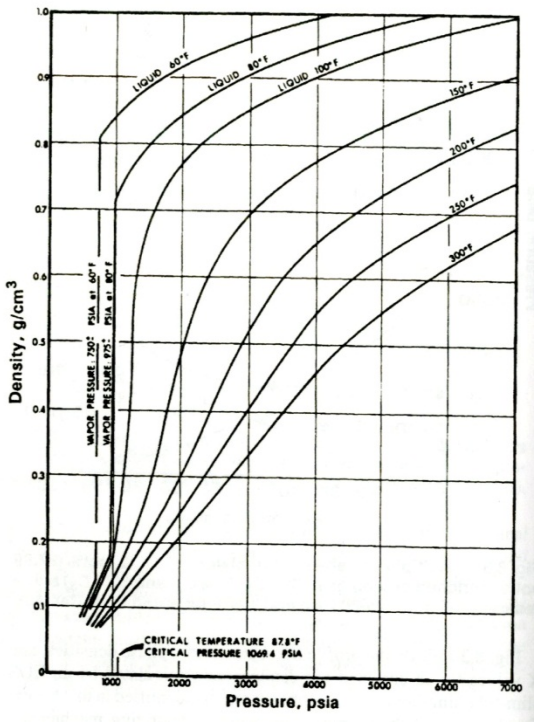

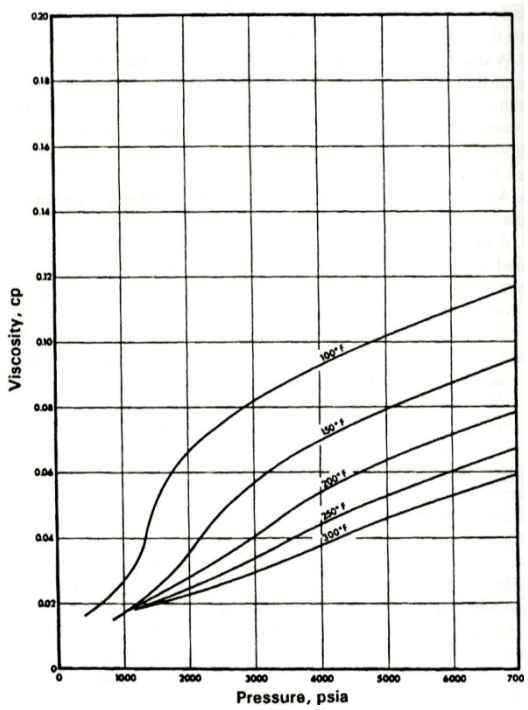

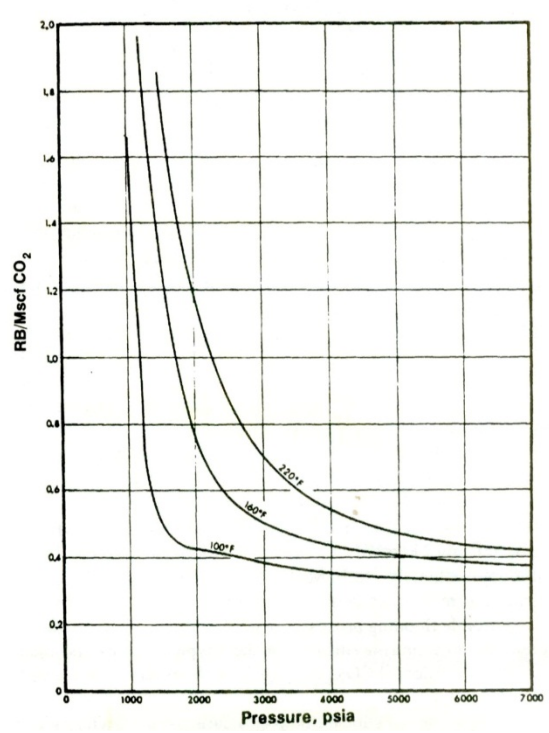

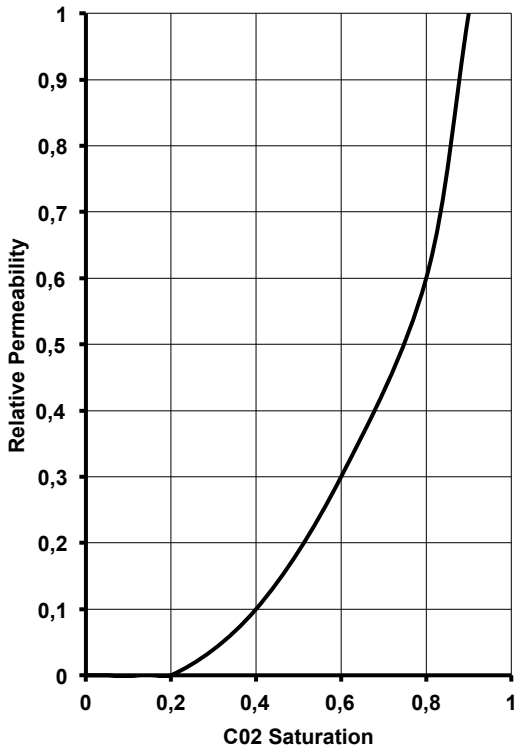

Appendix 2 : E100 simulation file for the one-dimensional case

```
RUNSPEC
TITLE
   ONE D CASE
DIMENS
   60   1    1  /
NONNC
OIL
WATER
GAS
DISGAS
FIELD
EQLDIMS
    1  100   10    1    1 /
TABDIMS
    1    1   16   12    1   12 /
WELLDIMS
    40    30    20    20 /
NUPCOL
    4 /
START
  17 'JAN' 2012  /
NSTACK
   24 /
--AQUDIMS
--1 1 1 36 2 100 /
--FMTOUT
--FMTIN
UNIFOUT
UNIFIN
--NOSIM

GRID
INIT
EQUALS
'PORO'  0.3       /
      'DZ'    3        1  60  1  1  1
1  /
      'DX'    3      /
      'DY'    3      /
      'PERMX' 500       /
      'MULTZ' 1      /
      'TOPS'  8325      /
/
COPY
      'PERMX'    'PERMY'   1  60  1  1
1  1  /
      'PERMX'    'PERMZ'   /
/

--AQUNUM
--1 5 5 4 1.0E+6 1000 1* 200 4* /
--/

--AQUCON
--1 5 5 5 5 4 4 'K-' 1.0 /
--/
EDIT
TRANZ
60*1 /

PROPS
SWFN
--Sw Krw Pcw
0.10 0.0  0.0


0.20 0.00 0.0
0.40 0.01 0.0
0.60 0.20 0.0
0.80 0.80 0.0
/


SGFN
-- Sg Krg Pcog
0.0    0.0    0.00
0.05   1*   0.00
0.2    0.0    0.00
0.4    0.1    0.00
0.6    0.3    0.00
0.8    0.6    0.00
0.9    1.0    0.00
/
SOF3
--So  Kro(o-w) Kro (o-g-wi)
0.05 0.00 0.0
0.1 0.00 0.01
0.21 0.05 0.05
0.4 0.10 0.10
0.6 0.40 0.40
0.9 0.60 0.60
/
-- PVT PROPERTIES OF WATER
--
--    REF. PRES. REF. FVF
COMPRESSIBILITY  REF VISCOSITY
VISCOSIBILITY
PVTW
       4014.7     1.029        3.13D-6
0.31            0 /
-- ROCK COMPRESSIBILITY
--
--    REF. PRES   COMPRESSIBILITY
ROCK
        14.7          3.0D-6
/
-- SURFACE DENSITIES OF RESERVOIR
FLUIDS
--        OIL   WATER   GAS
DENSITY
         49.1   64.79  0.12  /
--   PGAS   BGAS   VISGAS
PVDG
     14.7 166.666   0.008
    264.7  12.093   0.0096
    514.7   6.274   0.0112
   1014.7   3.197   0.017
   2014.7   1.614   0.03
   2514.7   1.294   0.035
   3014.7   1.080   0.04
   4014.7   0.811   0.054
   5014.7   0.649   0.062
   7014.7   0.386   0.08   /

--   RS      POIL  FVFO  VISO
PVTO
    0.001    14.7 1.062  1.04    /
    0.0905  264.7 1.15   0.975   /
    0.18    514.7 1.207  0.91    /
    0.371  1014.7 1.295  0.83    /
    0.636  2014.7 1.435  0.695   /
    0.775  2514.7 1.5    0.641   /
    0.93   3014.7 1.565  0.594   /
    1.270  4014.7 1.695  0.51
           5014.7 1.671  0.549
```

```
           9014.7 1.579  0.74    /
    1.618  5014.7 1.827  0.449
           9014.7 1.726  0.605   /
/
RPTPROPS
1  1  1  0  1  1  1  1  /

SOLUTION
RPTSOL
   1  11*0  /
--AQUFLUX
--1 10 /
--/
PRESSURE
60*4800/
SWAT
60*0
/
SGAS
60*0
/
RS
60*0.0
/

SUMMARY
RUNSUM
FOPR
FWPR
FGPR
FWIR
FOPT
FWPT
FGPT

WWPR
M
L
/
WGPR
M
L
/
WOPR
M
L
/
WOPT
M
L
/
WWIR
WATERA
/
WGIR
CO2
/
WBHP
M
L
WATERA
CO2
/
BGSAT
55 1 1
/
BOSAT
55 1 1
/
BFLOGI
55 1 1
/
BFLOOI
55 1 1
/
BFLOWI
55 1 1
/
BWSAT
55 1 1
/
BPR
10 1 1
50 1 1
20 1 1
30 1 1
40 1 1
60 1 1
/

SCHEDULE
RPTSCHED
   0 0 0 0 0 0 0 0 0 0 0
   0 2 0 0 2    /
DRSDT
 0 /
-- WELL SPECIFICATION DATA
--
--     WELL   GROUP LOCATION  BHP   PI
--     NAME   NAME    I  J   DEPTH
DEFN
WELSPECS
M 'G1'   40 1   8400 'OIL'  /
L 'G1'   60 1   8400 'OIL'  /
WATERA 'G2'    1 1   8400 'WATER'  /
CO2 'G3'    30  1    8400 'GAS'  /
/
-- COMPLETION SPECIFICATION DATA
--
--     WELL     -LOCATION- OPEN/ SAT
CONN  WELL
--     NAME     I  J K1 K2 SHUT  TAB
FACT  DIAM
COMPDAT
M  40 1 1  1 'OPEN' 0   -1   0.5  /
L  60 1  1 1 'OPEN' 0   -1   0.5  /
WATERA   1  1 1  1 'OPEN' 0   -1   0.5
/
CO2   30  1 1  1 'OPEN' 0   -1   0.5
/
/
-- PRODUCTION WELL CONTROLS
--
--      WELL     OPEN/  CNTL   OIL
WATER   GAS  LIQU   RES   BHP
--      NAME     SHUT   MODE  RATE
RATE  RATE  RATE  RATE
WCONPROD
M 'SHUT' 'BHP'    5*
4700 /
L 'OPEN' 'BHP'    5*
4600 /
/
-- INJECTION WELL CONTROLS
--
--      WELL     INJ   OPEN/  CNTL
FLOW
--      NAME    TYPE   SHUT   MODE
RATE
WCONINJ
```

```
WATERA 'WATER' 'OPEN' 'BHP' 4* 5000  /
CO2 'GAS'   'SHUT' 'BHP' 4* 4900  /
/
RPTSCHED
1 1 1 1 1 0 2 1 2 0
2 2 0 0 2 /
TSTEP
50*7 /
RPTSCHED
 1 1 1 1 1 0 2 1 2 0
 2 2 0 0 2 /
WCONPROD
M 'OPEN' 'BHP'   5*
4700 /
L 'OPEN' 'BHP'   5*
4600 /
  /
-- INJECTION WELL CONTROLS
--
--      WELL     INJ   OPEN/  CNTL
FLOW
--      NAME    TYPE   SHUT   MODE
RATE
WCONINJ
CO2 'GAS'   'OPEN' 'BHP' 4* 4900  /
/
RPTSCHED
1 1 1 1 1 0 2 1 2 0
2 2 0 0 2 /
TUNING
/
/
12 1 40 1 8 8 4*1E6 /
TSTEP
250*0.5 /
RPTSCHED
 1 1 1 1 1 0 2 1 2 0
 2 2 0 0 2 /
END
```

Appendix 3 : E300 simulation file for the two-dimensional case

```
RUNSPEC
METRIC
CO2SOL
OIL
GAS
WATER
FULLIMP
COMPS
1 /
EOS
PR /
DIMENS
60 60 1 /
TABDIMS
1 1 40 40 /
WELLDIMS
40    30    20    20 3* 20/
DIFFUSE
START
1 JAN 2007 /

GRID
EQUALS
'PORO'  0.3       /
      'DZ'    10        1  60  1  60
1  1  /
      'DX'    10      /
      'DY'    10      /
      'PERMX' 500       /
      'MULTZ' 1      /
      'TOPS'  2500    /
/
COPY
PERMX PERMY /
/
PERMZ
3600*500 /

PROPS
EOS
PR   /
CNAMES
CO2 /
OMEGAA
0.457 /
OMEGAB
0.077796 /
TCRIT
304.7 /
PCRIT
73.8 /
ZCRIT
0.274 /
ZCRITVIS
0.215 /
ACF
0.225 /
MW
44 /
ZI
1
/
DIFFCGAS
0.2 /
DIFFCOIL
0.01 /
RTEMP
75 /
BIC
0.1896 /
PARACHOR
78 /
LBCCOEF
0.1023 /
SGFN
--Sg Krg Pcg
0.0 0.00 0.0
0.1 0.00 0.0
0.2 0.05 0.0
0.4 0.10 0.0
0.6 0.40 0.0
0.8 0.60 0.0
0.99 0.70 0.0
/
SWFN
--Sw Krw Pcw
0.01 0.0  0.0
0.20 0.00 0.0
0.40 0.01 0.0
0.60 0.20 0.0
0.80 0.80 0.0
1.00 1.00 0.0
/
SOF3
--So  Kro(o-w) Kro (o-g-wi)
  0.0 0.00 0.0
0.1 0.00 0.0
0.2 0.05 0.05
0.4 0.10 0.10
0.6 0.40 0.40
0.8 0.60 0.60
0.99 0.70 0.70
/
ROCK
150 0.00005 /

SOLUTION
RPTSOL
PRESSURE SWAT SGAS DENG DENW VWAT XMF
YMF /
RPTRST
  'BASIC=2' /
FIELDSEP
1 25 50/
2 15 1/
/
PRESSURE
3600*320/
SWAT
3600*1.0
/
SGAS
3600*0
/
XMF
3600*0.0
/
RSW
3600*0.0
/
RS
3600*0.0
/
RSVD
```

```
2500 0.0
2501 0.0 /

SUMMARY
FGIR
FPR
FPRH
FPRP
FOPR
FWPR
FGPR
FWIR
FOPT
FWPT
FGPT
WGPR
M
R
/
WWPR
M
R
/
WOPT
M
R
/
WGOR
M
R
/
WBHP
M
R
CO2
WATERA
/
WWIR
WATERA
/
WGIR
CO2
/
BPR
1 1 1
60 1 1
20 1 1
10 1 1
30 1 1
40 1 1
50 1 1
/
RUNSUM
RPTONLY
SCHEDULE
SEPCOND
GAS/
/
OUTSOL
PRESSURE SOIL SWAT SGAS XMF YMF /
RPTSCHED
PRESSURE SOIL SWAT SGAS XMF YMF/
WELLSPEC
CO2 G3    30  30    1* GAS/
WATERA G2   1  30  /
M 40 30/
R G1   60 30   /
/
COMPDAT
M 40 30 1 1 /
R  60  30 1  1 /
WATERA     1 30 1  1 /
CO2   30  30 1  1/
/
WELLSTRE
CO2INJ 1.0 /
/
WINJGAS
CO2 STREAM CO2INJ /
/
WCONINJE
WATERA WATER OPEN BHP   2* 700/
CO2 GAS    SHUT BHP  2* 550/
/
WCONPROD
R 'OPEN' 'BHP'     5*
100/
M 'SHUT' 'BHP'     5*
250/
/
TUNING
/
/
2* 100/
TSTEP
1*365 /
WCONINJE
WATERA WATER  OPEN BHP  2* 700/
CO2    GAS    OPEN BHP  2* 550/
/
WCONPROD
R 'OPEN' 'BHP'     5*
100/
M 'OPEN' 'BHP'     5*
250/
/
TSTEP
1*365 /

END
```

Appendix 4: Rates for one-dimensional flow

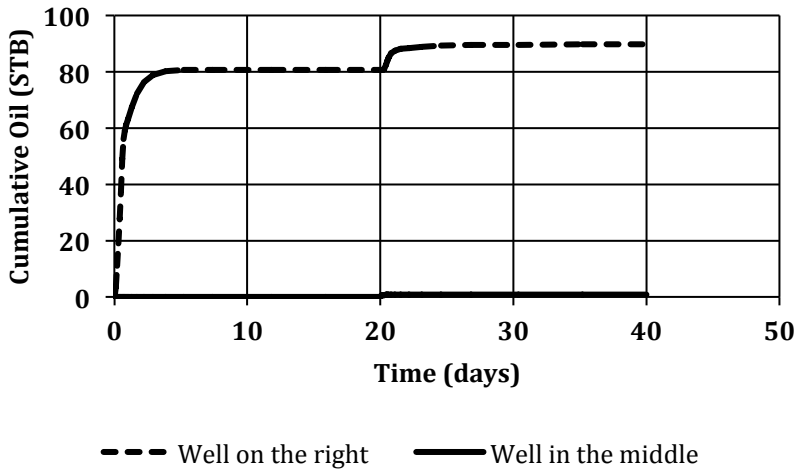

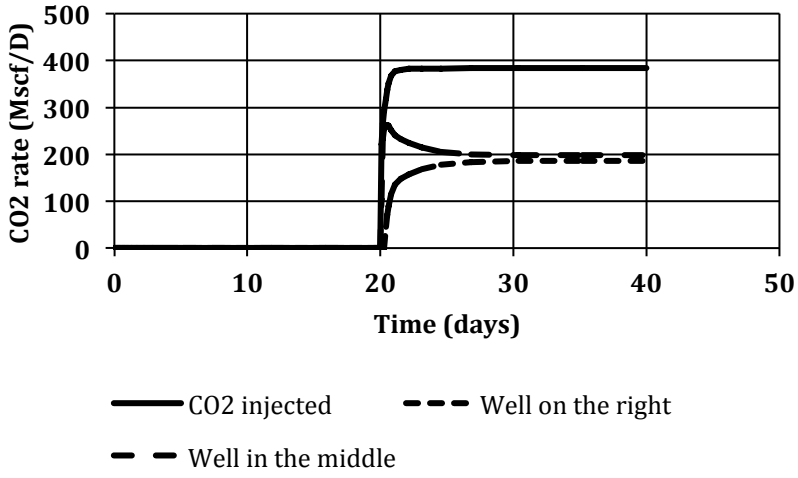

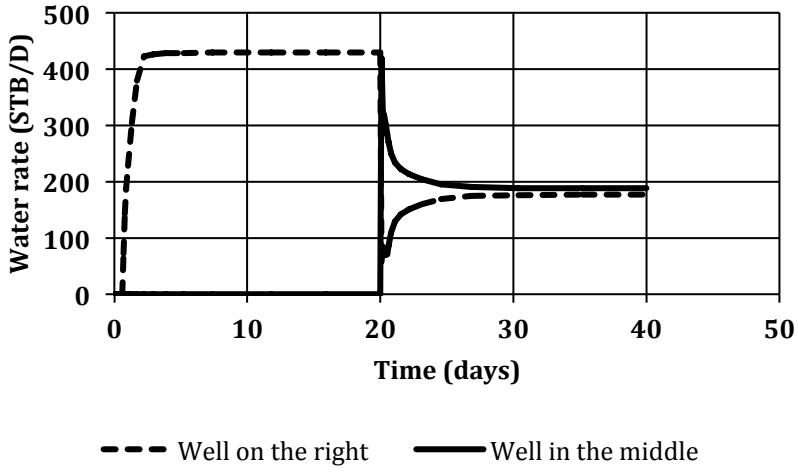

Appendix 5: Gas, water and Oil rates in the 1D simulation for different pressure profiles in the middle well (left) and right well (right).

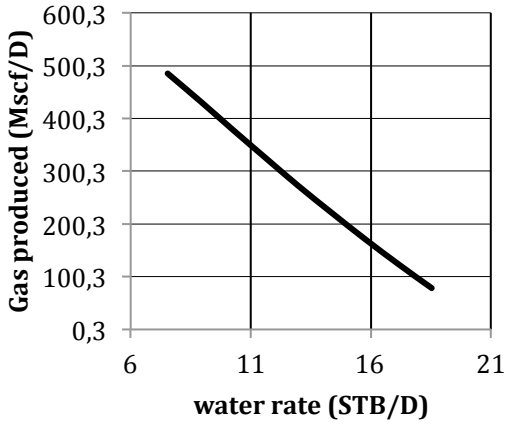

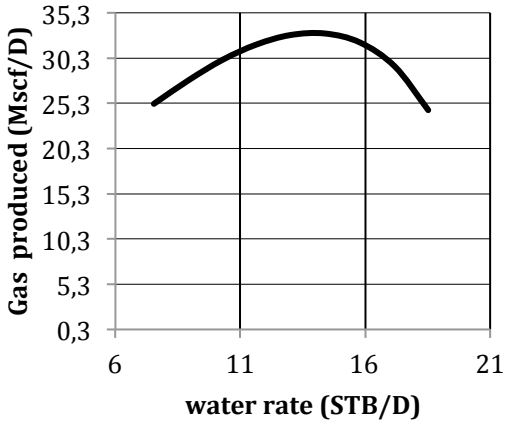

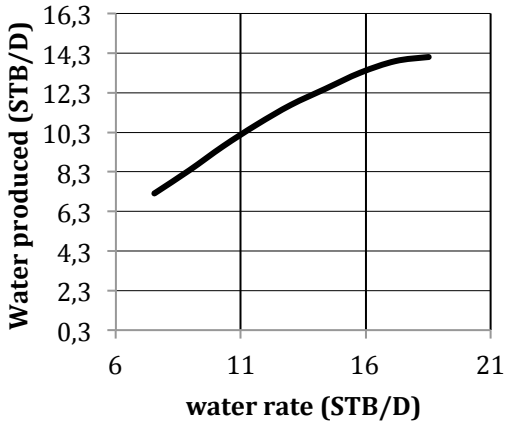

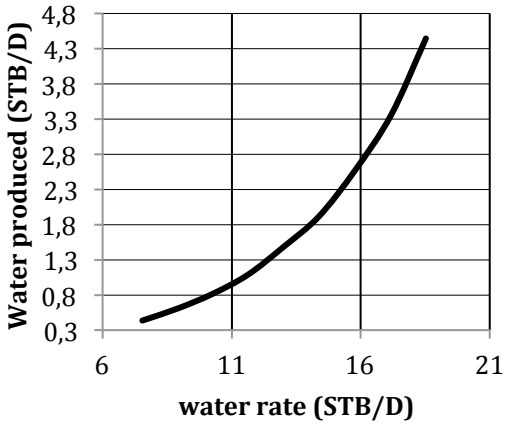

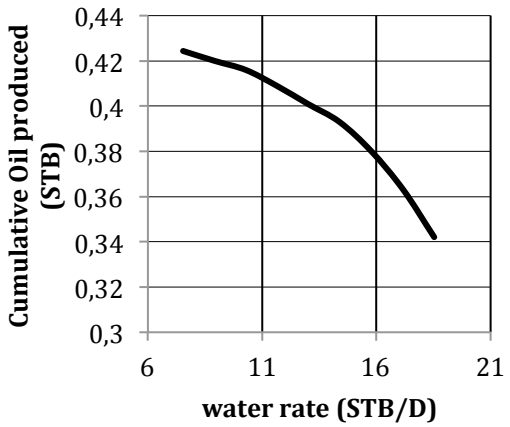

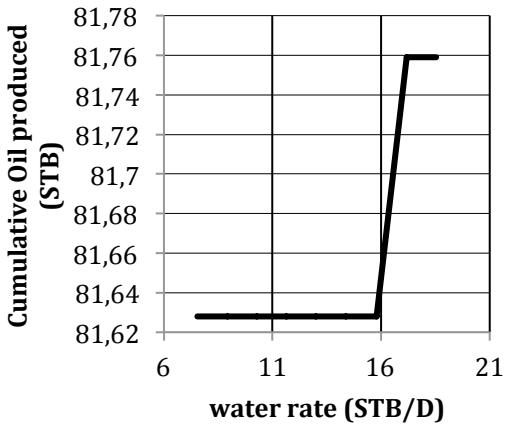

Appendix 6: Gas, water and Oil rates in the 1D simulation for different pressure profiles in the middle well (left) and right well (right), Eclipse 300.

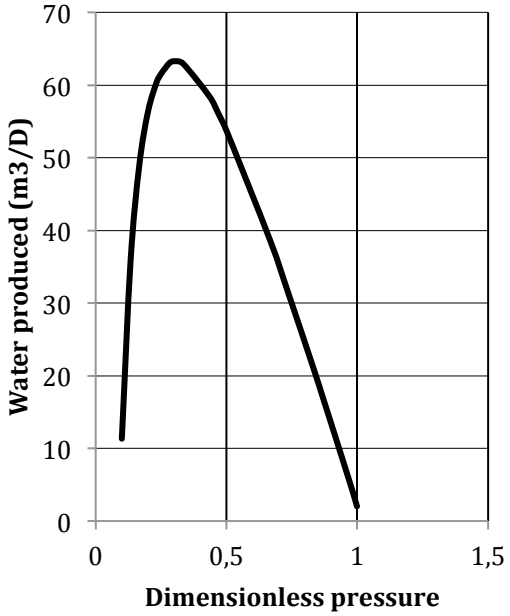

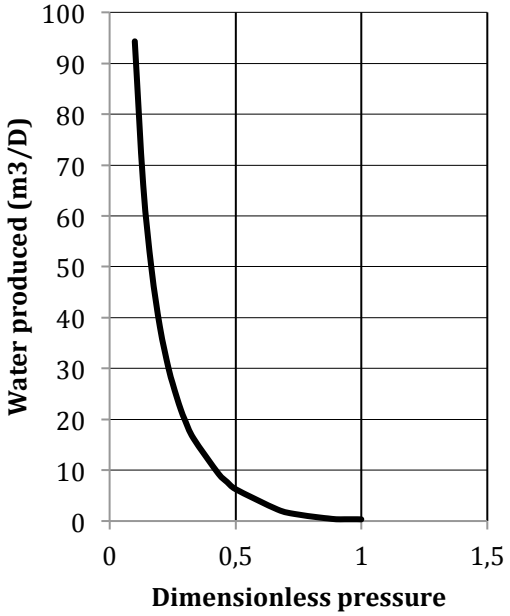

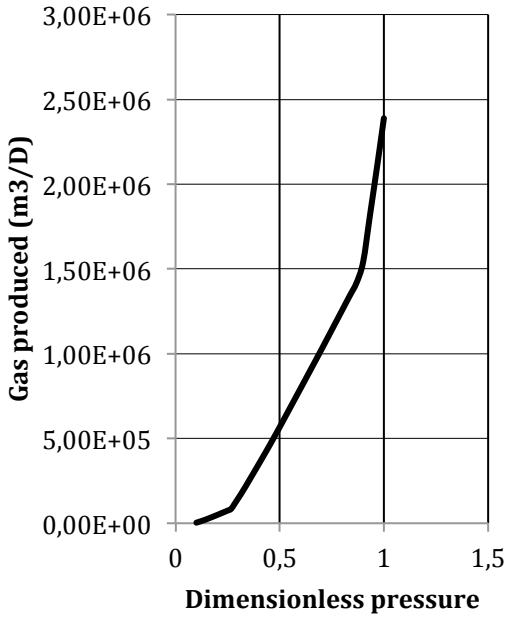

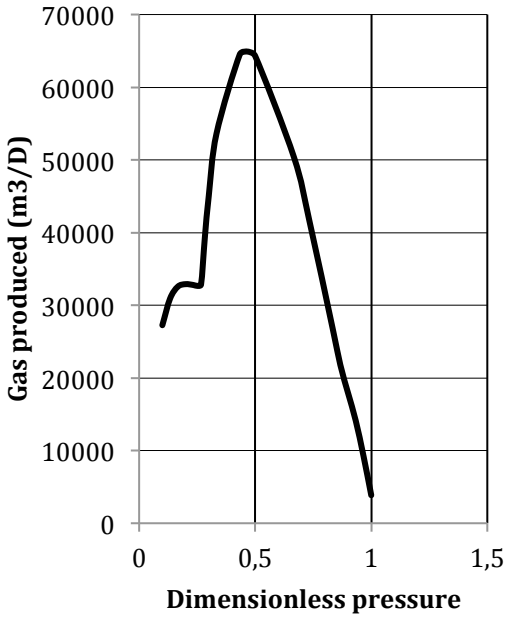

Appendix 7 : Matlab program

```
Im=imread('430-370.bmp');% Load the image file and store it as a matrix.
Rmat=zeros(890,955,1);%Matrix red intensity
Gmat=zeros(890,955,1);%Matrix green intensity
Bmat=zeros(890,955,1);%Matrix blue intensity
Tot=zeros(890,955,1);%Matrix blue intensity
check=zeros(890,955,1);%Matrix blue intensity

area=0;
Xleft=434;%window chosen
Xright=806;
Ybottom=560;
Ytop=180;

for i=Ytop:Ybottom %R,G,B matrix copy/paste in the chosen window
   for j=Xleft:Xright
      if Im(i,j,1)==128
      Rmat(Ybottom+1-i,Xright+1-j,1)=100;
      else Rmat(Ybottom+1-i,Xright+1-j,1)=Im(i,j,1);
      end
      if Im(i,j,2)==128
      Gmat(Ybottom+1-i,Xright+1-j,1)=100;
      else Gmat(Ybottom+1-i,Xright+1-j,1)=Im(i,j,2);
      end
      if Im(i,j,3)==255
      Bmat(Ybottom+1-i,Xright+1-j,1)=0;
      elseif Im(i,j,3)==128
      Bmat(Ybottom+1-i,Xright+1-j,1)=100;
      else Bmat(Ybottom+1-i,Xright+1-j,1)=Im(i,j,1);
      end
      Tot(Ybottom+1-i,Xright+1-j,1)=Bmat(Ybottom+1-i,Xright+1-j,1)+Rmat(Ybottom+1-
i,Xright+1-j,1)+Gmat(Ybottom+1-i,Xright+1-j,1);



      if Tot(Ybottom+1-i,Xright+1-j,1)~=10
         check(Ybottom+1-i,Xright+1-j,1)=1;
         area=area+1;
      else check(Ybottom+1-i,Xright+1-j,1)=0;
      end
   end
end

mesh(check)

grid on
```

Appendix 8: Pictures showing surface and cross section CO_2 saturation, from strong aquifer to weak aquifer.

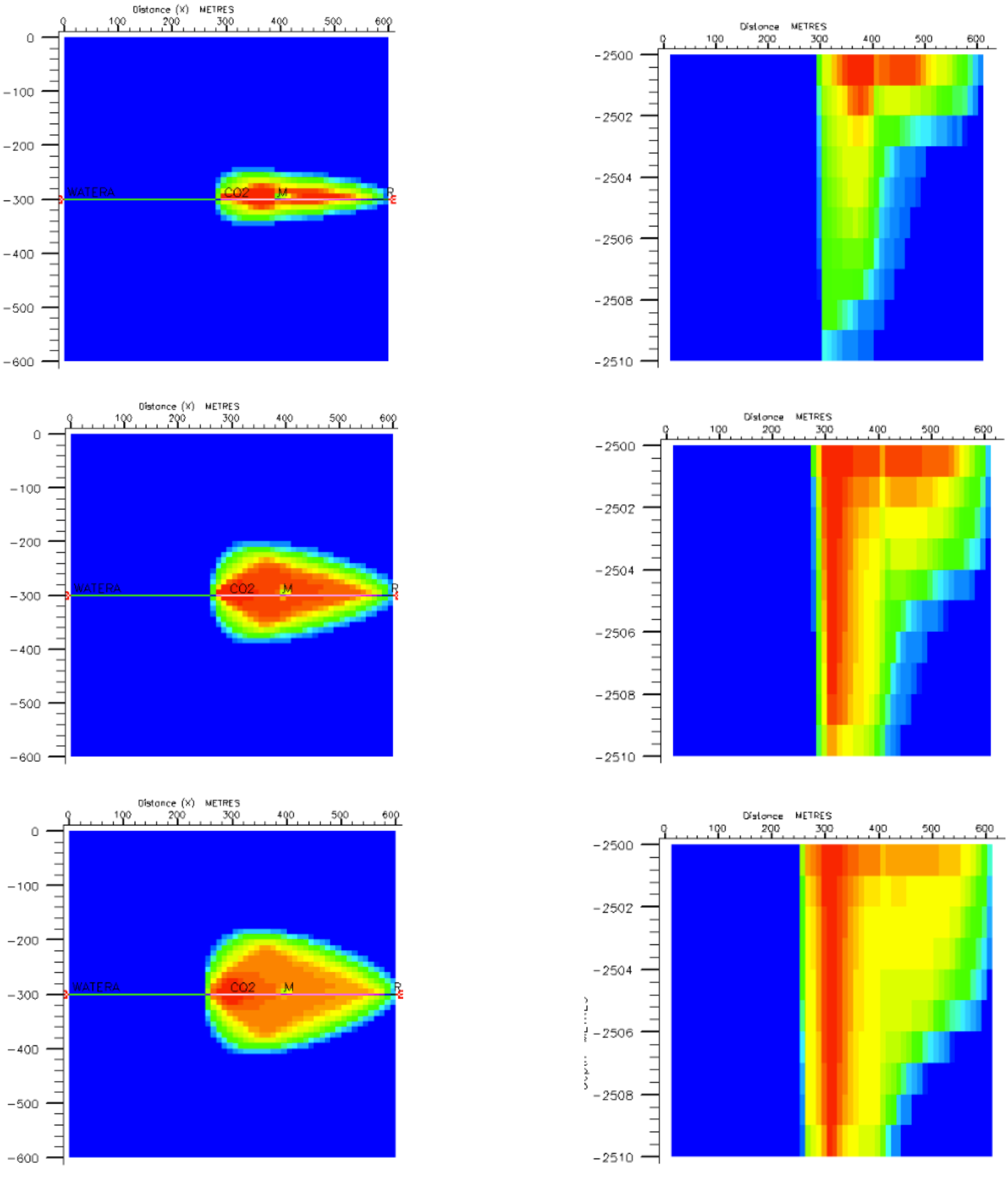

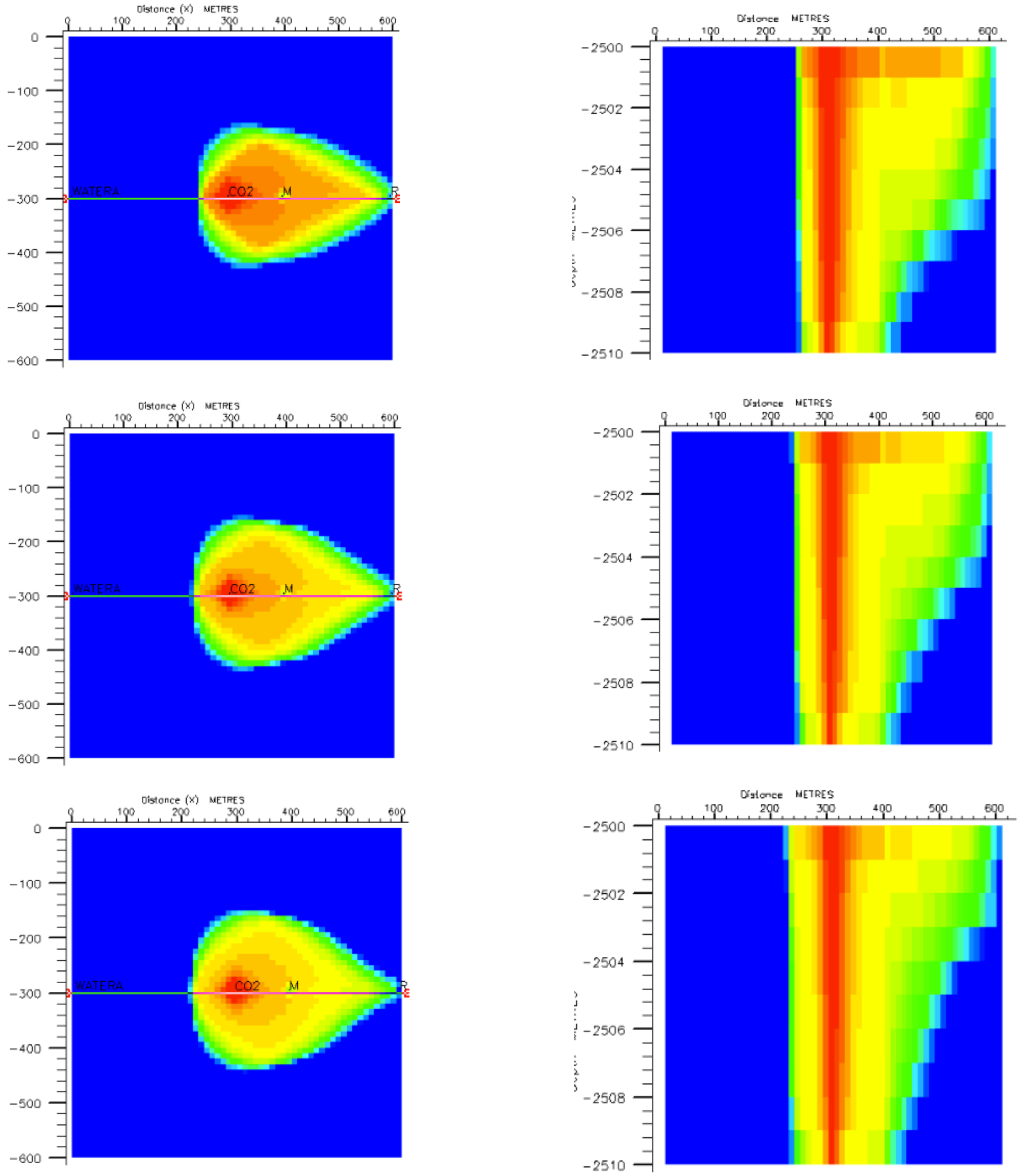
Distance (x) METRES
WATERA
CO2
M
Distance METRES